Neuronal Response to Experimental Autoimmune Encephalomyelitis

Dissertation
Zur Erlangung des Grades
Doktor der Naturwissenschaften

Am Fachbereich Biologie
Der Johannes Gutenberg-Universität Mainz

Vorgelegt von
Sabina Berl
geb. am 8. Juli 1985 in Frankfurt am Main, Deutschland

Mainz, 2019

Dekan: [redacted]

Berichterstatter 1: [redacted]

Berichterstatter 2: [redacted]

Tag der mündlichen Prüfung: _____17.12.2019_____

Für Stefan, Valentin und Rosalie

Table of Content

Table of Figures

Abbreviations

A	average
AD	Alzheimer's Disease
APC	antigen-presenting cells
Apoe	apolipoprotein E
Aspa	aspartoacylase
AMPA	α-amino-3-hydroxy-5-methyl-4-isoxazolepropionic acid
BBB	blood-brain-barrier
B2M	beta-2-microglobulin
CA^{2+}	calcium
Canx	calnexin
Calr	calreticulin
CFA	Complete Freund's adjuvant
CIP	primary progressive MS
CNS	central nervous system
cKO	conditional knockout
CSF	cerebrospinal fluid
Cspg4	chrondroitin sulfate proteoglycan 4
Cyp51	cytochrome P450 family 51
Dapi	4´,6-diamidino-2-phenylindole
DC	dendritic cell
Dcx	doublecortin
DE	differentially expressed
Dhcr7	7-dehydrocholesterol reductase
Dhcr24	24-dehydrocholesterol reductase
DNA	deoxyribonucleic acid
Dpi	days post injection
EAE	experimental autoimmune encephalomyelitis
ER	endoplasmatic reticulum
eYFP	enhanced yellow fluorescent protein
FACS	fluorescence activated cell sorting
Fdft1	farnesyl-diphosphat farnesyltransferase
Fl	floxed
FSC	forward scatter
Gfap	glial fibrillary acidic protein
GluR1	glutamate receptor 1
GM-CSF	macrophage colony-stimulating factor
HA	human influenza hemagglutinin
HDL	high density lipoprotein
HLA	human leukocyte antigen
Hmgcr	3-hydroxy-3-methylglutaryl-CoA reductase
Hmgcs1	3-hydroxy-3-methylglutaryl-CoA synthase 1
Hprt	hypoxanthine-guanine phosphoribosyl transferase
H2-D1	class I histocompatibility antigen D alpha chain
Iba1	ionized calcium binding adaptor molecule 1
Icam	intercellular adhesion molecule
IFNγ	interferon gamma
IFNγ-R1	interferon gamma receptor 1

IL-17A	interleukin 17 A
IL-17RA	interleukin 17 receptor antagonist
iNOS	inducible nitric oxide synthase
Itgam	integrin alpha M/macrophage-1 antigen
JAK	Janus kinase
KIR	killer cell immunoglobulin-like receptors
LDL	low density lipoprotein
LFA-1	lymphocyte function-associated antigen 1
Lss	lanosterol synthase
MACS	magnetic activated cell sorting
Mapk4	mitogen-activated protein kinase 4
MBP	myelin basic protein
MHC	major histocompatibility complex
MMP	matrix metalloproteinase
MOG	myelin oligodendrocyte glycoprotein
MS	multiple sclerosis
Mvd	mevalonate diphosphate decarboxylase
Mvk	mevalonate kinase
Nefh	neurofilament heavy chain
Nefm	neurofilament median chain
NeuN	neuronal nuclei
NG2	neuron-glial antigen 2
NGS	next generation sequencing
NK cells	natural killer cells
Nsdhl	NAD(P) dependent steroid dehydrogenase-like
OLG	oligodendrocytes
OPC	oligodendrocyte precursor cell
pAcc	perturbation accumulation
PCA	Principal component analysis
PCR	polymerase chain reaction
PirB	immunoglobulin-like receptor B
PLP	myelin proteolipid protein
Pmk	phosphomevalonate kinase
pORA	perturbation over-representation analysis
PPMS	primary progressive multiple sclerosis
Ptx	pertussis toxin
RIN	RNA integrity number
RNA	ribonucleic acid
RRMS	relapsing-remitting multiple sclerosis
Scap	SREBP cleavage-activating protein
SPMS	secondary progressive multiple sclerosis
Srebp	sterol regulatory element-binding protein
SSC	side scatter
Stat1	signal transducer and activator of transcription 1
Sqle	oxidosqualene cyclase
Tap-1	transporters associated with antigen processing-1
Tapbp	tapasin
T cell	thymus derived lymphocyte
TCR	T cell receptor
Tm7sf2	transmembrane 7 superfamily member 2
TNF	tumor necrosis factor

TRAIL	TNF-related apoptosis-inducing ligand
Tubb3	tubulin beta 3 class III
Tuj1	neuron-specific class III beta-tubulin 1
qPCR	quantitative polymerase chain reaction
WT	wildtype

1. Introduction

1.1. Structure and Function of Neurons in the CNS

The central nervous system (CNS) consists of the brain and the spinal cord and coordinates incoming information and the controlling of all parts of the body. The brain itself consists of the three main parts cerebrum, brain stem and cerebellum (Gilbert, 2000) (Figure 1A). The cerebrum is the largest region of the brain and is split in two cerebral hemispheres. It contains several regions like the cerebral cortex, hippocampus, basal ganglia and olfactory bulb. Cerebral functions are various and include memory, attention, language, consciousness and many others. The cerebral cortex is the outer layer of the grey matter, covering the core of white matter of the cerebrum. The surface of the cerebral cortex is folded in gyri and sulci, forming the prominent structure. Within the CNS, grey and white matter can be distinguish based on different content of white appearing lipid components. The grey matter mainly consists of neuronal cell bodies and unmyelinated axons and appears darker than the white matter primarily consisting of oligodendrocytes and lipid-rich myelinated axons, so called tracts (Jawabri and Sharma, 2019). The much smaller cerebellum is located posterior of the cerebrum and is covered with fine parallel grooves. These thin layers harbor several types of neurons, for example the purkinje cells and granule cells. Purkinje cells are a class of GABAergic (γ-aminobutyric acid) neurons and are the largest neurons in the human brain, whereas granule cells are found to be the smallest neurons in the human brain located in close proximity. The cerebellum is important for motor function as well as some cognitive function like attention and language. The brain stem is the most posterior part of the brain and connects the cerebrum to the spinal cord. Its comprised of the midbrain, pons and medulla oblongata (Purves et al., 2001). The brain stem functions as main innervation supply for face and neck via the cranial nerves. Furthermore it plays an important role in the regulation of cardiac and respiratory function (Gilbert, 2000).

The spinal cord extents from the brain stem to the lumbar and sacral region of the vertebral column. The main function of the spinal cord is signal transmission from the motor cortex towards the body and from the sensory neurons towards the sensory cortex. It is segmented in cervical, thoracic, lumbar and sacral regions. The butterfly shaped grey matter of the spinal cord consists of cell bodies of interneurons, motor neurons and unmyelinated axons. The outside of the spinal cord, the white matter, mainly consists of myelinated axons from motor

neurons and sensory neurons transmitting informative signals (Alsterberg et al., 1956) (Figure 1B).

Different types of neurons can be classified by their function. Motor neurons guide signals from the brain to spinal cord and further to muscles of all body parts for reaction and movement. Sensory neurons transmit signals from body to brain and spinal cord to process the feedback. The third group the interneurons connect the different neurons to each other forming this complex and unique network of signal transmission. The connection between neurons is made of synapses which transmit signals via neurotransmitter over the synaptic cleft from axon to dendrite or soma of different neurons (Foster, M.; Sherrington, 1897). The kind of neurotransmitter determines the class of neurons from which they are released. A broad diversity of neurotransmitter and neuroactive peptides are known until now. The four commonest ones which can be released from synaptic vesicles are acetylcholine, dopamine, GABA and serotonin. Depending on the receptor on the post-synaptic side, the signal can either be excitatory or inhibitory. Binding of a neurotransmitter to an excitatory receptor causes an influx of Na^+ and K^+ ions generating an action potential and transmission of the signal. In contrast binding to an inhibitory receptor leads to the opening of K^+ and Cl^- channels, inhibiting the action potential and stopping the signal (Lodish et al., 2000). Released neurotransmitter can be recycled or degraded to avoid overstimulation. Overactivation of neurological synapses can cause excitotoxicity and damage neurons by allowing high levels of Ca^{2+} to enter the cell. Ca^{2+} influx activates various enzymes of different pathways which harm cell components and leading to apoptosis (Jaiswal et al., 2009; Manev et al., 1989).

Brain and spinal cord are suspended in cerebrospinal fluid (CSF) and isolated from the bloodstream by the blood-brain-barrier (BBB). They are encased by the meninges, three membranes called the dura mater, the arachnoid mater and the pia mater. The subarachnoid space between arachnoid mater and pia mater is filled with cerebrospinal fluid (CSF) which continues down the spinal cord. The dura mater of the brain in attached to the skull, but in the spinal cord it is separated from the vertebrae by the epidural space (Maton, 1993). The BBB is formed by endothelial cells, astrocytes and pericytes creating a high selective semipermeable border between CNS and blood stream. Only the passage of selected molecules like water, glucose and amino acids is granted, whereas the entry of large molecules and pathogens is prevented. Accordingly, infections of the CNS are rare and immune cells relatively redundant. But an occurring infection is even more complicated to antagonize as the CNS is an immune privileged area since the BBB also prevents passage of immune cells (Ballabh et al., 2004;

Daneman and Prat, 2015). Opening of the BBB to immune cells is a pathological condition which can cause autoimmune disease like multiple sclerosis (MS) (Fletcher et al., 2010).

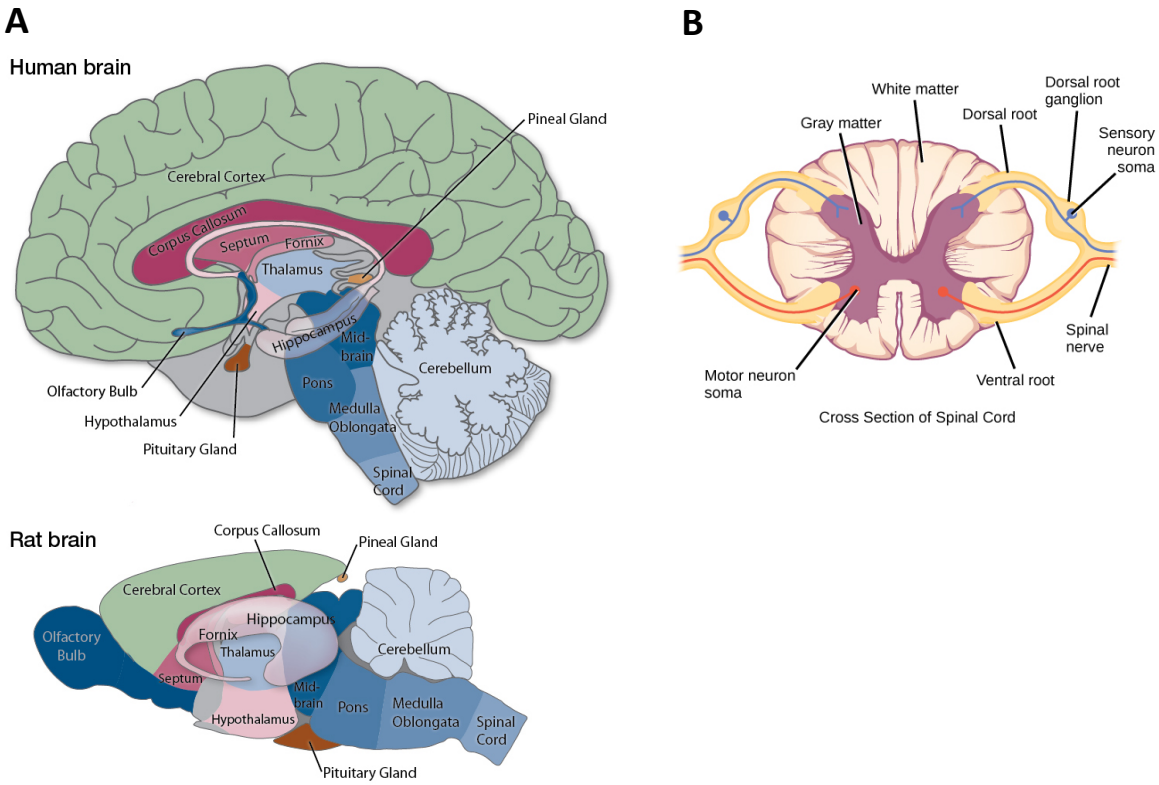

Figure 1: Structure of brain and spinal cord

A: The structure of the human and the rodent brain with cerebrum (cortex, olfactory bulb, hippocampus, thalamus and hypothalamus), cerebellum and brain stem (midbrain, pons and medulla oblongata) (adapted from Human versus rodent brain from Bryant Lab, Boston University).
B: Cross section of the spinal cord with grey and white matter showing motor and sensory neurons (adapted from Sensory-somatic nervous system from OpenStax, Rice University)

1.2. CNS Inflammation: Multiple Sclerosis and EAE

Multiple sclerosis (MS) is an autoimmune disease caused by chronic inflammation in the central nervous system (CNS). The disease is characterized by demyelination of neuronal axons causing severe neurological disorders like impaired vision, sensory modalities, motor performance and coordination (McDonald and Sears 1970; Steinman 1999). Thereby inflammatory lesions in brain and spinal cord are a direct cause of immigrating immune cells (Fletcher et al., 2010; Pender and Sears, 1986). Beside clinically isolated syndrome (CIS), primary progressive MS (PPMS) and secondary progressive MS (SPMS), the most common form is relapsing-remitting MS (RRMS) (Farrokhi et al., 2016; Fletcher et al., 2010). CIS is described as the first appearance of neurological symptoms evoked by inflammation and demyelination of axons, which has to last for 24 hours. CIS patients typically show

characteristics of MS but may not necessarily develop MS. Two third of these patients will convert to RRMS with further neurological dysfunctions (Brownlee and Miller, 2014). PPMS can be defined by continuous negative progressing neurological functions from the onset of symptoms and an absence of relapses and remissions (Iwanowski and Losy, 2015). In contrast SPMS follows an initial relapsing-remitting course with progressive worsening of neurological functions (Plantone et al., 2016). RRMS is characterized by episodes of relapse and remission but typically leads to a chronic disease. Approximately 85% of MS patients belong to this phenotype (Steinman, 1999).

Even though no animal model fully recapitulate all characteristics of MS it is still essential to develop and progress knowledge of the pathology of this disease to develop better treatments for the human disease (Handel et al., 2011; Robinson et al., 2014). Therefor the best studied and commonly used animal model for MS is experimental autoimmune encephalomyelitis (EAE). EAE can be either actively induced, passively transferred or develop spontaneously. Commonly active induced EAE is used for experiments by injection of myelin oligodendrocyte glycoprotein (MOG), Complete Freund's adjuvant (CFA) and Pertussis toxin (Ptx) (Stromnes and Goverman, 2006). Besides MOG, myelin proteolipid protein (PLP) and myelin basic protein (MBP) can be used as auto antigens as well (Mendel et al., 1995). The typical progression for MOG induced EAE is a monophasic curse of the disease (Bittner et al., 2014). It is characterized by rapid worsening of clinical symptoms and reaching a peak after several days. Afterwards the symptoms begin to resolve and end in a phase of clinical recovery. There, the animals still exhibit slight symptoms but never recover completely. Although not all mechanisms are fully understood to this point, the knowledge about the processes taking place after induction of this standard method of EAE is rather high (Billiau and Matthys, 2001).

After immunization with MOG peptide, antigen-presenting cells (APCs) like dendritic cells (DCs) in the para-aortic lymph nodes will present MOG to naïve $CD4^+$ T cells, which will then undergo maturation to leave the lymph nodes as T_H1 or T_H17 T cells (Furtado et al., 2008). Because of their myelin-specificity, the T cells recognize components of myelin sheaths after the passage through the blood-brain-barrier (BBB) into the CNS (Fletcher et al., 2010; Kerlero de Rosbo et al., 1993). Under normal condition the BBB is impermeable for the most cells and only specific water-soluble substances can pass (Hawkins, 2005). Which is not the case in EAE as well as in MS where the permeability of the BBB is impaired to the point that $CD4^+$ T cells or $CD8^+$ T cells become able to enter the CNS. After reactivation by their myelin-specific antigens coupled to major histocompatibility complex (MHC) class II molecules, in the case of $CD4^+$ T cells or class I molecules, in the case of $CD8^+$ T cells on local APCs, they start to recruit

other immune cells, like T_H17 cells, through the impaired BBB (Fletcher et al., 2010; Steinman, 1999).

As part of their natural program these reactivated T cells start to express cytokines like Interleukin-17A (IL17A), granulocyte-macrophage colony-stimulating factor (GM-CSF) and interferon-γ (IFNγ). IFNγ is the signature cytokine for T_H1 cells and is secreted to activate other immune cells, like macrophages or monocytes (Trinchieri, 1997). Macrophages and monocytes are also regulated by GM-CSF produced by invasive T_H17 cells during inflammation (Rostami and Ciric, 2013) as well as IL17A, which further promotes the inflammation (Harrington et al., 2005). As a result of the cytokine production and an activation of microglia, free oxygen radicals, proteases and glutamate are released, causing direct attack of the neuronal myelin sheath resulting in severe damage and loss of function (Fletcher et al., 2010; Steinman, 1999).

Besides the fact that MS and EAE are not perfectly identical in all aspects, they share several characteristic elements. Both show specific lymphocyte activation and cytokine secretion, CNS infiltration followed by demyelination and damage to neurons and glial cells. Even if the main principle of EAE is comparable to MS they differ in many details. MS is a chronic neurological disease whereas EAE is characterized by an acute progression with a clinical recovery with varying degrees of symptoms (Steinman, 1999). In MS patients most lesions are found in the white matter of the brain, while EAE is characterized by infiltrations mainly in the spinal cord (Pierson et al., 2012). But the most important difference between EAE and MS is the role of different T cell subtypes. In EAE the main effector T cells are $CD4^+$T cells, whereas in MS $CD8^+$ T cells located in lesion regions outnumber $CD4^+$ T cells by far (Van Kaer et al., 2019). Also, the role of involved cytokines exhibits variation. A good example is the case of Interferon γ (IFNγ), the administration of which was found to be protective in EAE, but was dramatically exacerbate MS progression. Still, a lot of functions in both diseases remain that have not been discovered yet (Fletcher et al., 2010).

However, the damage to neurons during MS or EAE is not necessarily permanent. Especially damage to the myelin sheaths can be repaired by remyelination which is from great relevance for the remission in RRMS and recovery phase of EAE (Kremer et al., 2015). This process helps to restore the axonal conduction necessary for neurological signalling (Trapp and Stys, 2009) and highly depends on oligodendrocyte precursor cells (OPCs) also referred to as NG2-cells, which differentiate into mature myelin forming oligodendrocytes (Franklin et al., 2012). Already during MS the OPCs are recruited into lesions in the brain, differentiate to oligodendrocytes and repair demyelinated lesions by producing new myelin for the axon sheaths (Chang et al., 2012, 2002; Prineas and Connell, 1979).

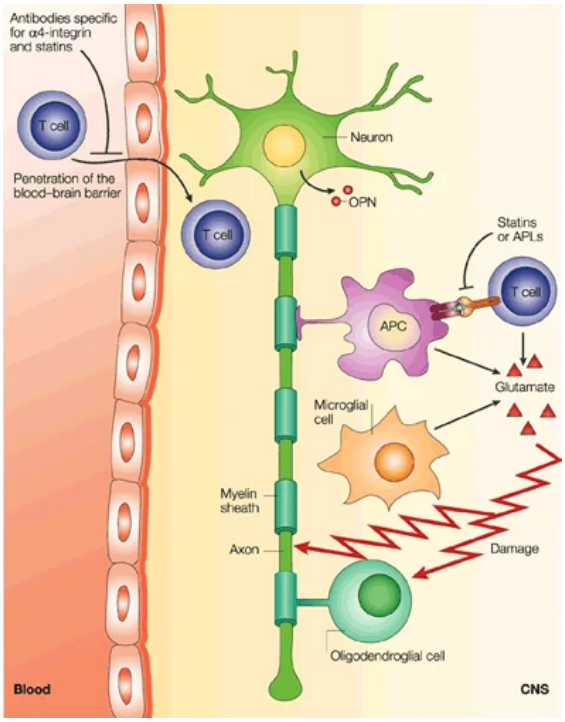

Figure 2: Process of neuronal damage in Multiple sclerosis and EAE

In the case of Multiple sclerosis or EAE immune cells, like T cells, pass the blood-brain-barrier and enter the CNS. Being present in this immune privileged area, they cause damage to neurons and other CNS resident cells by producing cytokines or attacking them directly. For example glutamate, which can be produced by T cells, antigen presenting cells like macrophages and microglia, is a toxic substance and harms oligodendrocytes and neuronal axons (from Steinman and Zamvil, 2003).

1.3. Neuronal Interaction with Invading Immune Cells during EAE

During EAE and MS the crosstalk between immune cells and CNS cells is unbalanced. Meaning the fine tuning of interaction between effector T cell and target neuron or glial cell is disturbed. But this finetuned crosstalk is important to fight pathogens and at the same time prevent too much damage to own tissue. Immune reactions within the CNS are restricted to as little as possible forming an immune privileged area (Galea et al., 2007; Ransohoff and Engelhardt, 2012). In the case of MS and its animal model EAE this privilege is corrupted, immune cells are able to pass the no longer fully intact blood brain barrier entering the CNS and cause damage to neurons and glial cells by producing cytokines and attacking them directly (Fletcher et al., 2010; Steinman, 1999). Thus the consequences for neurons and other CNS cells are highly dramatic if inflammation takes place in the CNS, like in MS and other neurodegenerative diseases, it becomes even more important that the knowledge of *in vivo* interaction of T cells and neurons expands. Still most studies were performed in *in vitro* experiments and confocal imaging (Medana et al., 2001).

Depending on the type of immune cells different contacts with neurons can be formed. It is known that once $CD8^+$ T cells reach the CNS they can form stable contacts to neuronal axons and dendrites dependent on antigen presentation by MHCI (Chevalier et al., 2011; Neumann et al., 1997). This contact will lead to damage in form of spheroids and beads as well as transection of neurites (Medana et al., 2001). Even if the full mechanism behind the damage of the CD8-neuronal contact is not fully understood it probably relies on the transfer of cytolytic granules (Suidan et al., 1994) as well as Fas/Fas-ligand binding which induces an apoptosis cascade in the target cell (Medana et al., 2001). The contact of neurons to $CD4^+$ T cells, in contrast to $CD8^+$ T cells, is antigen independent as neurons do not express MHCII molecules by which they could interact with $CD4^+$ T cells. Instead the contact and interaction can be formed by TNF-a binding to the TNF-related apoptosis-inducing ligand (TRAIL) (Aktas et al., 2005). Also the interaction between ICAM on neurons and the ligand LFA-1 on T_H17 cells resulting in neuronal dysfunction could be proven (Siffrin et al., 2010). Even if $CD4^+$ T cells are the main effector T cells during EAE, the consequences of MHCI expression and recognition by $CD8^+$ T cells during EAE will be of high value in this thesis.

1.4. Cytokines and Chemokines in EAE and their Effect on Neurons

Beside the direct interaction of $CD8^+$ and $CD4^+$ T cells, which can lead to massive damage of neurons and other CNS cells during EAE, invading immune cells and also CNS resident cells can secrete various different cytokines and chemokines, which can cause damage as well, either by inducing downstream cascades in the target cell or by attracting even more immune cells to the site of inflammation. T cells, which can have a direct connection to neurons as described above, are together with microglia and macrophages the main cytokine and chemokine producers. The cytokine production of T cells is shown to directly contribute to the disturbance of electrical signalling in neurons (Medana et al., 2000; Mizuno et al., 2008).

In EAE both activated $CD4^+$ and $CD8^+$ T cells are able to release IFNγ during inflammation. Binding of IFNγ to its receptor leads to an activation of the Janus kinase/signal transducers and activators of transcription (JAK/STAT) pathway. It is a cascade used to transduce a multitude of signals for development and homeostasis. In mammals, the JAK/STAT pathway is the principal signalling mechanism for a wide array of cytokines and growth factors. Following the binding of cytokines to their receptor, STATs are activated by members of the JAK family of tyrosine kinases. Once activated they form dimers and translocate to the nucleus to modulate expression of target genes which can function anti-apoptotic, regulate the cell cycle as well as enhancing cell survival (Harrison, 2012; Kiu and Nicholson, 2012). IFNγ is produced by

encephalitogenic T cells during EAE and is known to cause opposing effects on CNS resident cells. In a dose-dependent manner it can either induce protection in microglia and oligodendrocytes when present in low dose, whereas in high doses it promotes effects worsening the disease. In astrocytes the role of IFNγ seems to be primarily promoting of the disease (Ottum et al., 2015). In spinal cord neurons IFNγ receptor expression, which can be upregulated by nerve growth factor (NGF), is known to be involved in neuron survival and reduction of disease severity (Stampachiacchiere and Aloe, 2005). This shows that fine-tuning of IFNγ with its receptor is of high value for EAE progression and further knowledge in neuronal function very important.

The IFNγ receptor is a heterodimer of two subunits, which assembles after binding of its ligand IFNγ. In neurons, after binding of IFNγ, the subunit IFNγR1 can interact to the neuron specific GluR1 subunit of the α-amino-3-hydroxy-5-methyl-4-isoxazolepropionic acid (AMPA) receptor, which are localized in close proximity on the surface. This interaction can cause a calcium influx to the neuron as well as inducing of the JAK/STAT pathway (Mizuno et al., 2008). It was already shown that blockage of this GluR1 subunit can eliminate neurological disorders in EAE rats (Abdarasulova et al., n.d.).

It was shown that neurons indeed upregulate their expression of Fas on the surface after incubation with IFNγ *in vitro* (Medana et al., 2000). The main damage to neurons seems to be an interplay of secreted cytokines and direct interaction, like Fas and Fas-ligand and MHCI - T cell receptor binding. Binding of neuronal MHCI by $CD8^+$ T cells causes a higher release of IFNγ, which on the neuronal side leads to the upregulation of Fas, resulting in an enhancement of downstream cascades promoting apoptosis. Following an impaired electric activity in neurons, MHCI is upregulated for the sake of signalling, but on the other hand will cause an increased CD8 mediated killing (Neumann et al., 1997). How exactly IFNγ functions on neurons and how they react in an autoimmune reaction like EAE and MS needs to be further investigated to unravel the neuronal response to this key player cytokine.

Very controversy studies existing about the strong indication that IL17 is another key player during MS and EAE (Waisman et al., 2015). IL17 is mainly produced by T_H17 $CD4^+$ T cells and targets CNS resident cells when secreted. The best-studied cell type expressing the IL17 receptor are astrocytes, but also neurons are shown to express it to a certain extent (Chisholm et al., 2012; Li et al., 2013; Sarma et al., 2009). It was found that MS patients obtain highly enriched levels of IL17A in their cerebrospinal fluid (CSF), which on top directly correlated with the glutamate levels in the CSF, indicating that T_H17 cells could be a direct origin of glutamate excitotoxicity (Kostic et al., 2014). It was found by intravital microscopy, that in

spinal cord of EAE animals infiltrating T_H17 cells and neurons form immune synapses in active lesions, which is an indirect evidence of the cytotoxic properties of IL17 (Siffrin et al., 2010). The direct effect and the specific response of neurons to IL17 by binding to their IL17 receptor is so far unknown and needs to be further studied to understand the full mechanism of neuron and T_H17 $CD4^+$ T cell interaction during the time course of EAE and in comparison to MS patients.

1.5. The Role of MHCI in Neurons

As already described above, $CD8^+$ T cells can interact with neurons by antigen-dependent binding of MHCI to their T cell receptor (Chevalier et al., 2011; Neumann et al., 1997). The expression of MHCI on neurons is not common and differs between different subpopulations. For example on cortical neurons in the brain MHCI is downregulated after development, but purkinje neurons in the cerebellum constitutively express MHCI molecules on their surface (McConnell et al., 2009; Shatz, 2009). In cell culture it was documented that neurons increase their MHCI expression upon incubation with IFNγ (Chevalier et al., 2011). In line *in vivo* experiments showed that under inflammatory conditions and neurodegeneration MHCI becomes activated and enriched in expression (Foster et al., 2002; Maehlen et al., 1988). To present functional MHCI proteins on the cell surface including peptides from the cytosol not only MHCI itself needs to be expressed by neurons, but also all molecules involved in the process of protein degradation, peptide transfer to the endoplasmatic reticulum (ER), peptide binding on MHCI as well as its transport to the cell surface. The proteasome, which is a protease complex, degrades proteins in the cytosol until they have the right size to be actively transported to the ER by specific transporters, Tap1 and -2 (transporters associated with antigen processing-1 and -2). Newly synthesized MHCI molecules are bound to calnexin (Canx) until dimerization with $ß_2$-microglobulin. For loading of this hetero-dimer with peptides, binding to calreticulin (Calr) and the chaperon molecule BRp57 is necessary, as well as binding to the peptide transporter TAP via tapasin (Tapbp). After this complex procedure MHCI complexes can be released and transported to the cell membrane. All these involved enzymes and molecules have to be expressed in neurons to obtain functional MHCI molecules that can be recognized by the TCR of $CD8^+$ T cells. And indeed, all of them were shown to be expressed in neurons (Díaz-Hernández et al., 2003; Neumann et al., 1997; Pickering and Davies, 2012).

An essential role for the development of the nervous system is the binding of MHCI molecules to the paired immunoglobulin-like receptor B (PirB-receptor). PirB was firstly discovered to be expressed in B lymphocytes and myeloid cells (Kubagawa et al., 1997), but was also found to

be expressed in neurons of particular brain regions, including the cerebral cortex, the olfactory bulb and the cerebellum. Interestingly PirB is especially located in growth cones and axons of cortical neurons (Syken et al., 2006). It could be shown that MHCI is located postsynaptically in close proximity of neuron specific glutamate receptors (AMPA receptors) whereas PirB can be found at the presynaptical side. PirB can signal across the synapsis if bound to MHCI. As MHCI expression is related to neuronal activity, PirB could also regulate downstream cascades in an activity-dependent manner and so facilitates axonal regeneration. As it was also shown that PirB signalling can inhibit axonal outgrowth, binding of MHCI is able to limit synaptic plasticity during development of the nervous system (Shatz, 2009). In EAE the role of PirB is unclear so far and is examined in this thesis.

1.6. Cholesterol Metabolism in the CNS

As the brain is the most cholesterol-rich organ, cholesterol plays an essential role for the health of the CNS (Dietschy and Turley, 2004). It is highly important for the maintenance of the optimal level of energetic metabolism, the composition of cell membranes and myelination (Czuba et al., 2017). The metabolic pathways of cholesterol in the CNS involve neurons, cerebral blood vessels and neuroglia. Especially for the proper function of neurons and their electrical excitation as well as the synaptic transmission and the morphology of nervous tissue, cholesterol is indispensable (Czuba et al., 2017; Dietschy and Turley, 2004). Particularly important is the main production of cholesterol by astrocytes and neurons during embryogenesis where most of the synthesis happens (Dietschy and Turley, 2004; Morell and Jurevics, 1996a). In maturity astrocytes by far become the main suppliers for cholesterol and the cholesterol synthesis in the brain is minimized to a very low turnover (Morell and Jurevics, 1996a; Nieweg et al., 2009a). If cholesterol synthesis is somehow deficient, the myelination process can be delayed (Saher et al., 2005).

Thus cholesterol is significant for the myelination of neurons, as the majority of it is found in myelin sheaths (Dietschy and Turley, 2004). It has also an impact on brain disorders if the homeostasis of cholesterol is imbalanced. This could lead to pathological processes and neuronal death (Vance, 2006) and a greater permeability of the BBB. A compromised BBB integrity can cause lesion formation as consequence of an increased permeability to macromolecules like immunoglobulins and so lead to an inflammation in the CNS. This can result in chronic neurodegenerative diseases such as Alzheimer's Disease (AD) or MS (Czuba et al., 2017; Lucchinetti et al., 2011). Therefore, the maintenance of the BBB is very essential. Cholesterol levels, particularly lipoproteins have a great impact on the permeability of the BBB.

High Density Lipoprotein (HDL) is claimed to be protective for the BBB integrity during MS and is associated with reduced lesions as it can modulate the phenotype of immune cells by altering cellular cholesterol (Fellows et al., 2015; Weinstock-Guttman et al., 2011). In contrast, Low Density Lipoprotein (LDL) and high total cholesterol levels are claimed to worsen disease progression of MS (Tettey et al., 2014).

However, cholesterol is not only important for myelination as it is found in almost any vertebrate cell and has several additional functions. It is a very important component of cell membranes in higher eukaryotes and particularly enriched in plasma membranes. There, it regulates the membrane fluidity, ion permeability, the modulation of membrane proteins and transmembrane signalling processes (Ikonen, 2008). Cholesterol subsequently has a great effect on biophysical properties of cell membranes. Through its interaction with lipids it can decrease the fluidity of the membrane and reduce the permeability for polar molecules (Simons and Vaz, 2004). Further, the membrane bending rigidity depends on cholesterol too. The more cholesterol is found in the membrane, the more energy is required to bend it (McIntosh and Simon, 2006). Moreover, cholesterol is enriched in synaptic membranes and if it is deficient in neurons, it has crucial impacts as it can lead to impaired synaptic vesicle endo- and exocytosis, increases spontaneous vesicle release and decreases evoked post-synaptic currents. These several functions indicate that neuronal cholesterol could have another purpose except the supply of sufficient cholesterol levels (Mailman et al., 2011).

1.7. Cholesterol Biosynthesis and Feedback Mechanisms

As lipoproteins like cholesterol cannot be imported from the peripheral blood circulation through the BBB, synthesis in the CNS is uncoupled to the rest of the synthesis in the body and as a consequence the cholesterol metabolism has to take place in the CNS (Jeske and Dietschy, 1980). The biosynthesis of cholesterol is a very complex and source-intense pathway which includes about 20 steps of transforming acetyl-CoA to cholesterol. Many enzymes are involved in this conversion. The mevalonate pathway starts with Acetoacetyl-CoA thiolase, which builds acetoacetyl-CoA by condensation of two molecules Acetyl-CoA. The next step from acetoacetyl-CoA to 3-hydroxy-3-methylglutaryl-CoA is catalysed by the enzyme 3-hydroxy-3-methylglutaryl-CoA-synthase (HMG-CoA synthase). The further production of mevalonate is implemented by 3-hydroxy-3-methylglutaryl-CoA reductase (HMGCR). HMGCR is associated with the endoplasmatic reticulum and interacts through membrane spanning helices in the N-terminal domain. HMGCR is the rate limiting enzyme in the cholesterol biosynthesis and the target of statin pharmacotherapy. The following step from mevalonate to mevalonate-

5-phosphat is dependent on ATP and is catalysed by the mevalonate kinase (Mvk). This enzyme is highly important for the feedback inhibition by downstream intermediates in the polyisoprenoid biosynthetic pathway, geranyl diphosphate and farnesyl diphospate. Mevalonate-5-phosphat is processed to mevalonate-5-diphoasphate by the enzyme phosphomevalonate kinase (Pmk). Mevalonate diphosphate decarboxylase (Mdd/Mvd) forms isopentenyl-5-diphosphate through ATP dependent decarboxylation of mevalonate-5-diphosphate (Miziorko, 2011).

Beginning with isopentenyl-5-diphosphate cholesterol is formed by following steps and enzymes belonging to the cholesterol biosynthesis. Isopentenyl-5-diphosphate is converted to dimethyl-allyl-diphosphate by the isopentenyl-diphosphate isomerase, which then is further processed by geranyl-diphosphate synthase to geranylphosphate. Farnesyl-diphosphate synthase then synthesises farnesyl-diphosphate, which together with geranyl-diphosphate can inhibit the mevalonate kinase (Mvk) in a negative feedback loop. Squalene is formed by farnesyl-diphosphat farnesyltransferase (Fdft1), and after cyclization of squalene by oxidosqualene cyclase (Sqle) lanosterol can be synthesized by lanosterol synthase (Lss). Finally, lanosterol is converted to cholesterol by a 19-step process containing NADPH and oxygen. Enzymes involved in this conversion are lanosterol 14-alpha demethylase (Cyp51), transmembrane 7 superfamily member 2 (Tm7sf2), NAD(P) dependent steroid dehydrogenase-like (Nsdhl), 24-dehydrocholesterol reductase (Dhcr24) and 7-dehydrocholesterol reductase (Dhcr7) (Waterham, 2006).

The cholesterol production in adult mice's brains is a *de novo* synthesis. It takes place in the ER of astrocytes and the product cholesterol is then transported to the plasma membrane (DeGrella and Simoni, 1982; Nieweg et al., 2009a). Some amount of cholesterol is constantly exchanged, for so far unexplored reasons it is excreted or degraded in cell plasma membranes all the time (Dietschy and Turley, 2004). Regarding the severe consequences of a disturbed cholesterol homeostasis, the permanent supply of new cholesterol and a strict regulation of the synthesis are even more essential. One important enzyme contributing to this process is the 3-hydroxy-3-methylglutaryl-CoA reductase (HMGCR). It converts 3-hydroxy-3-methylglutaryl-CoA to mevalonate. This step is considerably important as it is rate-limiting and irreversible (Ohashi et al., 2003a). A feedback mechanism helps to monitor constantly intracellular cholesterol levels. By transcriptional activation and deactivation of *hmgcr* the level of cholesterol in cells can be controlled (Sever et al., 2003). One transcription factor for activating the expression of the HMGCR gene is the sterol regulatory element-binding protein (SREBP) (Yokoyama et al., 1993). Another important protein for sensing cholesterol levels is the SREBP

cleavage-activating protein (SCAP). It is able to regulate the activity of SREBP and accordingly the HMGCR expression (Rawson, 2003). If there is a lack of cholesterol in the cell, SCAP activates SREBP by cleavage and increases thereby the transcription of *hmgcr*. Consequently, the cholesterol synthesis is enhanced. Conversely, if the cell is saturated, in the ER cholesterol itself induces binding of SCAP and prevents activation of SREBP and thus the interruption of cholesterol synthesis. In this way, the optimal cholesterol supply for the cell is provided and an overload of cholesterol is prevented (Chen et al., 2014).

As described, HMGCR plays a very important role in the regulation of cholesterol synthesis. If its expression is somehow affected, the consequences could be an insufficient cholesterol supply. But so far, the role of HMGCR in neurons and especially during EAE is poorly investigated and remains unclear. Indeed, this could be a very important information as it could be an approach to a possible therapy for MS. Indeed statins are already used as a treatment for the disease (Willey and Elkind, 2010a), so if the relevance of HMGCR could be elucidated, maybe new treatment strategies could be developed.

1.8. Aim of the Study

Damage of neurons, with disruption of signal transmission, by invading immune cells during MS and EAE is the main reason for the pathological phenotype and potential death of mice and human patients. However the role of neurons and the mechanism of neuronal response *in vivo* during MS and EAE is elusive, most likely due to the lack of techniques and difficulties of neuronal isolation from adult mice or humans.

In this thesis I will test three different methods of isolating neuronal RNA from adult mouse CNS in high quality and quantity. The best suitable method will be used to perform NGS with isolated neuronal RNA from three different time point of EAE (control, peak and recovery). I hope to unravel the neuronal response during the time course of EAE and discover target genes to further analyse their specific role in neurons during EAE. Also the comparison of mouse NGS data to human MS patients data will be accomplished.

2. Material and Methods

2.1. Mouse Experiments

2.1.1. Mice

C57BL/6J, RiboTag$^{fl/fl}$ (from Prof. Dr. Emmanuel Valjent, Paris), NFH-Cre (from Paul Heppenstall, Rome), IL17RA$^{fl/fl}$, IFNgR1$^{fl/fl}$ and HMGCR$^{fl/fl}$ (generated in our lab, (Lacher et al., 2017)) mice were bred in the animal facility at the University of Mainz, Germany. All strains were kept on the C57BL/6 background. TgN (Thy1.2-eYFP)$_{TYFA}$ mice on C57Bl/6N background (Hirrlinger et al., MCN, 2005 PMID: 16169246) were bred in the animal facility of the CIPMM at the University of Saarland, Germany. Camk2-Cre/PirB$^{fl/fl}$ mice (Bochner et al., 2014) were bred in the animal facility of the Beckman Center at the University of Stanford, USA.

All experiments were carried out under the terms of the guidelines of the Central Animal Facility Institution of Mainz and in agreement with relevant laws according to German and European guidelines for animal experimentation.

2.1.2. Experimental Autoimmune Encephalomyelitis (EAE)

Mice were immunized subcutaneously at the base of the tail with 50 µg MOG$_{35–55}$ peptide (Gene Script) emulsified in Complete Freund's adjuvant (Difco Laboratories, Detroit, MI, USA) supplemented with 1.1 mg of heat-inactivated Mycobacterium tuberculosis (Difco). 200 ng of pertussis toxin (List Biological Laboratories) was intraperitoneal injected on the same day and a second dose 2 days later. Mice were scored each day for clinical signs of EAE as previously described with modifications. The clinical assessment scale was graded from 0 to 6 as follows: 0, no disease; 0.5, partial loss of tail tonicity; 1, complete loss of tail tonicity; 1.5, partially impaired righting reflex on attempt to roll over (within 3 s); 2, impaired righting reflex; 2.5, partial hind limb paresis resulting in staggering gait; 3, one hind limb fully paralysed; 4 full hind limb paralysis; 4.5, starting forelimb paresis; 5, forelimb paresis resulted in inability to move the body; 5.5, moribund; and 6, dead animal.

2.2. Cell Biology

2.2.1. Dissociation of Adult Mouse Brains

Dissociation of adult mouse brains was performed using the "Neural Tissue Dissociation Kit – Postnatal Neurons" (*Miltenyi Biotec*, 130-094-802) following the user manual with slight modifications in combination with the gentleMACS Dissociator (*Miltenyi Biotec*). Mice were killed using CO_2 and perfused with 30ml NaCl (0.9%), the brains isolated and cut into 15-20 pieces with a sterile and sharp razor blade. Per brain, two C Tubes (*Miltenyi Biotec*, 130-093-237) and the double recommended volume of enzyme mixes (3920µl enzyme mix 1, 90 µl enzyme mix 2) were used. C tubes with brain pieces and enzyme mix 1 are attached to the gentle MACS Dissociator. After running of program m_brain_01, C tubes are detached and incubated with rotation at 37°C for 15min. Enzyme mix 2 is added before running the gentleMACS program m_brain_02. C tubes are detached and incubated for 10min at 37°C under slow rotation. C tubes are attached to the gentle MACS Dissociator and run program m_brain_03. Samples are collected at the bottom of the tube by briefly centrifugation, resuspended and applied to a MACS SmartStrainer, 70µm, placed on a 50ml tube. 10ml of D-PBS with PBS are added. After centrifugation for 10min at 300xg at room temperature each brain was finally resuspended in 3.6 ml PBS++/BSA (0.5%) (*life technologies, 14040-091*) for myelin removal.

2.2.2. Myelin Removal from Adult CNS Cell Suspension

After dissociation of adult mouse brains the remaining myelin has to be removed. Therefor 400 µl of Myelin-Removal Beads II (*Miltenyi Biotec*, 130-096-733) were added to the cell suspension from each brain and incubated for 15min at 4°C. After incubation cells are washed with 40ml buffer from the kit and centrifuged at 300xg for 10min. Each brain was resuspended in 8000µl buffer and distributed to eight LS columns (*Miltenyi Biotec*, 130-042-401) to properly remove the myelin. This procedure was repeated a second time with 900 µl PBS++/BSA (0.5%), 100 µl Myelin-Removal Beads and 6 columns per brain. The cell fraction purified of myelin was resuspended in 3 ml PBS++ per brain for fluorescence activated cell sorting (FACS); 3200 µl PBS++/BSA (0.5%) per brain for depletion of non-neuronal cells; or 350 µl RLT buffer with 1% ß-mercaptoethanol per $2x10^5$ cells for RNA isolation of all brain cells.

2.2.3. Fluorescence Activated Cell Sorting (FACS) of Neurons

Cells collected after myelin removal were incubated with mouse Fc-receptor block (*BioXCell*, BE0008), stained for CD11b (*eBioscience*, 25-0112) and the viability dye PO-PRO™-1 iodide (Invitrogen, P3581) for 30 min, washed once with PBS++ and resuspended in 3 ml PBS++/BSA (0.5%) for FACS sorting. Gates were set using isotype antibody-stained controls and wild type cells without eYFP expression. All samples were sorted with a FACSAria I (*BD Bioscience*) with a 100µm nozzle. Post-acquisition data analysis was carried out using FlowJo software. The sorted cells were either assessed with Flow-cytometry assay or resuspended in 350 µl RLT buffer with 1% ß-mercaptoethanol for RNA isolation.

2.2.4. Depletion of Non-Neuronal Cells/Isolation of Neurons

For the isolation of neurons from a mixed brain cell suspension without myelin, the Neuron Isolation Kit (*Miltenyi Biotec*, 130-098-752) was used. To each 3200µl brain cells suspension from 2.3 400µl non-neuronal cell specific biotinylated antibodies are added, mixed and incubated 5min at 4°C before cells are washed by adding 40ml buffer and centrifuged at 300xg for 10min at room temperature. Cells were resuspended in 3200µl PBS++/BSA (0,5%) and 400µl Anti-Biotin MicroBeads are added, mixed and incubated for 10min at 4°C. Volume of cell suspension is adjusted to 4000µl per brain with PBS++/BSA (0,5%) and distributed to eight LD columns (*Miltenyi Biotec*, 130-042-901) to deplete non-neuronal cells. Isolated neurons were either used for Flow-cytometry assay or resuspended in 350 µl RLT buffer with 1% ß-mercaptoethanol for RNA isolation.

2.2.5. Flow-Cytometry Assay of Enriched and Isolated Neurons

Samples enriched for neurons or isolated neurons and samples of all brain cells as controls were washed once with PBS++, incubated with mouse Fc-receptor (*BioXCell*, BE0008), stained for CD11b (*eBioscience*, 25-0112) and the Fixable Viability Dye eFluor®780 as a dead cell marker (*eBioscience*, 65-0865-14) for 30 min, fixed and permeabilized with a PE Anti-Mouse/Rat Foxp3 staining set (*eBioscience*, 72-5775-40) according to the user manual. The cells were then stained for NeuN (*Merck Millipore*, FCMAB317PE) for 30 min and washed with the permeabilization buffer before resuspending in 100 µl permeabilization buffer. All samples were acquired on a FACSCanto II (*BD Bioscience*). Post-acquisition data analysis was carried out using FlowJo software.

2.2.6. Flow-Cytometry Assay of CNS Infiltrates

Single cell suspensions were blocked with Fc-Block (BioXCell) in FACS buffer and surface stained with the following monoclonal antibodies: CD4 (Biolegend), CD40L (eBioscience), CD44 (eBioscience), CD90.2 (eBioscience), TCRbeta (Biolegend), CD11b (eBioscience). Ly6C (BD), Ly6G (BD). To exclude dead cells, cells were also stained with the fixable viability dye ef780 (eBioscience). Cells were usually pregated for a lymphocyte gate, singlets and living cells. Samples were acquired with FACS Canto II.

2.3. Molecular Biology

2.3.1. RiboTag Technique

RiboTag experiments were performed as previously described (Sanz et al., 2009) using tissue from the lumbar region of the spinal cord or brain stem from RiboTagfl/wt/NFH-Cre mice at different time points after EAE induction (dpi 16 and dpi 30) or healthy control animals.

2.3.2. Quantitative Real Time Polymerase Chain Reaction (qPCR)

RNA was isolated by using the RNeasy Plus Micro Kit (*Qiagen*, 74034) according to the user manual. cDNA was synthesized out of 200–1,000 ng of RNA via SuperscriptII (*Invitrogen*). Quantitative real-time PCR for Hprt, Tubb3, Dcx, Gfap, Aspa and Itgam was performed using primers from *Qiagen* (http://www.qiagen.com/products/pcr/quantitect/primerassays.aspx) or self-designed primers (Dcx forward: 5'-cctctttcttctctttttatttgcctta-3'; Dcx reverse: 5'-ggaaccacagcaacttttccaa-3'). The expression is normalized to the housekeeping gene Hprt. Relative expression was normalized to Hprt and quantified with delta delta ct. The experiment was performed three times. Quantitative real-time PCR was measured in an AB StepOnePlus Real Time PCR "Thermocycler" (Life Technologies) with SYBR green (*Qiagen*).

2.3.3. Next Generation Sequencing (NGS)

NGS was performed in collaboration with the Genetic Institute of the University of Mainz with Illumina Sequencing. RNA was isolated with the RNeasy Micro Kit (Qiagen) according to the manufacturer's instructions from material of RiboTag experiments. RNA amounts were measured by Q-bit 2.0 fluorometer (Life Technologies) and the quality was assessed on a Bioanalyzer (Agilent) using a High Sensitivity Chip. Samples with a RNA integrity number (RIN) > 8 were used for library preparation with Sample Prep v2 Kit (Illumina) according to

the manufacturer's manual. Library size distribution was assessed on a Bioanalyzer 2100 using a High Sensitivity DNA Chip (Agilent). Sequencing was performed on an Illumina sequencer.

2.4. Bioinformatic Analysis

2.4.1. NGS Data Analysis

Quality control of the sequencing data (51 base pairs, single end, unstranded library preparation) was performed with the FastQC tool (available at http://www.bioinformatics.babraham.ac.uk), as well as the comprehensive Qorts suite. Inspecting the produced reports, all samples were deemed of good quality for further processing. Short reads alignment was performed with the ENSEMBL Mus_Musculus.GRCm38 chosen as the reference genome. The corresponding annotation (ENSEMBL v76) was also retrieved from the ENSEMBL FTP website (http://www.ensembl.org/info/data/ftp/index.html). The STAR aligner (version 2.4.0b) was used to perform mapping to the reference genome, resulting in 10.1 million uniquely mapped reads per sample (uniquely mapping rates: 88.1-90.3%). Subsequent analyses were performed with the R statistical software (version 3.5.0), leveraging core packages of the Bioconductor project. Alignments were processed with the featureCounts function of the Rsubread package, using the annotation file also used for supporting the alignment. Exploratory data analysis and functional annotation to Gene Ontology terms was performed with the pcaExplorer package. Principal component analysis (PCA) was performed using the 500 genes showing the highest variability across samples, with regularized logarithm (rlog) transformed expression values. Differential expression analysis was performed with the DESeq2 package (version 1.22.0), setting the False Discovery Rate to 0.05. Gene expression profiles were plotted as heatmaps (color-coded z-scores for the rlog transformed expression values) with the heatmap package.
The three contrasts between available conditions generated sets of 1778 (peak vs ctrl), 308 (recovery vs ctrl), and 1084 (peak vs recovery) DE genes respectively. MA plots show the comparisons of the two different EAE time points compared to healthy controls. The raw counts for the genes were first normalized by the size factor corresponding to each library size as in the DESeq normalization method and then for each gene a combination of M-A values (M = log2 fold change, A = average) was derived and plotted.

2.4.2. Data Analysis of qPCR and NGS with Statistics

Statistical analysis was performed with Prism Graph Pad (v.5.0b) and statistical environment R (v.3.5.0). The unpaired Student's t test was used and all bar graphs were represented as means ± SEM and statistical differences were determined using unpaired Student's t test indicated as follows: $*p < 0.05$; $**p < 0.01$; $***p < 0.001$. Biological replicates are used for standard error.

2.5. Histological Analysis and Immunohistochemistry

For vibratome sections, tissues were fixed overnight with 4% PFA, embedded in 2% agarose, and cut at 40 µm. The sections were stained with antibody to HMGCR (1:200, rabbit, Sigma-Aldrich), SMI32 (1:10000, mouse, Biolegend), GFAP (1:500, mouse, eBioscience), Iba1 (1:750, rabbit, Wako), MBP (1:500, rat, BioRad). Cy3 (1:500, anti-mouse IgG), Cy3 (1:500, anti-rat IgG), FITC (anti-rabbit IgG) and Alexa488 (1:200, anti-mouse)-labelled secondary antibodies were supplied by Sigma-Aldrich. To label neurons NeuroTrace from Thermo Fisher Scientific was used. Images were acquired with a Leica SP5 confocal microscope or an Olympus ix81 fluorescence microscope and further processed with ImageJ64 and Adobe Illustrator CS4.

3. Results

3.1. Isolation of Pure Neuronal RNA from Adult Mouse CNS

Isolation of neurons from adult mice is almost impossible due to the packed arrangement of CNS cells (mostly neurons, astrocytes, oligodendrocytes, NG2 cells and microglia) with strong cell-cell interactions. The wrapping of neuronal axons with myelin sheets is another fact contributing to the difficulty to isolate these cell types. Current methods used to isolate neurons from adult mice are based on the dissociation of CNS tissue resulting in a single cell suspension. The separation of fully intact neurons without destroying dendrites and axons is a major task for analysing them *in vivo*.

For this purpose, three different methods were tested to obtain neuronal RNA in the best quality and quantity for further analysis (Figure 3). Two of these methods relied on dissociation of CNS tissue and myelin removal. For the latter, two different methods were established. The first method is based on transgenic mice where neurons express eYFP, which makes it possible to isolate these neurons by fluorescent activated cell sorting (FACS) (Figure 3A). The second method did not require transgenic animals and was based on depletion of all non-neuronal cells by MACS separation (Figure 3B) (Berl et al., 2017). A third method called RiboTag was tested as well, which does not require isolation of neurons prior to isolation of neuronal RNA (Figure 3C). The RiboTag method requires specific RiboTag transgenic mice. These mice harbour a modified ribosomal protein L22 gene, which includes the sequence for an human influenza haemagglutinin (HA) -tag in an additional exon 4 at the end of the sequence. By crossing RiboTag mice to the neuronal specific NFH-Cre mouse line, the original exon 4 is removed and the modified one with the included HA-Tag is expressed, resulting in HA-tagged ribosomes specifically in neurons. Instead of CNS tissue dissociation using a papain kit and myelin removal, a Dounce and Homogenization buffer were used to separate and break up CNS cells. With the use of specific HA-Tag antibodies coupled to magnetic beads, neuronal ribosomes with incorporated RNA can be immunoprecipitated and separated from ribosomes and RNA of other cell types. This makes it redundant to isolate neurons before isolation of neuronal RNA for further analysis, which is normally the most harmful step in isolation of pure neuronal RNA. The next chapters describe the results of the tested methods with their advantages and disadvantages.

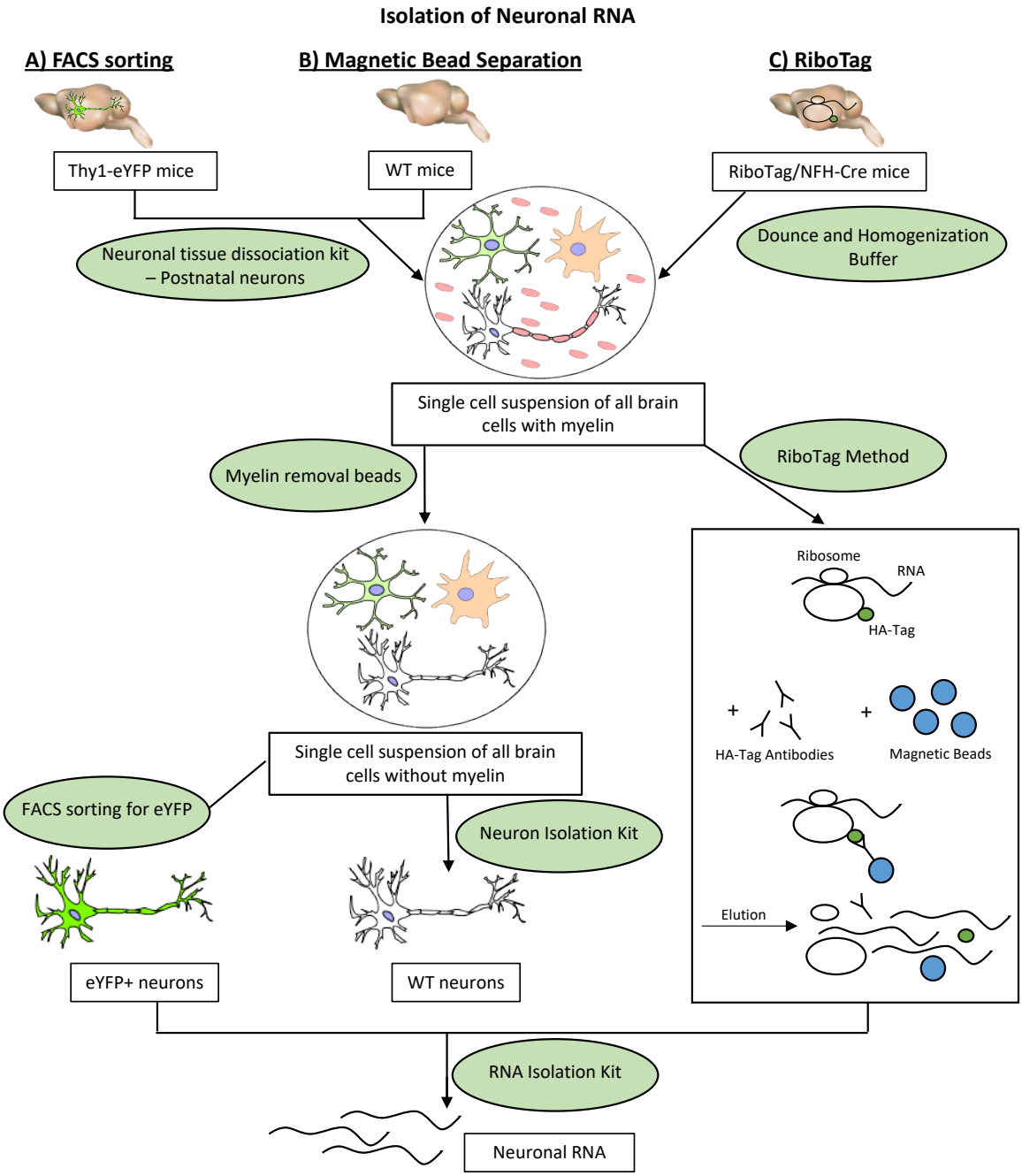

Figure 3: Overview of neuronal RNA isolation methods

For enrichment or isolation of neurons from adult mouse CNS three different methods were tested. For FACS isolation **(A)** and magnetic bead seperation **(B)** the tissue was dissociated with the Neural tissue dissociation Kit (*Miltenyi Biotec*). Myelin was removed from the single cell suspension by Myelin-Removal Beads (*Miltenyi Biotec*). eYFP^{+} Neurons could be further enriched by FACS sorting for eYFP. WT neurons could be isolated by the Neuron Isolation Kit (*Miltenyi Biotec*). For the RiboTag method **(C)** a Dounce and Homogenization buffer were used to obtain a single cell suspension. With the use of specific HA-Tag antibodies and magnetic beads neuronal ribosomes with incorporated RNA can be immunoprecipitated and separated from ribosomes of other cell types. For isolation of neuronal RNA for all three methods a RNA Isolation Kit was used (Adapted from (Berl et al., 2017)).

3.1.1. Enrichment of Adult Neurons by FACS Sorting

To isolate neurons by flow cytometry sorting, a mouse line expressing eYFP specifically in neurons, controlled by a murine Thy1.2 minigene, is used (Hirrlinger et al., 2005). This gives the opportunity to sort the $eYFP^+$ neurons based on eYFP expression without further fixation or manipulation of the neurons, which results in a higher yield and higher quality of isolated RNA which is highly necessary for RNA sequencing and high-throughput analysis of the neuronal RNA profile. After the use of the brain tissue dissociation with the kits of *Miltenyi Biotec* (Neural Tissue Dissociation Kit – Postnatal Neurons and Myelin-Removal Beads II) mentioned before, the cells were stained for the dead cell marker PO-PRO^{TM}-1 iodide to exclude dead neurons and the microglia marker CD11b to have a reference population. In the analysis 70-75% of the living cells were $eYFP^+$ and, as expected, negative for CD11b (Figure 4A). After this promising result, FACS sorting was used to isolate the $eYFP^+$ cells. From a single brain it was possible to sort between 6 x 10^6 to 13 x 10^6 $eYFP^+$ $CD11b^+$ cells. The reanalysis of these sorted cells confirmed that indeed over 95% of the sorted cells were $eYFP^+$. Analysis of the sorted $eYFP^+$ cells using intra-cellular staining for NeuN showed that only 65% of these cells expressed this neuronal marker, suggesting that not all $eYFP^+$ cells were neurons (Figure 4B). The RNA which was isolated from the $eYFP^+$ sorted cells was subsequently analysed for different marker genes of neurons and glial cells. The results showed that the neuronal marker Tubb3 (ß-III-tubulin) is enriched up to eight times compared to the sample of all brain cells before FACS sorting. Dcx (doublecortin), a marker for neuronal precursor cells, is enriched up to ten times compared to pre-FACS sorted cells. Non-neuronal markers for microglia, oligodendrocytes and astrocytes like Itgam (integrin alpha M/macrophage-1 antigen), Aspa (aspartoacylase) and Gfap (glial fibrillary acid protein) respectively, were still present, suggesting that not all glial cells could be excluded by FACS sorting (Figure 4C) (Berl et al., 2017).

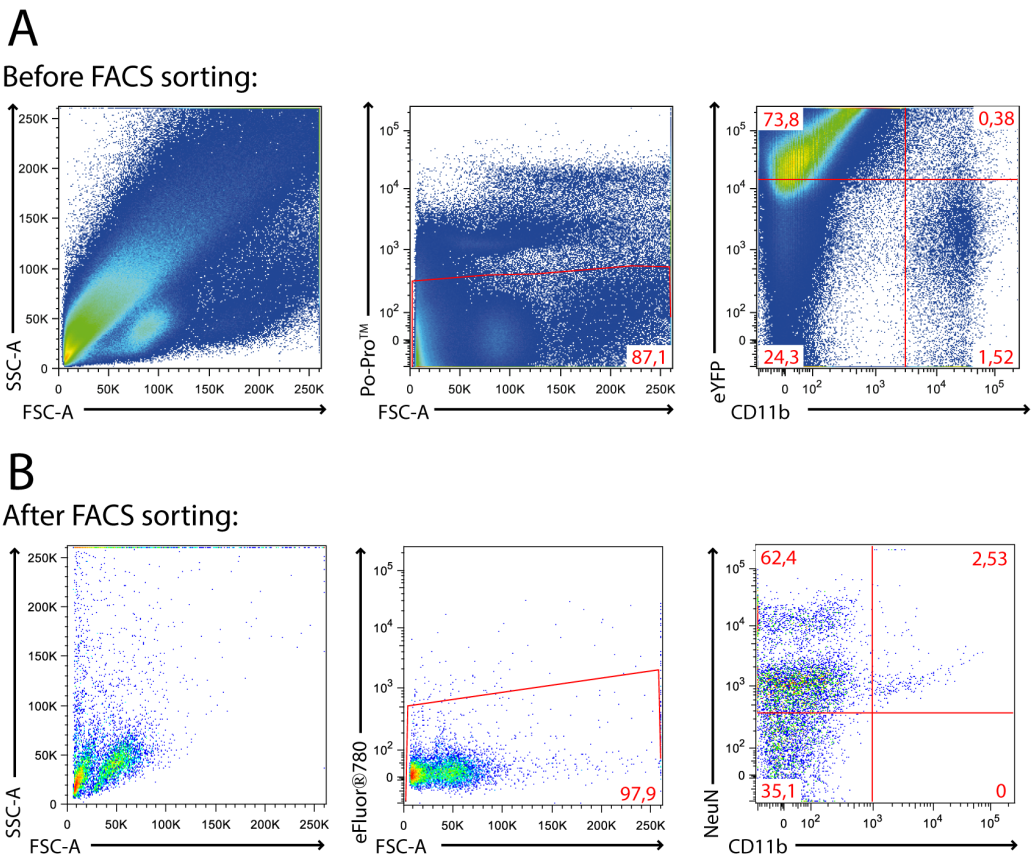

Figure 4: FACS sorting of adult neurons

A: The enrichment of neurons by FACS sorting is based on PO-PRO™-1 iodid staining and neuronal expression of eYFP.
B: Staining of sorted eYFP positive and CD11b negative cells reveals 62.4% NeuN positive fixable ViaDye eFluor®780 negative neurons.
C: qPCR data of enriched neurons shows increased expression of Tubb3 and significant increase of Dcx (p=0,008) compared to all brain cells relative to Hprt expression (N=3). Each experiments was performed three times. (Adapted from (Berl et al., 2017))

3.1.2. Depletion of Non-Neuronal Cells comes to Sparse Isolated Adult Neurons

The second method to isolate neurons is based on the depletion of all non-neuronal cells by MACS (magnetic cell sorting) technology. The big advantage of this method is that the procedure does not require transgenic animals like FACS sorting of $eYFP^+$ cells or the RiboTag method. After the first steps of dissociation of the brain and myelin removal, which are the same as in the first method, adult neurons are isolated by magnetic depletion of all non-neuronal cells. We established a protocol for the adult mouse brain based on the protocol of the kit for isolation of postnatal neurons (Neuron Isolation Kit, *Miltenyi Biotec*). Since the brain cells of postnatal mice are not as packed and do not form as many cell-cell interactions as the brain of adult mice, the isolation with this method is already well stablished. Isolation of up to 5×10^4 neurons from a single adult mouse brain was possible by modifying the user manual (details in material and methods 2.2.4). Before depletion of all non-neuronal cells, up to 80% of cells were alive and out of those, 40-46% cells were $NeuN^+$ neurons and 17% were $CD11b^+$ microglia (Figure 5A). After isolation of neurons, the control population of $CD11b^+$ microglia, for determining contaminating non-neuronal cells, is no longer detectable, which proofs the adaption of the kit for adult mouse brain. From the resulting cells, over 86% out of living cells were $NeuN^+$ neurons (Figure 5B). Further analysis of the isolated RNA from these cells, showed a high enrichment of both neuronal markers Tubb3 (30-fold) and Dcx (60-fold) concurrently with a coincidentally nearly complete absence of tested glial markers such as Itgam, Aspa and Gfap, representing microglia, oligodendrocytes and astrocytes (Figure 5C). With the improved protocol based on the neuron isolation from P7 mice, it is possible to isolate a highly pure population of 5×10^4 neurons from a single mouse brain. This indeed is too little for our purpose as we cannot be sure that those neurons being isolated represent the neurons, which are affected by immune cells during EAE.

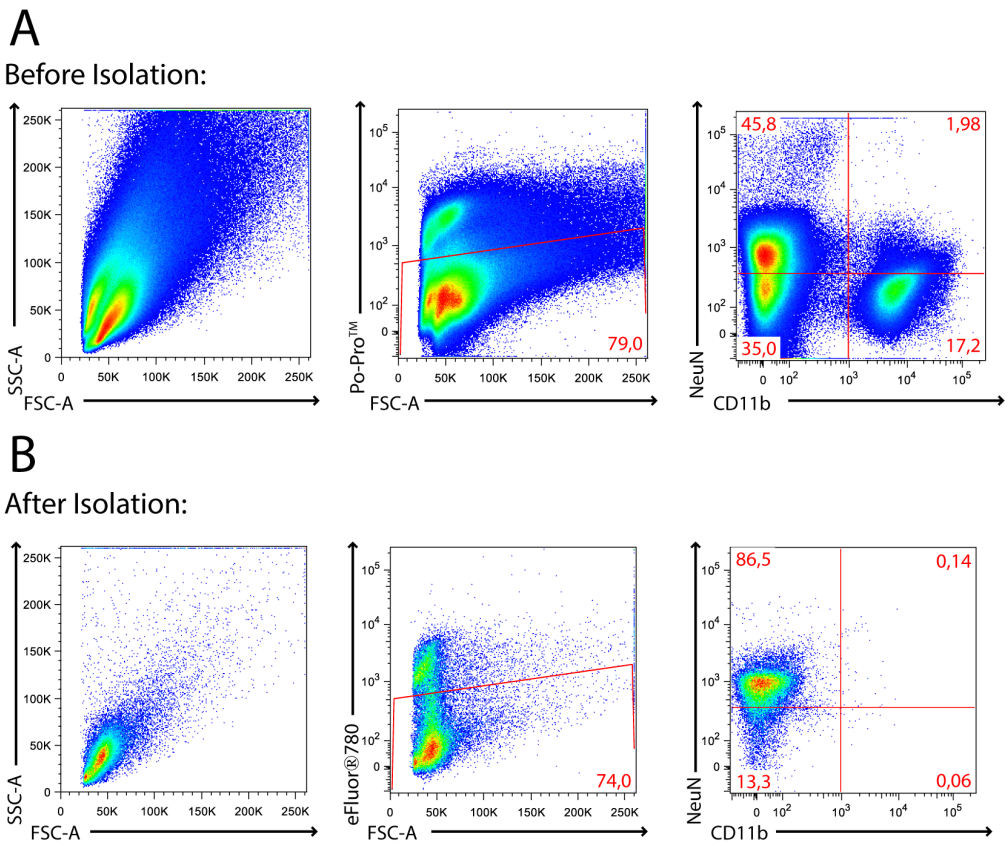

Figure 5: Isolation of neurons by depletion of non-neuronal cells

A+B: The Isolation of neurons to a purity ranging from 45.8% up to 86.5% out of living cells is based on depletion of non-neuronal cells by Neuron Isolation Kit (*Miltenyi Biotec*).
C: qPCR data of isolated neurons shows an significantly increase in Tubb3 (p=0,0006) and Dcx (p=0,0001) and an absence of glial marker compared to all brain cells relative to Hprt expression. Experiments were repeated three times. (Adapted from (Berl et al., 2017))

3.1.3. RiboTag Method ensures Neuronal RNA in High Quality and Quantity

The third method to isolate pure neuronal RNA from adult mice is based on immunoprecipitation of HA-tagged ribosomes with incorporated RNA. With this procedure the most harmful step of dissociation of the neurons from other neurons or glial cells by which axons and dendrites mostly get damaged is abdicable. On the other hand, the use of specific RiboTag transgenic mice is necessary. With specific HA-Tag antibodies and magnetic beads HA-tagged neuronal ribosomes with incorporated RNA can be immunoprecipitated and easily separated from RNA of other cell types, without isolation of neurons before (Figure 6B). To guarantee the specificity of the HA-Tag, histology in the spinal cord lumbar region was performed, to show exclusive overlapping of the staining for HA-Tag and NeuN as neuronal marker. Staining of the identical HA-Tag antibody which is used for the immunoprecipitation only shows co-staining with the neuronal marker NeuN and absence in other non-neuronal cells in the spinal cord lumbar region (Figure 6C). The purity of neuronal RNA was also tested by quantitative real time PCR (qPCR) before further processing of mRNA for Next generation sequencing (NGS). It can be shown that the RiboTag method for isolation of neuronal RNA leads to an enrichment of the neuronal markers neurofilament heavy chain (Nefh) and neurofilament median chain (Nefm) and a total absence of glial markers, like Gfap for astrocytes, Itgam for microglia, Aspa for oligodendrocytes and Cspg4 for NG2 cells, compared to control RNA from total spinal cord lumbar region. This is not only true for healthy control mice, also in EAE mice the same results can be obtained (Figure 6D). This is the proof of principle for the isolation of pure neuronal RNA with the RiboTag method in healthy adult mice and mice afflicted with EAE.

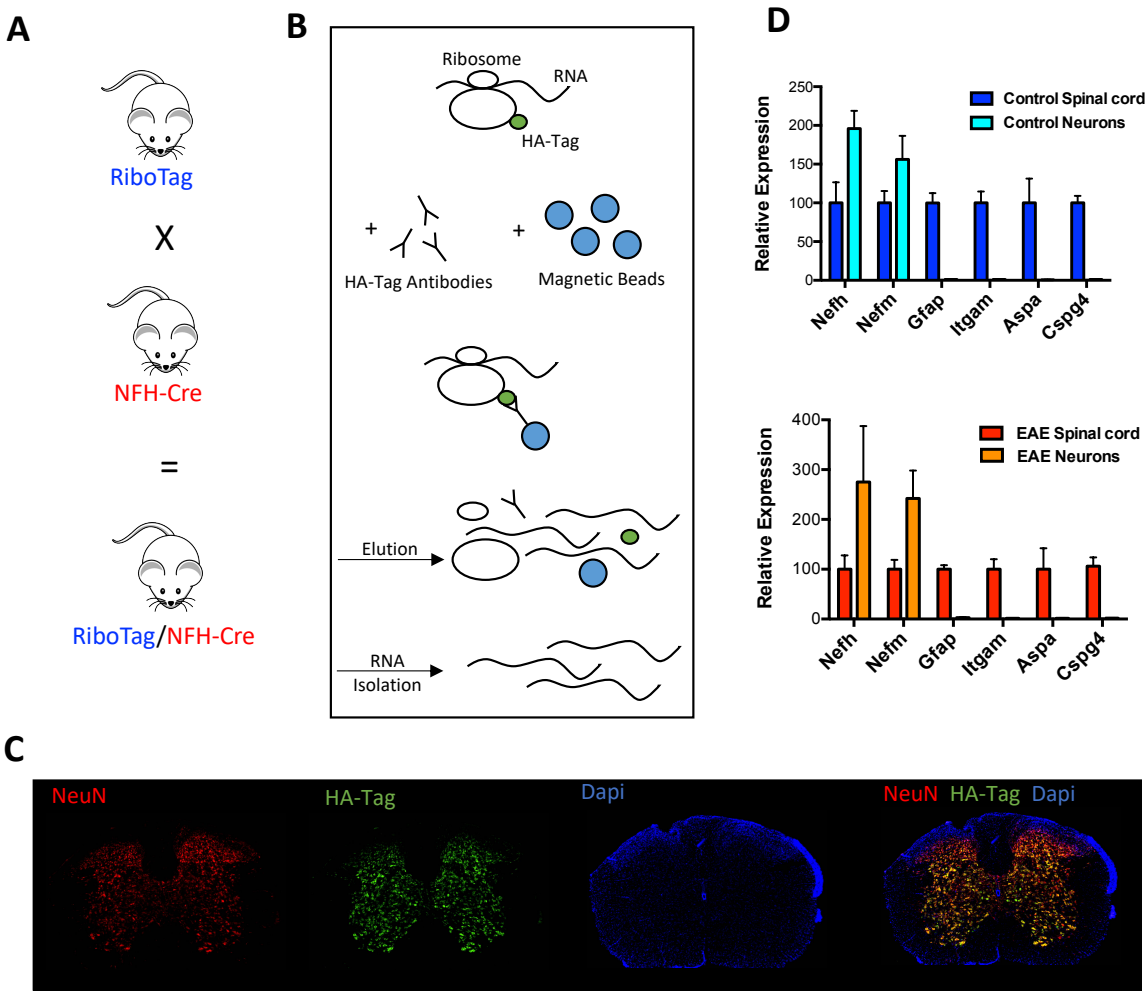

Figure 6: RiboTag method and RNA isolation from control, peak and EAE recovery

A: RiboTag mice are crossed to neuron specific NFH-Cre mice to obtain RiboTag/NFH-Cre mice with neuronal tagged ribosomes.
B: Neuronal HA-tagged ribosomes can be immunoprecipitated by the RiboTag method to obtain pure neuronal RNA.
C: Histological staining of the neuronal marker NeuN and HA-Tag together with Dapi proofs specificity of the HA-Tag to neurons in the lumbar region of the spinal cord by co-localization. Each experiment was repeated three times.
D: Analysis by qPCR shows an enrichment of neuronal markers *nefh* and *nefm* in the immunoprecipitated neuronal RNA compared to RNA from total spinal cord samples. Marker genes for astrocytes (*gfap*), microglia (*itgam*), oligodendrocytes (*aspa*) and NG2-cells (*cspg4*) are eliminated in the neuronal samples compared to total spinal cord controls. This is true for RNA from naive mice as well as for RNA from EAE mice (N=3).

3.2. High-Seq Analysis of Neuronal RNA during the Time Course of EAE

To unravel the neuronal response during the time course of EAE, EAE is induced. Mice show the first symptoms of EAE at day 10 post injection and further develop an ascending paralysis until they reach the peak of disease at day 16. Afterwards they start to recover until they reach a plateau level of disease but never recover completely (Stromnes and Goverman 2006). To study the time course of neuronal response during EAE, RNA of neurons at the peak of disease, neurons during the recovery phase and neurons from healthy control mice was isolated (Figure 7A+B). Only neurons of the lumbar region from the spinal cord were used for this study as immune cells start to invade the CNS early and numerous in this region (Ludowyk et al., 1992). Using different time points we were able to develop a time-line of neuronal response during EAE. A deep sequencing analysis using illumina sequencing was performed to identify differential expressed genes during the time course of EAE specifically in neurons. The sequencing data was analyzed as described in material and methods (2.4.1).

The PCA plot (principal components analysis) is constructed based on hierarchical clustering of the DE gene expression and shows the variance between the different samples according to the top 5000 expressed genes. The three different groups, control (red), peak (green) and recovery (blue) show the expected distribution and variance for this kind of approach and sequencing showing the triplicates clustering closer together then the different groups (Figure 7C). The heat map of the top 250 differentially expressed genes nicely clarifies that the triplicates cluster according their experimental groups (control, peak and recovery). Each row represents one specific gene and the columns represent different samples. The shown values are normalized and standardized by each row to show variations across the different samples, whereas red represents upregulation and blue downregulation (Figure 7D). Comparison of the expression profiles of the different time points of EAE revealed higher numbers of differential expressed genes at the peak of EAE than during recovery of EAE, compared to control samples. Many of the differentially expressed genes during peak of disease are back to control level during the recovery phase. Comparatively less genes are differentially expressed only during recovery of EAE. This is especially represented by the volcano plots showing significant differential expressed genes with their adjusted P value (-log10 adjPVal) at peak or recovery relative to their expression level as fold change (logFC). Analysing the differential expressed genes in detail most of these genes at the peak of disease are up regulated whereas only a limited number of genes is down regulated (Figure 7E).

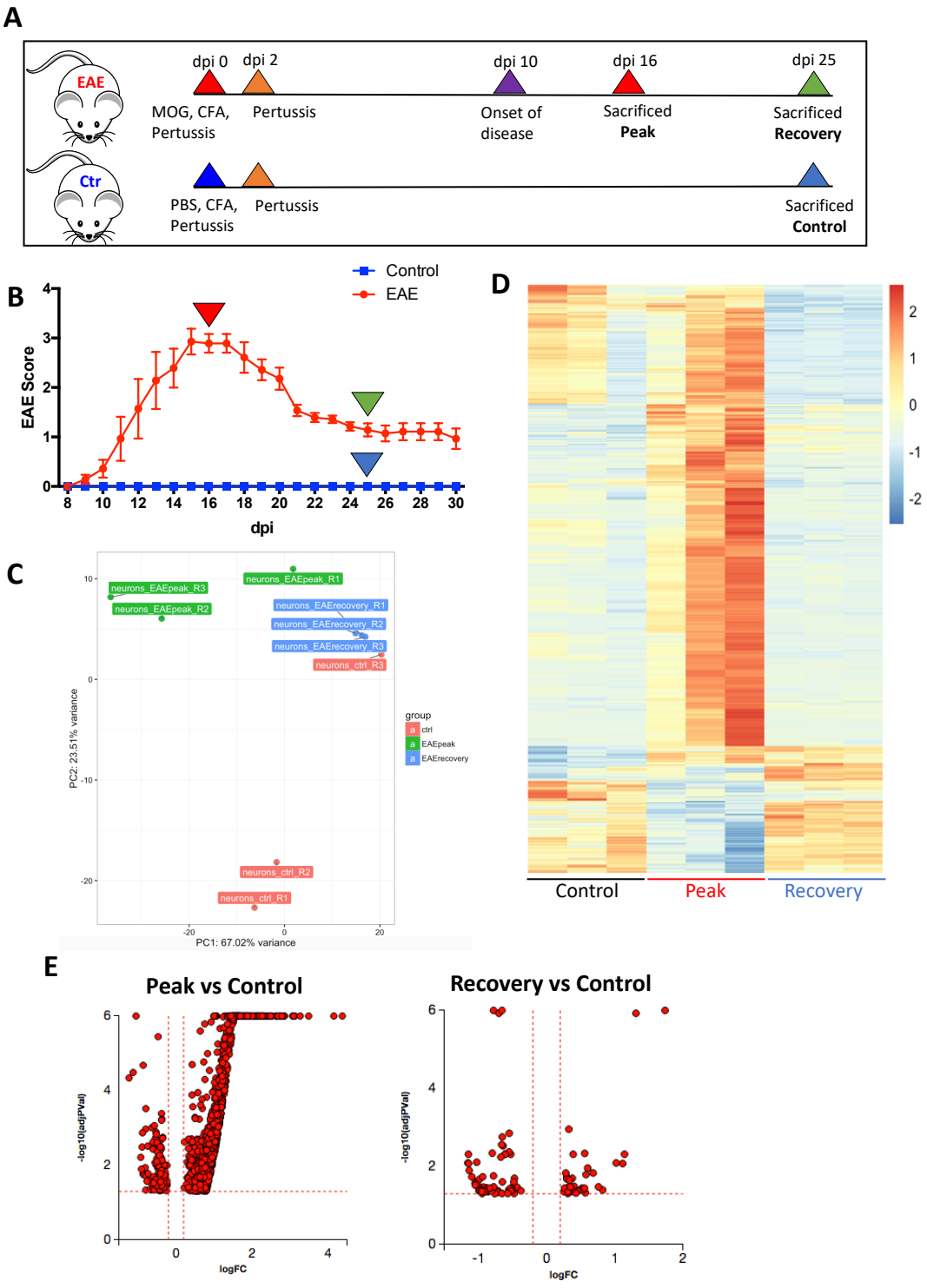

Figure 7: Sequencing analysis of neuronal RNA from control, EAE peak and EAE recovery

A+B: EAE is induced with MOG, CFA and Pertussis toxin and a second Pertussis injection on dpi 2, whereas control mice which are injected with PBS instead of MOG do not develop EAE. EAE mice have an onset of disease at day 10 and are either sacrificed at peak of disease on dpi 16 or in recovery phase together with control mice on dpi 25 (N=10). Sequencing was performed in triplicates for each experimental group.
C: The PCA plot (principal components analysis) shows the variance between the different samples according to the top 5000 expressed genes (N=3).
D: Heatmap of NGS data of most differential expressed neuronal genes shows a nice clustering of genes according to their experimental groups (control, peak and recovery), highlighting reproducibility of the experiment (N=3).
E: Volcano plots of significant differential expressed genes in Peak and Recovery compared to Control samples (N=3).

Meta-Analysis (Performed with iPathwayGuide https://apps.advaitabio.com/oauth-provider) revealed in total 1108 differentially expressed genes at the peak of EAE whereas only 113 genes show differential expression during recovery of EAE, and only 21 genes overlap significantly (Figure 8A). Neuronal gene expression of the different time points of EAE were validated by qPCR. Both experiments show similar results for the tested genes, which focused on highly differential expression at peak or during recovery of EAE. The genes *b2m* (beta-2-microglobulin), *h2-d1* (class I histocompatibility antigen D alpha chain), *stat1* (signal transducer and activator of transcription 1) and *apoe* (apolipoprotein E), which were highly up regulated in the sequencing data are also up regulated in the qPCR analysis. *Mapk4* (mitogen-activated protein kinase 4) which is one of the genes being down regulated at peak of disease shows the same result in qPCR analysis (Figure 8B+C). For recovery, the genes *hmgcs1* (3-hydroxy-3-methylglutaryl-CoA synthase 1), *dhcr24* (24-dehydrocholesterol reductase), *cyp51* (cytochrome P450 family 51) and *mvk* (mevalonate kinase) were significantly down regulated. This could be confirmed with the qPCR analysis as well (Figure 8D+E).

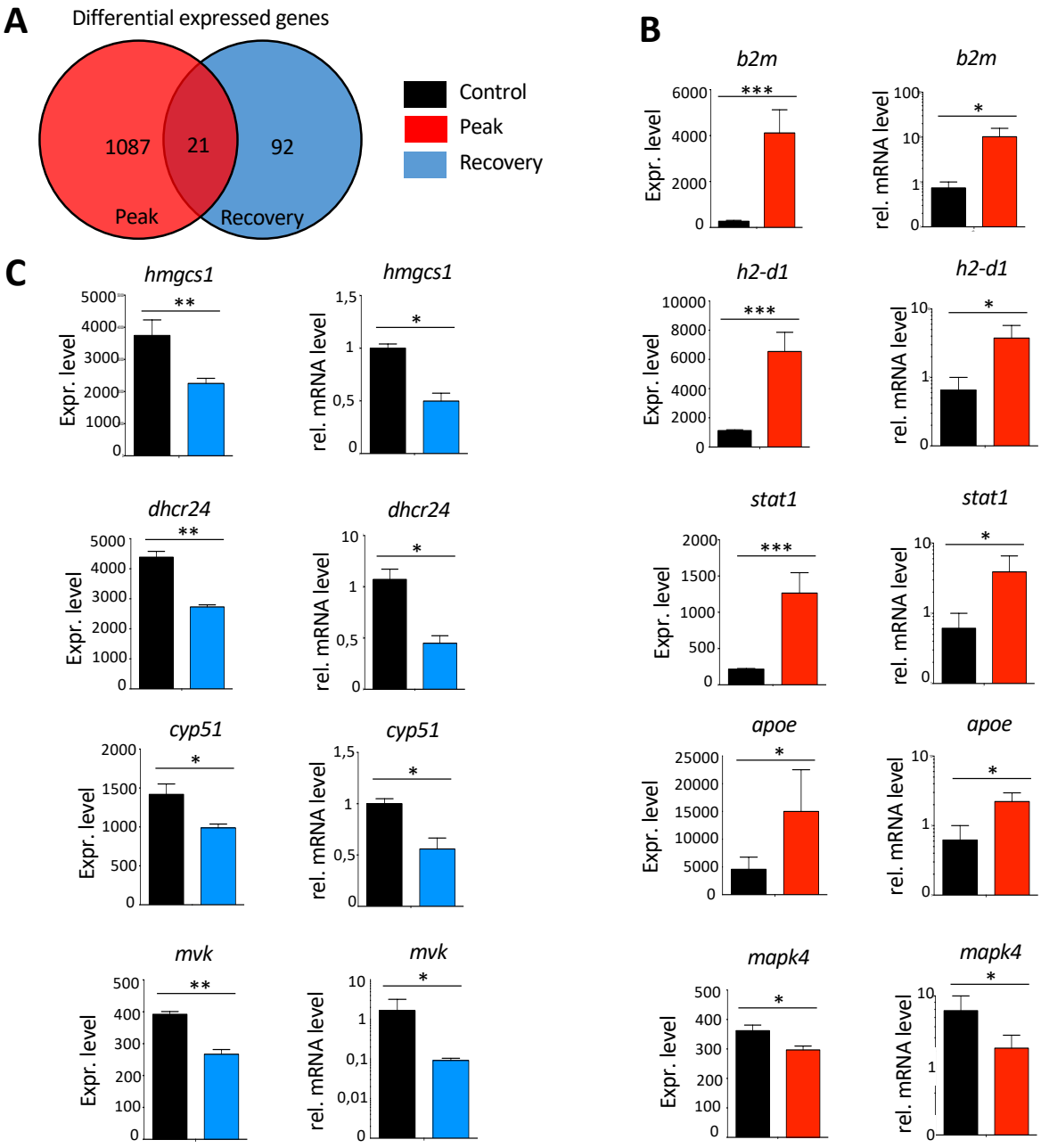

Figure 8: Validation of differential expressed genes in peak and recovery

A: Meta-Analysis of all differential expressed genes at peak and during recovery of EAE (according to iPathwayGuide).
B: Expression values (±SEM) of the differential expressed genes *b2m*, *h2-d1*, *stat1*, *apoe* and *mapk4* at EAE peak and qPCR validation (N=3).
C: Expression values (±SEM) of the differential expressed genes *hmgcs1, dhcr24, cyp51* and *mvk* during EAE recovery and qPCR validation (N=3).
Expression values and qPCR validation are shown in ±SEM, the statistical significance (unpaired Student's t test) is indicated as *$p < 0.05$, **$p < 0.01$, and ***$p < 0.001$ (N=3). Validation by qPCR was repeated three times.

3.3. Pathway Analysis and Selection of Candidate Genes

Performing a detailed pathway analysis the 1108 differentially expressed genes at peak of disease can be sorted to 114 different pathways. The 113 genes of the recovery fall into 30 different pathways. Only 6 pathways contain differential expressed genes at peak of EAE as well as during the recovery phase (Figure 9A). Different regulated pathways at the peak of disease compared to control are represented by red dots and outnumber by far the differentially expressed pathways during recovery, represented by blue dots. This points out that the regulation of neuronal response during EAE differs predominantly during the peak and is again more similar with minor changes in expression during recovery phase (Figure 9B).

For the peak of EAE the pathways of Phagosome, Lysosome, Hematopoietic cell lineage, Cell adhesion molecules, Primary immunodeficiency, Antigen processing and presentation, Ribosomes, Natural killer cell mediated cytotoxicity, Tuberculosis and Chemokine signaling pathway can be found. Recovery related top 10 pathways are Steroid (Cholesterol) biosynthesis, Metabolic pathways, Terpenoid backbone biosynthesis, Fatty acid metabolism, Renin secretion, Huntington`s disease, Pertussis, Insulin secretion, Alzheimer`s disease and Peroxisome. The genes of the top 10 differential expressed pathways for peak and recovery can be found in the table below (Figure 9C+D).

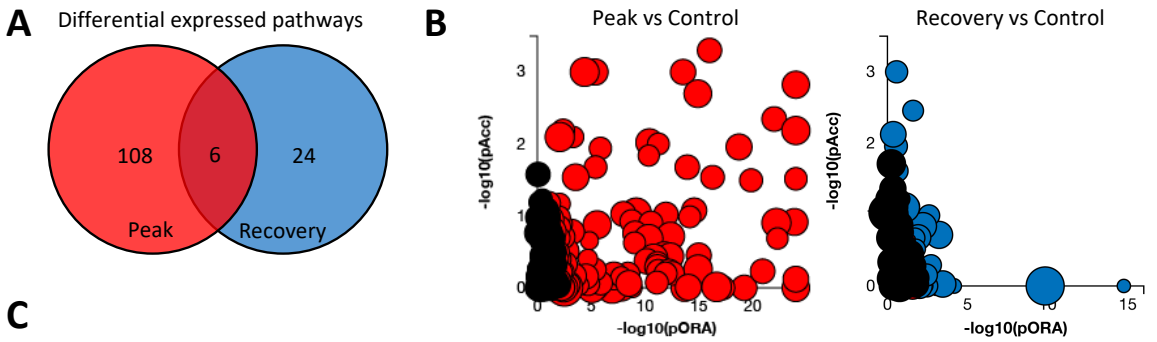

C

Pathway	Genes
Phagosome	Fcgr2b, Fcgr3, Fcgr1, H2-T23, H2-DMb1, H2-DMa, H2-T22, H2-Q7, H2-Q4, H2-D1, H2-K1, Ncf1, Ncf4, Itga5, Itgb2, Msr1, Tap1, Tlr2, H2-Q6, C1ra, Clec7a, Fcgr4, Tcirg1, Cyba, Ncf2, Cd36, H2-M3, Itgam, Tap2, C3, Tlr4, H2-M2, Atp6v0d2, Thbs1, H2-Oa, Olr1, Ctss, Tuba1c, Tubb6, Tuba1b, Coro1a, Itgb1, Ctsl, H2-DMb2, Atp6v1g1, Lamp2, Actb, Sec61b, Tlr6
Lysosome	Acp5, Ctsc, Cd68, Slc11a1, Tcirg1, Ctsb, Ctsd, Ctsz, Napsa, Ctsh, Gusb, Fuca1, Gns, Atp6v0d2, Hexa, Man2b1, Npc2, Ctss, Ap1g2, Naglu, Dnase2a, Asah1, Ctsl, Pla2g15, Hexb, Lgmn, Lamp2, Laptm5, Galns, Ctsw, Lipa, Ctsa, Psap
Hematopoietic cell lineage	Csf3r, Cd22, Fcgr1, Il7r, Itga5, Cd33, Csf2ra, Il4ra, Cd14, Cd36, Il1b, Itgam, Il3ra, Il1a, Itga4, Cd44, Cd3e, Csf1, Il6ra, Cd37, Tnf, Cd2, Cd3d, Cd5, Csf1r, Cd24a
Cell adhesion molecules (CAMs)	Cd86, Cd22, H2-T23, H2-DMb1, H2-DMa, H2-T22, H2-Q7, H2-Q4, H2-D1, H2-K1, Icam1, Itgb2, Itgb7, Sdc1, H2-Q6, Cd274, Siglec1, H2-M3, Itgam, Spn, H2-M2, Itga4, H2-Oa, Icos, Cd2, F11r, Itgb1, H2-DMb2, Cd40, Cd28, Pdcd1
Primary immunodeficiency	Il7r, Tap1, Jak3, Tap2, Lck, Blnk, Btk, Cd3e, Icos, CD40, ZAP70
Antigen processing and presentation	Ifi30, B2m, H2-T23, H2-DMb1, H2-DMa, H2-T22, H2-Q7, H2-Q4, H2-D1, H2-K1, Tapbp, Tap1, H2-Q6, Ctsb, H2-M3, Tap2, Psme1, H2-M2, H2-Oa, Ctss, Tnf, Ctsl, H2-DMb2, Lgmn, Psme2
Ribosome	Rpl41, Rps15, Rps4x, Rps14, Rps9, Rplp0, Rplp2, Rplp37a, Rps5, Rps25, Rps26, Rps20, Rpl36al, Rpl32, Rps19, Rpl7, Rpl13a, Rps11, Rpl22, Rpl23, Rplp1
Natural killer cell mediated cytotoxicity	Fcer1g, Ptpn6, H2-T23, H2-D1, H2-K1, Icam1, Itgb2, Rac2, Vav1, Tyrobp, Syk, Sh3bp2, Plcg2, Fcgr4, Lcp2,Cd48, Lat, Pik3r5, Lck, Ifgr1, Tnf, Cd244, Ptk2b, Ifnar2, Zap70, Cd247
Tuberculosis	Fcgr2b, Fcgr3, Fcgr1, Fcer1g, H2-DMb1, H2-DMa, Il10ra, Nos2, Itgb2, Itgax, Tgfb1, Syk, Stat1, Tlr2, Clec7a, Fcgr4, Tcirg1, Clec4e, Ctsd, Cd14, Il1b, Itgam, C3, Lsp1, Il1a, Casp8, Tlr4, Atp6v0d2, H2-Oa, Ifngr1, Tlr9, Ctss, Tnf, Tnfrsf1a, Irak4, Coro1a, H2-DMb2, Cebpb, Lamp2, Il10rb, Myd88, Apaf1, Malt1, Card9, Tlr6
Chemokine signaling pathway	Cxcl16, Ccr5, Ccr2, Ccr1, Fgr, Hck, Gngt2, Cxcl10, Ncf1, Ccl9, Ccl6, Ccl5, Rac2, Vav1, Stat2, Stat1, Dock2, Cxcr4, Lyn, Jak3, Plcb2, Rap1b, Cxcr6, Pik3r5, Adcy7, Plcb1, Ccl2, Ccr7, Prkcd, Stat3, Cxcl9, Elmo1, Ccl7, Ptk2b, Ccl12

D

Pathway	Genes
Steroid (Cholesterol) biosynthesis	Fdft1, Dhcr24, Sqle, Lss, Nsdhl, Cyp51, Dhcr7, Tm7sf2
Metabolic pathways	Fdtf1, Mvd, Dhcr24, Sqle, Lss, Mvk, Nsdhl, Hmgcr, Hmgcs1, Atp5h, Aldoc, Hsd11b1, Ndufv2, Uqcrh, Nme1, Mocs2, Cyp51, Fasn, Cmpk1, Ak1, Dhcr7, Gpt, Hprt, Tm7sf2
Terpenoid backbone biosynthesis	Mvd, Mvk, Hmgcr, Hmgcs1
Fatty acid metabolism	Fads1, Fads2, Fasn
Renin secretion	Adcyap1, Calm2
Huntington`s disease	Atp5h, Hip1, Ndufv2, Uqcrh, Sod1
Pertussis	Cfl2, Calm2, Jun
Insulin secretion	Adcyap1
Alzheimer`s disease	Atp5h, Ndufv2, Uqcrh, Grin2c, Calm2
Peroxisome	Mvk, Sod1, Hacl1

Figure 9: Pathway analysis of differential expressed genes at EAE peak and during EAE recovery

A: Meta-Analysis of all differential expressed genes distributed to their associated pathways at peak and during recovery of EAE (according to iPathwayGuide).
B: Dot plots representing differential expressed pathways in peak (significant in read) and recovery (significant in blue). The pathways are positioned by their total perturbation accumulation (pAcc) vs. a classical Over-representation analysis (pORA). The size of each dot denotes the total number of genes in the corresponding pathway (iPathwayGuide).
C: Top 10 differential expressed pathways at peak of disease compared to control.
D: Top 10 differential expressed pathways during recovery of EAE compared to control.

3.4. Upregulation of MHCI in Neurons at the Peak of EAE

After this deep pathway analysis we focused on potentially candidate genes to further analyze their role in neuronal response to EAE. The first group of genes which caught the attention were MHC class I genes (major histocompatibility complex). Those genes can be found in different pathways which all show a high upregulation at the peak of disease. MHCI genes play a role in 4 of the top 10 differentially expressed pathways at the peak of disease, represented by the yellow dots, namely Phagosome, Cell adhesion molecules, Antigen processing and presentation and Natural killer cell mediated cytotoxicity (Figure 10A). The function of MHCI molecules is to present peptides derived from the cytosol on the cell surface, so T cells can identify these peptides as "self" or "non-self" and eliminate infected cells and pathogens. Differential expressed genes of the process to load peptides on MHCI molecules and transport to their surface are shown in the pathway diagram of "Antigen processing and presentation" and described in detail in the introduction (1.5). Pathway analysis revealed that the genes for MHCI, B2M, Tapbp, Tap1/2 as well as PA28 and TNF-a are upregulated at the peak of disease in neurons (Figure 10B). The decision if a target cell is attacked and eliminated by CD8 T cells or NK cells, is mediated by various activating and inhibitory signals. Inhibitory receptors of NK cells, like Ly49A, Ly49C, Ly49G2 and Ly49I interact with different MHC class I types like H-2D^{b}, H-2D^{d}, H-2D^{k}, H-2K^{b} and H-2K^{d}. All genes for those inhibitory ligands are highly up regulated in neurons at the peak of EAE (Figure 10C).

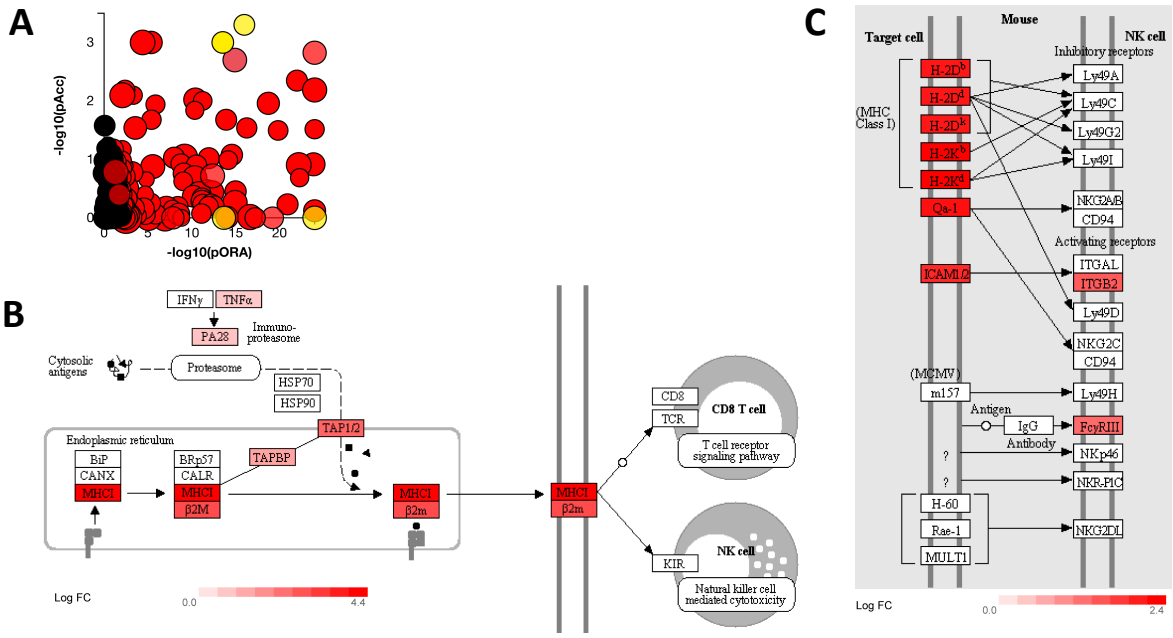

Figure 10: Antigen processing and presentation and Natural killer cell mediated cytotoxicity

A: Yellow dots of the dot plot represent the pathways „Phagosome“, „Cell adhesion molecules“, **„**Antigen processing and presentation“ and „Natural killer cell mediated cytotoxicity“.
B: The pathway diagram of Antigen processing and presentation shows an upregulation of MHCI genes and their interactions at the peak of EAE compared to the control group. The change in expression is illustrated in different shades of red, in a scale from 0 to 4.4 as log fold change (N=3).
C: The diagram provides a succinct representation of the interaction of upregulated MHCI genes in the pathways „Cell adhesion molecules“ and „Natural killer cell mediated cytotoxicity“ (adapted from iPathwayGuide). The scale indicates the log fold change from 0 to 2.4 of differentially expressed genes at the peak of disease compared to healthy controls (N=3).

3.5. The Role of PirB with MHCI Interaction in EAE

We focused on a neuron specific role of MHCI beside common antigen presentation. An essential role for the development of the nervous system is the binding of MHCI molecules to the PirB (immunoglobulin-like receptor B) receptor (Shatz, 2009; Syken et al., 2006) (Figure 11A).

The NGS data shows not only an upregulation of the different MHCI genes like *h2-d1* (p=0.001) and *b2m* (p=0.001), but also a significant enrichment of *pirb* (p=0.001), at the peak of EAE (red) compared to healthy control animals (black). The expression of all upregulated genes is back to control level when animals are in the recovery phase of EAE (blue) (Figure 11B).

To confirm that the upregulation of MHCI is not only true for the RNA level we did histology analysis to confirm the results on protein level. A staining of Tuj1 as a marker for neurons in combination with an antibody for H2-D1 (MHCI) together with Dapi was performed in the spinal cord lumbar region. Whereas in the control MHCI is hardly detectable due to low expression of the protein in neurons, the neurons in the spinal cord lumbar region highly upregulate MHCI on their surface at the peak of EAE. This confirms the finding of the sequencing data and points out the fact that also on protein level MHCI is highly increased at the peak of EAE (Figure 11C).

We picked PirB as one of our candidate genes to reveal its function in EAE by using knockout animals. In collaboration with the labs of Shatz and Steinman, EAE experiments with Camk2-Cre/PirB$^{fl/fl}$ mice (Bochner et al., 2014) and WT mice as controls were performed to identify a potential difference in the phenotype of the knockout animals. This Camk2-Cre/PirB$^{fl/fl}$ mice lack PirB not only in neurons, but also in some glial cells of the CNS, like astrocytes and microglia. Both groups developed the typical signs of EAE and were scored for 27 days after immunisation. Even though the WT mice started a bit earlier (day 8 instead of day 9) and developed slightly higher scores (A=2.5) compared to the knockout animals (A=2), none of this differences were significant (Figure 11D).

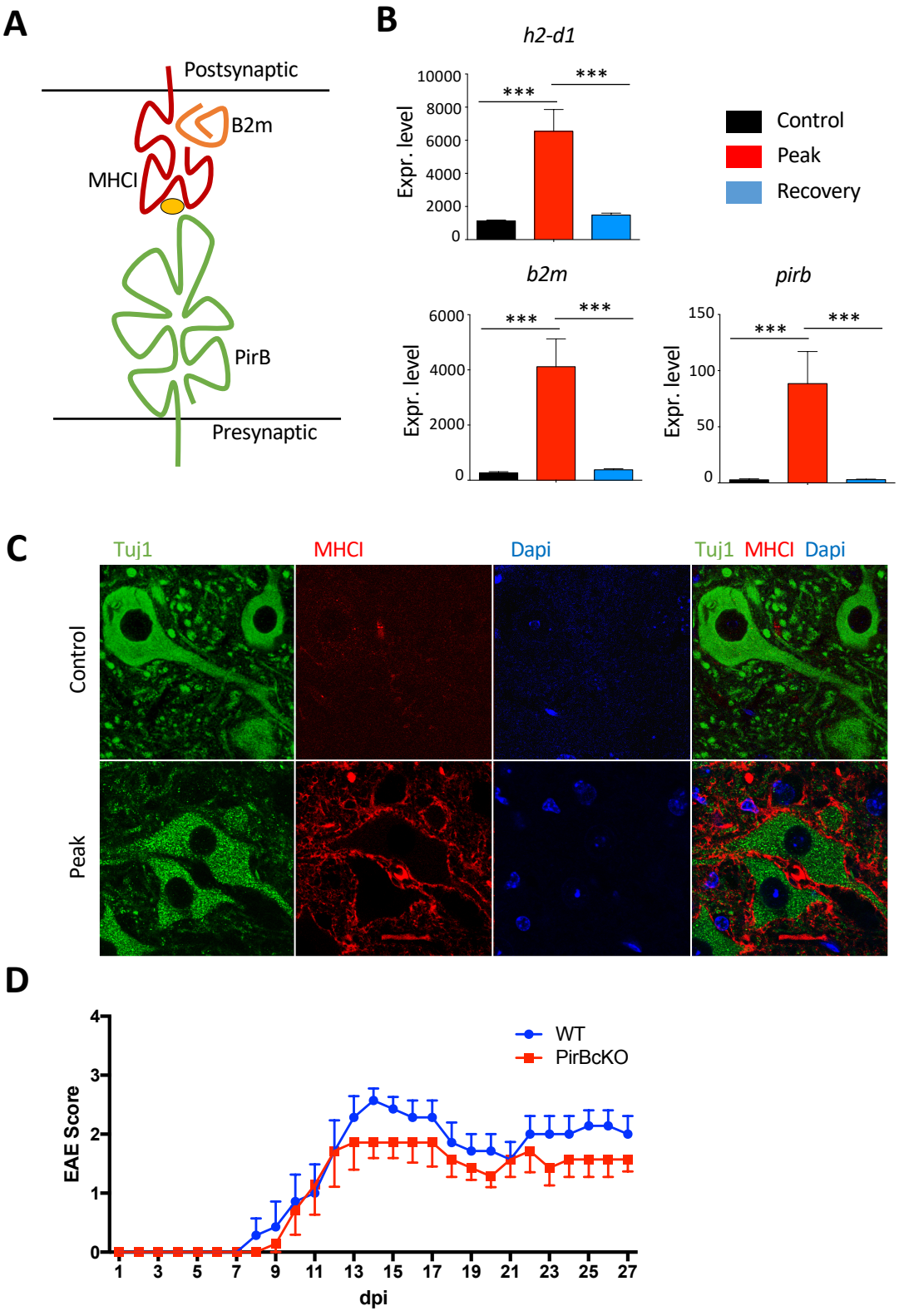

Figure 11: Knockout of PirB, the MHCI interaction partner, does not cause a phenotype in EAE

A: H2-D1 (MHCI) with B2m on the postsynaptic neuron interacts with PirB on the postsynaptic side of the neuron (Adapted from Shatz et al.,2009).
B: Expression level of the genes *h2-d1, b2m* and *pirb* in control, peak and recovery of EAE. ***p < 0.001 (N=3).
C: Histological staining of MHCI, the neuronal marker Tuj1 and Dapi. MHCI is highly upregulated at the surface of neurons at the Peak of EAE compared to control. The experiments was repeated three times.
D: EAE with PirB cKO mice compared to WT mice show a slightly less severe phenotype during EAE, but not to a significant extent (N=7).

3.6. Upregulation of IFNγR1 and Downstream Pathways at Peak of EAE

As it is already known that cytokines produced by immune cells as well as CNS cells play one of the major roles in cell damage during EAE we also examined cytokines and their receptors. One gene which got our attention was IFNγR1 with the downstream pathway of JAK-STAT signalling, due to high upregulation at the peak of EAE (Figure 12A). In neurons, IFNγR1 can interact with GluR1, a subunit of the AMPA receptor, leading to calcium influx to the neuron as well as inducing of the JAK/STAT pathway (Mizuno et al., 2008) (Figure 12B). After binding of IFNγ to the IFNγ-receptor, a cascade including several enzymes is induced, leading to proliferation and differentiation as well as cell survival. The downstream pathway of IFNγ signalling is described in detail in the introduction (1.4) (Figure 12C).

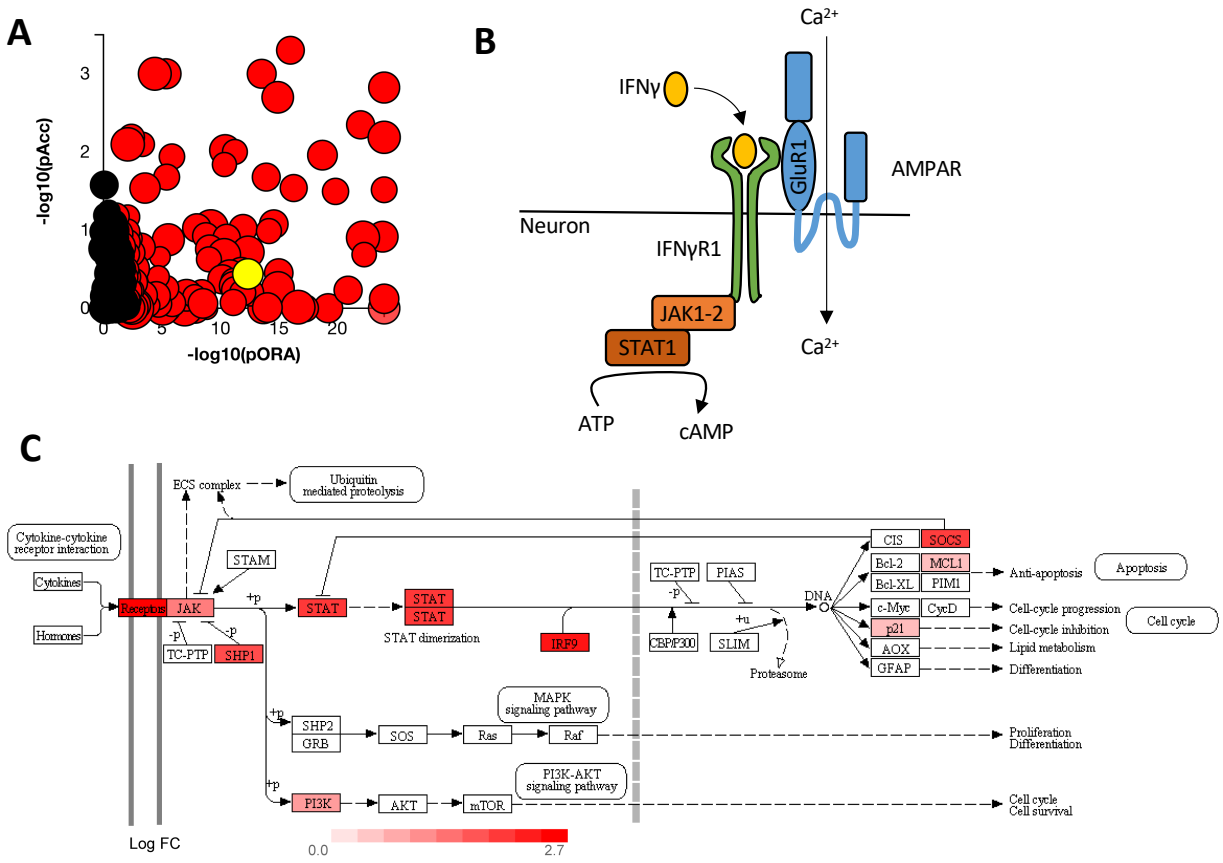

Figure 12:Upregulation of IFNγR1 and JAK-STAT pathway in neurons during EAE

A: Position of the JAK-STAT Pathway (yellow) in the distribution of differential regulated pathway at the peak of EAE compared to control animals.
B: By binding of IFNγ, the IFNγR1 on the neuronal surface can interact with the neuronal GluR1 subunit of the AMPAR receptor causing an CA^{2+} influx as well as the activation of the JAK-STAT pathway (Adapted from (Mizuno et al., 2008)).
C: Pathway diagram of the JAK-STAT Pathway with significant upregulated genes in neurons at peak of EAE. Upregulation indicated by scale in log FC from 0 to 2.7 (N=3) (Adapted from iPathwayGuide).

Analyzing the NGS data focusing on IFNγ and the downstream JAK/STAT pathway, we found *ifnγr1* (p=0.05), *stat1* (p=0.001) and *jak2* (p=0.05) significantly up regulated, at the peak of disease (red) whereas *ifnγr2*, *glur1* and *jak1* are expressed but not differentially regulated during EAE compared to healthy control animals (black). During recovery phase all differential expressed genes in this pathway are back to control levels of expression (blue) (Figure 13A). To confirm the differential expression of *ifnγr1* by sequencing, histology with antibody staining was performed. A staining of anti-IFNγR1 and anti-Tuj1, as a neuronal marker, together with nucleus labelling (Dapi) in spinal cord lumbar region in animals at the peak of disease were compared to healthy control animals. The results show a clear enrichment of IFNγR1 staining at the peak of disease. IFNγR1 labelling in neurons is exclusively recognized at the surface prominently on large motor neurons (Figure13B). Also other cells like astrocytes, microglia and oligodendrocytes upregulate their expression of IFNγR1, which can be seen by IFNγR1 positive but Tuj1 negative cells (Ding et al., 2015). With the confirmation of differential expression also on protein level the decision was made to knockout the gene of IFNγR1 specifically in neurons to study its role in neurons during EAE. For this purpose, The neuron specific NFH-Cre mice were crossed to IFNγR1$^{fl/fl}$ mice (C57BL/6N-Ifngr1tm1.1Rds/J; JacksonLaboratory) to obtain IFNγR1$^{fl/fl}$/NFH-Cre mice which lack IFNγR1 specifically in neurons (Figure 13C). We used IFNγR1$^{fl/fl}$/NFH-Cre mice and littermate IFNγR1$^{fl/fl}$ mice as Cre-negative controls to induce EAE and followed the disease progression for 30 days. In the investigated period we could not detect any significant phenotype of this mice according to EAE clinical scores (Figure 13D).

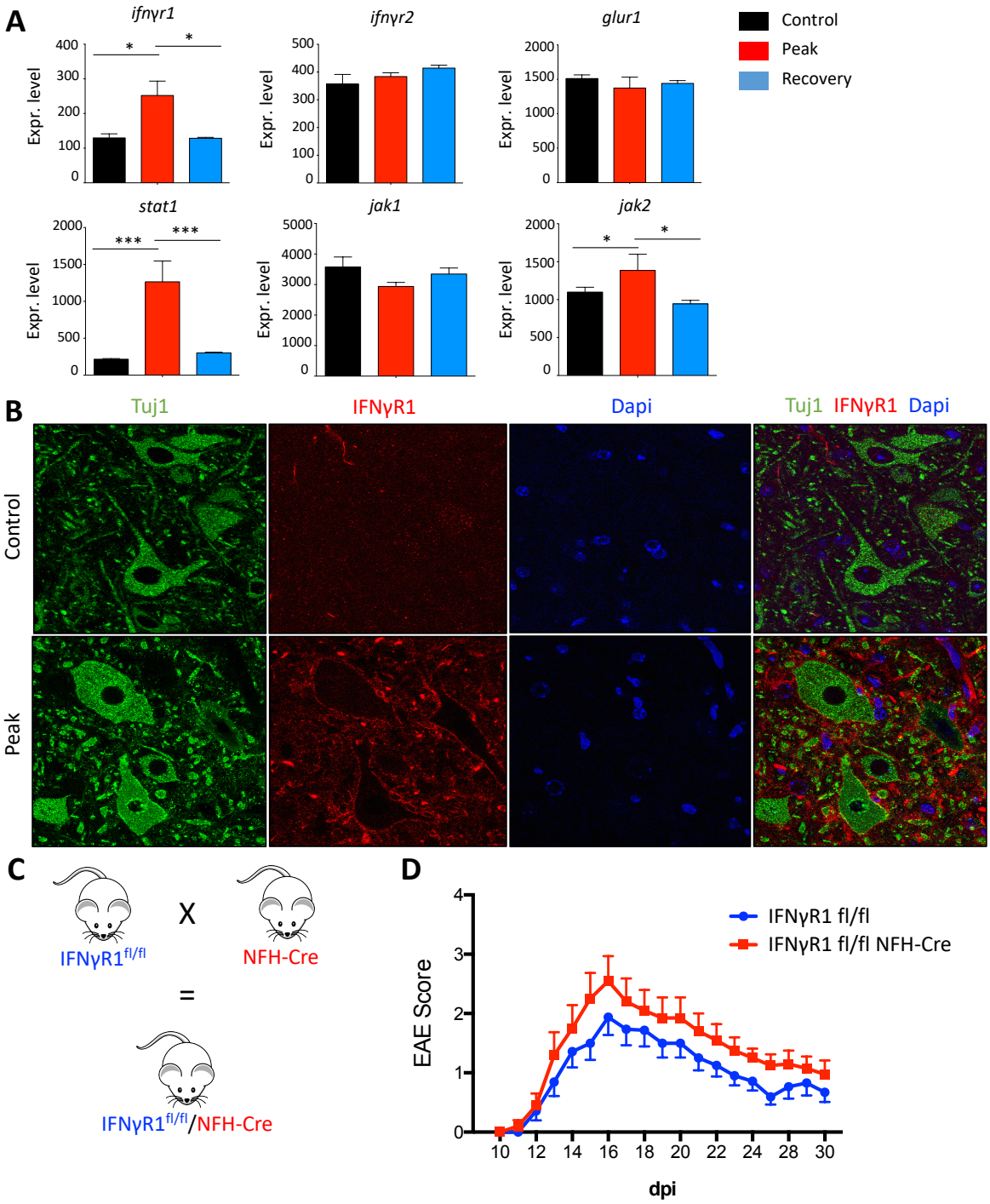

Figure 13: Neuronal KO of IFγR1 does not cause an altered phenotype in EAE

A: Gene expression of *ifnγr1, ifnγr2, glur1, stat1, jak1* and *jak2* during the time course of EAE. Whereas *ifnγr2, glur1* and *jak1 do not show a differential expression, ifnγr1, stat1* and *jak2* are significantly upregulated at peak of disease and back to control level during recovery phase. Statistical significance (unpaired Student's t test) is indicated as *p < 0.05, **p < 0.01, and ***p < 0.001 (N=3).
B: Histological co-staining of the neuronal marker Tuj1 and IFNγR1 show an upregulation of IFNγR1 on the neuronal surface at peak of disease compared to naive control animals. The experiment was repeated three times and performed with biological triplicates.
C: IFNγR1$^{fl/fl}$ mice are crossed to NFH-Cre mice to receive experimental IFNγR1$^{fl/fl}$/NFH-Cre mice.
D: IFNγR1$^{fl/fl}$/NFH-Cre mice do not show any significant phenotype in EAE compared to littermate IFNγR1$^{fl/fl}$ control mice (N=8).

3.7. IL17RA is Upregulated in Neurons during Peak of Disease

Another important pathway, which is not one of the top 10 effected pathways, but still from high interest for EAE, is the cytokine – cytokine-receptor interaction pathways (Figure 14A). Il17A and Il17F can bind as homo- or heterodimers to the IL17 receptor, which in the CNS consists of two subunits, IL17RA and IL17RC. Other forms, like IL17RB and IL17RE, appeared to be not expressed in the sequence data (Figure 14B). Whereas the gene for IL17RC seems to be only slightly upregulated at the peak of disease, the IL17RA gene is significantly upregulated at the peak ($p=0.04$), compared to control mice. During the recovery phase of EAE the expression values of the IL17RA gene are back to control levels ($p=0.01$) (Figure 14C).
These promising results lead to the decision to further study the role of IL17 and its receptor in neurons during EAE. Therefor a neuron specific knockout of IL17RA was created by crossing $IL17RA^{fl/fl}$ mice to the neuron specific NFH-Cre mice, resulting in the $IL17RA^{fl/fl}$/NFH-Cre knockout mice and $IL17RA^{fl/fl}$ littermate controls which are NFH-Cre negative (Figure 14D). These mice were used for EAE experiments to unravel potential effects of the IL17RA knockout specifically in neurons. The $IL17RA^{fl/fl}$/NFH-Cre mice showed the first signs of EAE similar to their littermate controls but develop slightly higher clinical scores compared to the control animals, especially in the beginning logarithmic phase of EAE. But overall the EAE experiments did not show significant differences between the different genotypes of mice for IL17RA, even if the scores are slightly lower in the knockout it is not consistent enough to take further conclusions (Figure 14E).

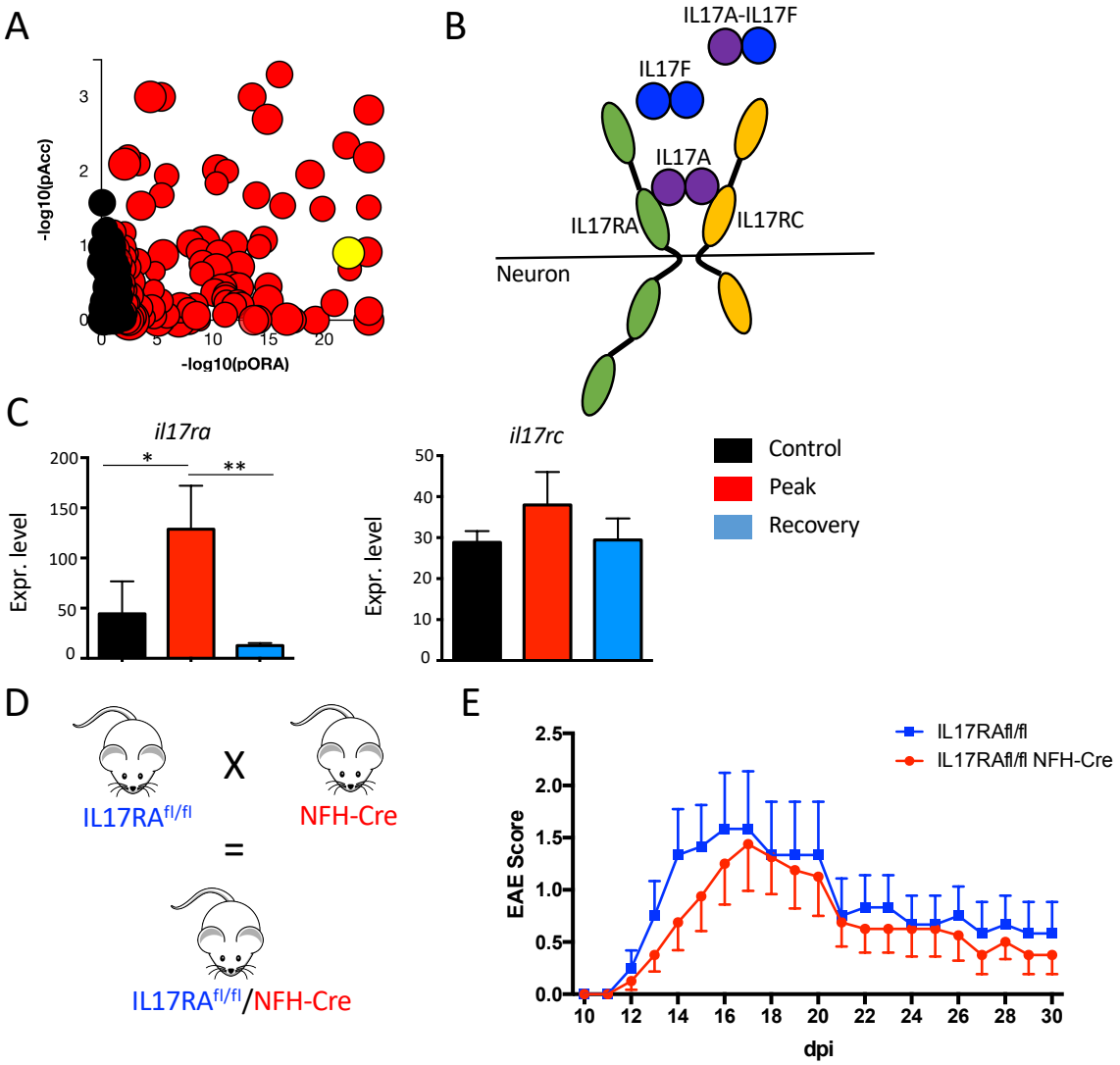

Figure 14: IL17RA is upregulated during peak of disease but has no influence on EAE itself

A: Pathway analysis shows that cytokine – cytokine receptor interactions (yellow dot) are differentially expressed during the peak of EAE, illustrated in the distribution dot plot (iPathwayGuide).
B: IL17A can bind as homo- or heterodimer with IL17F to the IL17R, in neurons only the subunits IL17RA and IL17RC are expressed (Adapted from (Amatya et al., 2017)).
C: IL17RA is significant upregulated during peak of disease (p=0,04/p=0,001) in neurons of the spinal cord lumbar region. Expression values are back to control level during recovery phase of EAE. The IL17RC is expressed in neurons but not significant differentially expressed in the time course of EAE (N=3).
D: IL17RA knockout mice specifically in neurons are created by crossing IL17RA$^{fl/fl}$ mice to NFH-Cre mice.
E: EAE of IL17RA$^{fl/fl}$ mice and IL17RA$^{fl/fl}$ NFH-Cre mice do not show a significant difference, also the knockout mice have the tendency to a less severe EAE in the logarithmic phase of EAE from day 12 to day 16 at the peak of disease (N=14). The EAE experiment was repeated three times.

3.8. Downregulation of Cholesterol Biosynthesis during Recovery of EAE

Two of the most affected pathways we found during recovery of EAE are the mevalonate pathway and the cholesterol biosynthesis (Figure 15A). As described in the introduction (1.7), those pathways include many enzymes and are important to produce cholesterol and other steroid hormones (Waterham, 2006) (Figure B). Focussing on genes involved in the mevalonate pathway and the cholesterol biosynthesis it is conspicuous that the majority of all genes are downregulated already at peak of disease, but even more and also significant during recovery of EAE. Following genes are significantly downregulated during recovery phase: *hmgcs1, hmgcr, mvk, mvd, fdft1, sqle, lss, cyp51, tm7sf2, nsdhl, dhcr24 and dhcr7* (Figure 15C). This is not only true for the lumbar region of the spinal cord, but also for the brain stem of mice at the peak of disease and during recovery. For *hmgcs1,cyp51, dhcr24 and sqle* we saw the same tendency, although it was not significant. But this might be due to the different composition of neuronal types in the brain stem compared to the spinal cord lumbar region and different amount of invading immune cells.

The 3-hydroxy-3-methylglutaryl coenzyme A (HMG-CoA) reductase (HMGCR) is an endoplasmatic reticulum residing enzyme, which catalyses the rate-limiting step of cholesterol biosynthesis within the mevalonate pathway. It catalyses HMG-CoA conversion to mevalonate. We picked this gene as one of our candidate genes to further analysis to study its role in neurons during EAE to unravel the role of the mevalonate pathway and cholesterol biosynthesis. As the next step we examined if the RNA data we found by deep-sequencing can be mirrored on protein level. We performed a staining of HMGCR and NeuN in the lumbar region of the spinal cord in healthy control animals in comparison to miceat the peak and in the recovery phase of EAE. We found that also on protein level HMGCR can be found in the motor neurons of control animals but is almost absent in neurons of the same region during recovery but no difference can be seen at the peak of EAE (Figure 15D). This proofs that the differential expression is not only present on mRNA level but rather also present on protein level, which means that it is translational relevant and points out the importance of the role of HMGCR in neurons during the recovery phase of EAE.

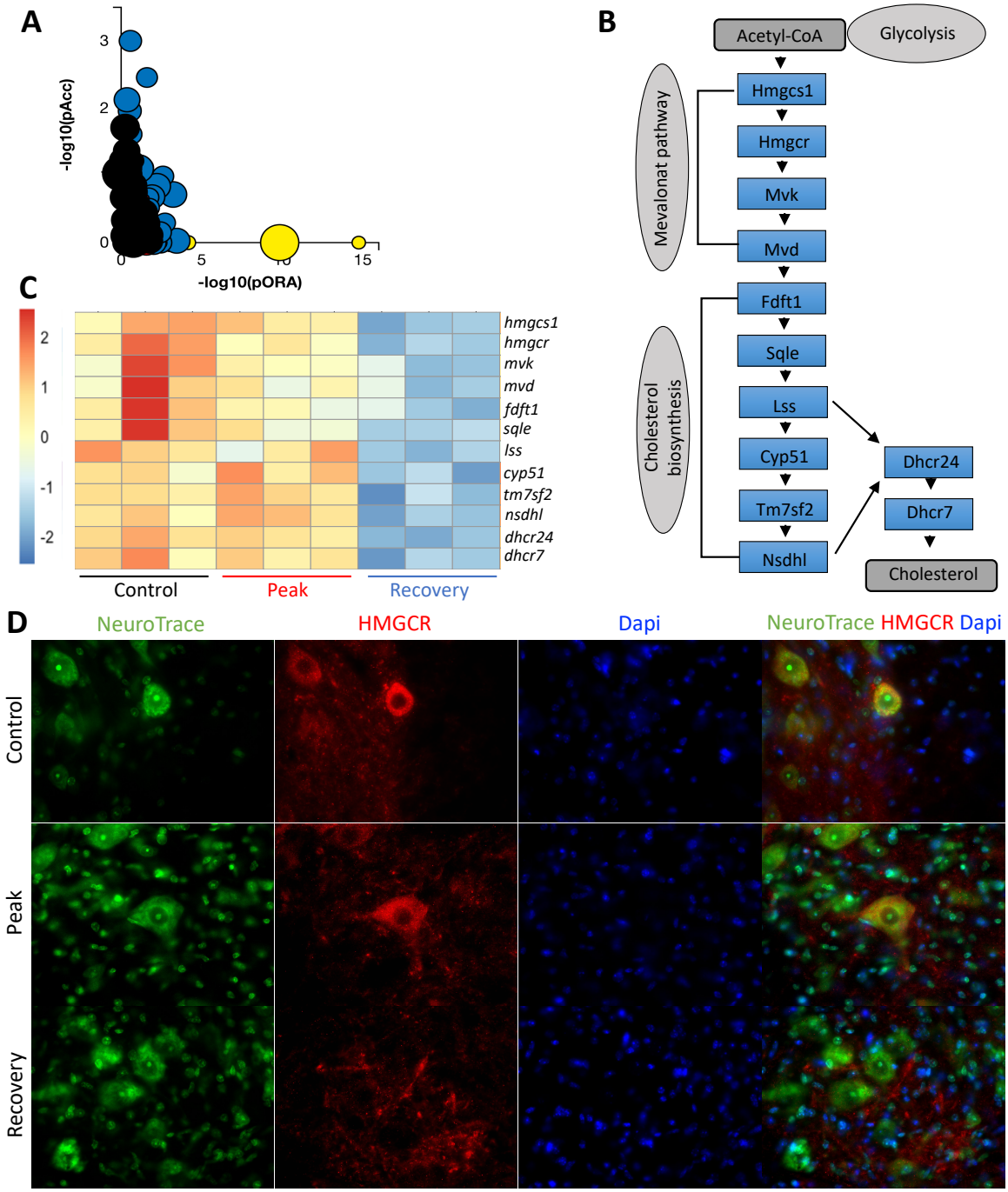

Figure 15: Downregulation of Cholesterol biosynthesis during recovery of EAE

A: Cholesterol biosynthesis, Metabolic pathways and Terpenoid backbone synthesis (indicated by yellow dots) are highly downregulated in neurons during recovery of EAE illustrated in the distribution dot plot n comparison to healthy controls (iPathwayGuide).
B: Mevalonate pathway and Cholesterol biosynthesis with involved genes show the transmission from Acetyl-CoA to Cholesterol.
C: Gene profile of significant differential expressed genes involved in the Mevalonate Pathway and Cholesterol biosynthesis during the time course of EAE in the three experimental groups Control, Peak and Recovery. Upregulation and downregulation are illustrated in red and blue respectively (N=3).
D: Histology shows the staining of NeuroTrace and HMGCR with Dapi. Downregulation of neuronal HMGCR on protein level occurs only during recovery, but not at the peak of EAE. Experiments were performed in triplicates and repeated three times.

3.9. Neuron Specific Heterozygous HMGCR Knockout Mice

To study the role of HMGCR specifically in neurons during EAE a knockout mouse was created. As total knockout of HMGCR in neurons ($HMGCR^{fl/fl}$/NFH-Cre) turned out to be embryonic lethal, a heterozygous neuron specific knockout for HMGCR was used. By crossing $HMGCR^{fl/fl}$ mice with the neuron specific NFH-Cre mouse line, $HMGCR^{fl/wt}$/NFH-Cre can be generated (Figure 16A). $HMGCR^{fl/wt}$/NFH-Cre mice are born healthy and with no observable phenotype. By eye they cannot be distinguished from their $HMGCR^{fl/wt}$ littermates, which are NFH-Cre negative (Figure 16B). They develop and grow normally and do not show any obvious differences in behaviour which could be a hind for neurological deficits or disorders, neither in young age nor as adult mice. Within the observed time frame of 6 months the mice develop and behave like their NFH-Cre negative littermates. Illustrated in the graph, the genotypes of the born mice in percentage show a distribution of 1/3 instead of 1/4 according to Mendelian genetics, confirming the embryonic lethality of the forth genotype. To evaluate the result of the heterozygous knockout of HMGCR on the protein level we performed histological antibody staining for HMGCR together with NeuroTrace, labelling all neurons, and Dapi. We found that probes from $HMGCR^{fl/wt}$/NFH-Cre mice show a reduced staining of HMGCR in neurons compared to $HMGCR^{fl/wt}$ controls in steady-state, confirming that the heterozygous knockout of HMGCR is relevant on protein level too, but does not have any obvious effects on the phenotype of the mice in steady-state (Figure 16C).

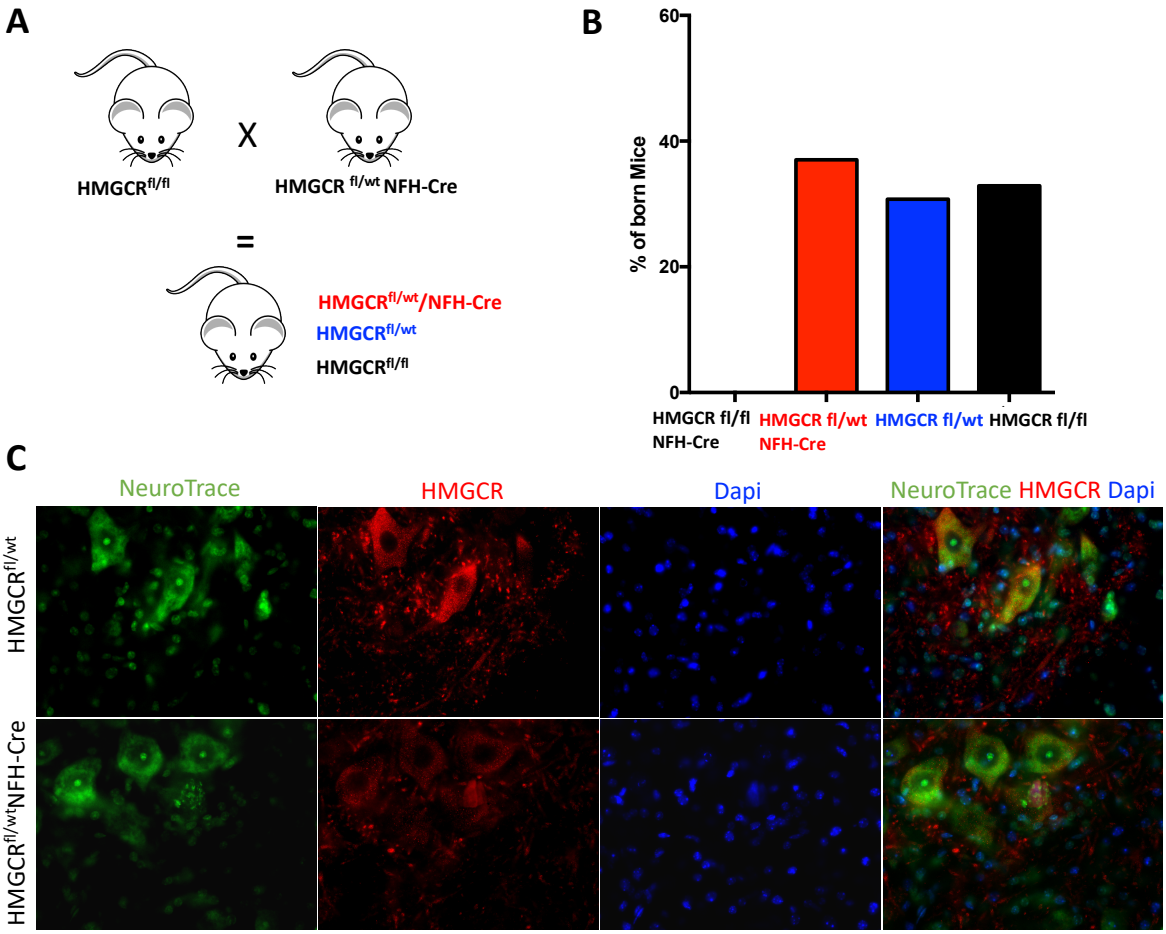

Figure 16: Generating and analysis of HMGCR$^{fl/wt}$/NFH-Cre mice with a heterozygous knockout of HMGCR in neurons

A: HMGCR$^{fl/fl}$ mice are crossed to HMGCR$^{fl/wt}$/NFH-Cre mice with three different genotypes as offspring being HMCGR$^{fl/wt}$/NFH-Cre, HMCGR$^{fl/wt}$ and HMGCR$^{fl/fl}$ mice. The genotype HMGCR$^{fl/fl}$/NFH-Cre cannot be born from this cross, indicating embryonal lethality with a homozygous knockout of HMGCR.
B: The graph shows the distribution of born mice from the three different genotypes in percentage, pointing out a 1/3 relation, confirming the embryonic lethal forth genotype (N=25).
C: Histological analysis of the spinal cord lumbar region with staining for neurons (NeuroTrace), HMGCR and Dapi was performed for HMGCR$^{fl/wt}$/NFH-Cre mice and HMGCR$^{fl/wt}$ mice as controls in steady-state. The protein level of HMGCR in neurons is lower in the heterozygous knockout mice (N=3). The histology was performed with biological triplicates and repeated three times.

3.10. HMGCR$^{fl/wt}$/NFH-Cre Mice show a Severe EAE and Reduced Recovery

After inducing EAE in HMGCR$^{fl/wt}$/NFH-Cre and HMGCR$^{fl/wt}$ controls EAE progression was documented for 30 days post induction (Figure 17A). Both groups start to develop first signs of EAE around dpi 9 and reach the peak of the disease at dpi 16. Comparing the scores the experimental mice show a significantly more severe EAE in line with obviously worse disease condition as compared to the control mice (Figure 17B). During the EAE progression after the peak, the control mice start to recover and reach a plateau at an average score of 1. The HMGCR$^{fl/wt}$/NFH-Cre mice start to recover two to three days later. The recovery phase

transition into a plateau phase already four to five days post the peak. This final phase is accompanied with an average clinical scores of 2,25 and so significantly higher compared to control animals (Figure 17C).

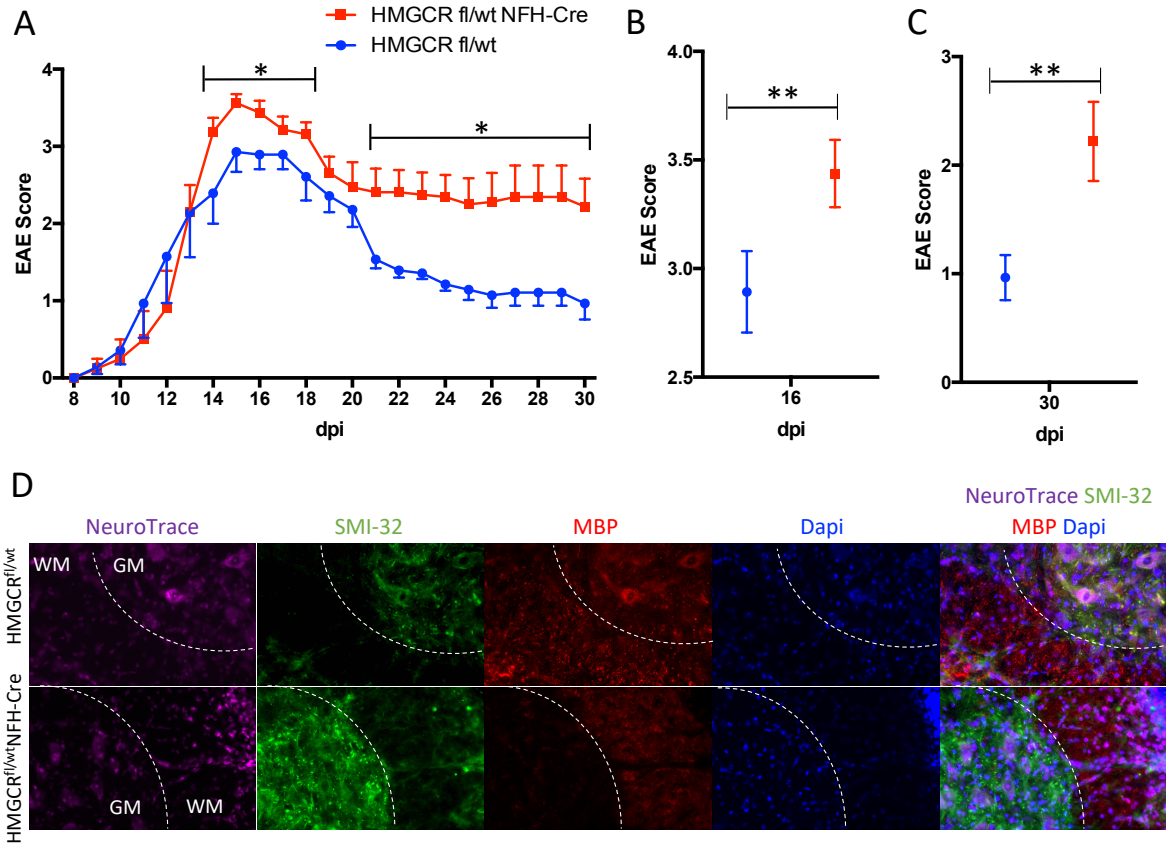

Figure 17: HMGCR$^{fl/wt}$/NFH-Cre mice have a more severe EAE and higher neuronal damage with lower myelination

A: EAE of HMGCR$^{fl/wt}$/NFH-Cre mice is more severe and shows reduced ability to recover. Higher scores reach significance for the days 13-17 at the peak and day 21- 30 during recovery phase. *p < 0.05, (N=7). The EAE experiment was repeated three times.
B: Average score of mice at day 16 at the peak of EAE is significantly higher in HMGCR$^{fl/wt}$/NFH-Cre mice compared to Cre-negative littermates (p=0,001).
C: Average score of mice at day 30 during recovery phase reaches significance with highly enriched scores in the heterozygous knockout mice compared to control mice (p=0.008).
D: Histological analysis of HMGCR$^{fl/wt}$/NFH-Cre mice and HMGCR$^{fl/wt}$ mice at the peak of EAE show higher neuronal damage by staining of SMI-32 and lower myelination in the grey matter by staining of MBP with co-staining of NeuroTrace and Dapi. Border between white and grey matter is indicated by white dotted line. Histology was performed with biological triplicates (N=3).

3.11. HMGCR$^{fl/wt}$/NFH-Cre Mice have More Neuronal Damage and Less Myelination during EAE

CNS tissue was analysed by histological staining to evaluate the myelination and neuronal damage of the HMGCR$^{fl/wt}$/NFH-Cre mice compared to tissue of their littermate controls (HMGCR$^{fl/wt}$). We used tissue of the spinal cord lumbar region derived from mice in the

recovery phase to examine if the higher scores of the HMGCR$^{fl/wt}$/NFH-Cre mice and the incapacity to recover like the controls is also due to more damage in the CNS. Staining for the myelin basic protein (MBP) as a marker for myelin (Dietschy und Turley 2004) was performed. Knowing that HMGCR is important for the myelination of neurons during the development of the CNS, we hypothesised that it also might be important for the remyelination during recovery of EAE and mice lacking one allele will have a disadvantage here. Indeed, we found considerably less MPB staining in the experimental mice compared to controls in the grey-matter of the spinal cord (Figure 17D). This shows that the lack of one HMGCR allele has an effect on the myelination of neurons, even if the knockout is heterozygous and exclusively in neurons and not in oligodendrocytes, the main myelinating cell type.

On top of the fact that there is less myelination in the HMGCR$^{fl/wt}$/NFH-Cre mice they also show obviously higher neuronal tissue damage compared to HMGCR$^{fl/wt}$ mice, represented by the staining of SMI32. SMI32 is a marker for non-phosphorylated neurofilaments, a sign for neuronal damage, staining cell body, dendrites and thick axons of destructed neurons (Budde et al. 2008). The increased staining of SMI32 in neurons of the experimental mice during the recovery phase proofs the existents of more damage to neurons, which is a possible reason for the weaker recovery of these mice (Figure 17D). The reason for the lower myelination and the higher neuronal damage in HMGCR$^{fl/wt}$/NFH-Cre mice need to be further studied and FACS analysis of infiltrating cells could give further view on the process of severe EAE.

3.12. Increased Amount of T Cells and Granulocytes in HMGCR$^{fl/wt}$/NFH-Cre Mice at the Peak and during Recovery

3.12.1. Gating Strategy

To focus on CNS infiltrating and CNS resident immune cells a FACS analysis was performed at the peak of disease and during recovery to reveal any possible differences in the heterozygous knockout mice compared to control littermates. Two different staining protocols were carried out to examine microglia, neutrophils and monocytes on one site and MOG reactive T cells on the other side. For all FACS plots the same gating strategy was applied for each following experiment. For both strategies the first gate was set for lymphocytes according on the forward and side scatter. In the next step doublets are excluded twice with different forward and side scatters. Viable cells were included depending on negative signal for a viability dye (material and methods 2.2.6 for details). After this, the gates were set according to the different used markers (Figure 18+19).

For granulocytes the gating strategy is performed by gating on CD45 positive cells, as CD45 is expressed by all cells of the haemopoietic system, except erythrocytes. T cells were excluded by staining for TCRβ, which is part of the T cell receptor (Parrish et al. 2016). The $CD45^+/TCR\beta^-$ cells can be divided into subpopulations of microglia (CD45 low) and myeloid cells (CD45 high) by staining for CD11b and CD45. Further classification can be seen by staining for Ly6C and Ly6G by which neutrophils and monocytes can be separated (Figure 18).
In the second gating strategy, performed to analyse T cells, CD4 and CD90.2 antibodies were used to detect $CD4^+$ T cells, after gating for single and viable lymphocytes.
Staining with antibodies against CD44 and CD40L were performed to obtain the activated T cells ($CD44^+$) and specifically the MOG reactive ones ($CD40L^+$). The intracellular staining for the MOG reactive T cells enabled to detect cytokines as IL17A, IFNγ and GM-CSF expressed by the T cells (Figure19).

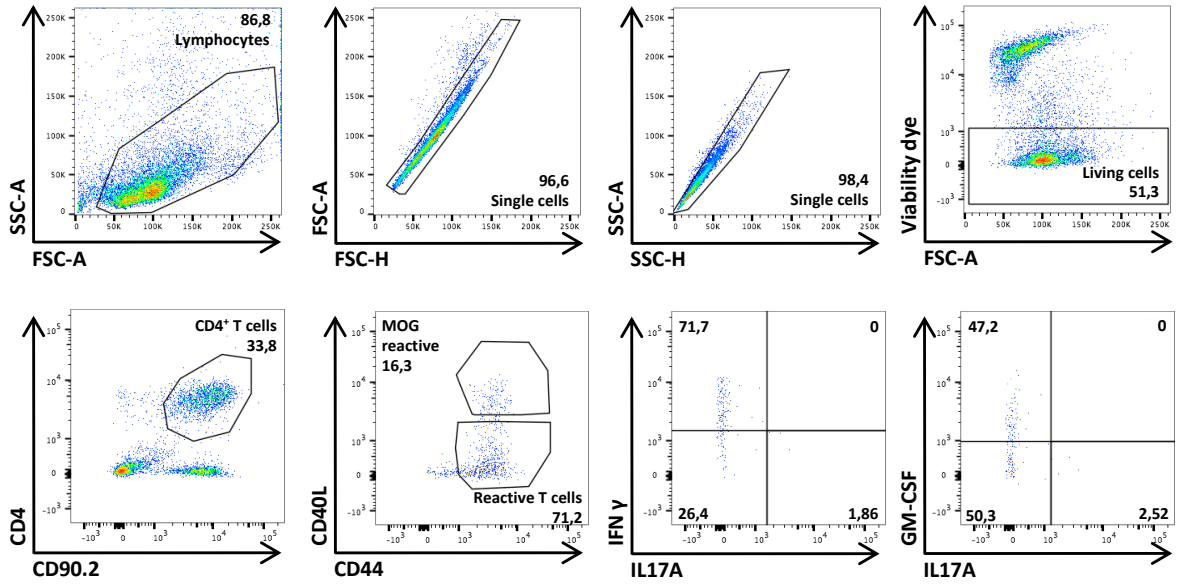

Figure 18:Gating strategy for T cell staining in the CNS, lymph nodes and spleen (example: control brain during recovery)

After staining with a viability dye, CD4, CD90.2, CD40L, CD44, IFNγ, IL17A and GM-CSF, it was gated an lymphocytes with SSC-A and FSC-A, twice for single cells with different forward and sideward scatters (FSC-A and FSC-H; SSC-A and SSC-H) and living cells according to viability dye negative cells.
Then $CD4^+$ and $CD90.2^+$ $CD4^+$ T cells were picked to distinguish between MOG reactive and activated T cells by CD40L and CD44. The MOG reactive $CD4^+$ T cells can be separated in subpopulation expressing IFNγ, IL17 and GM-CSF.

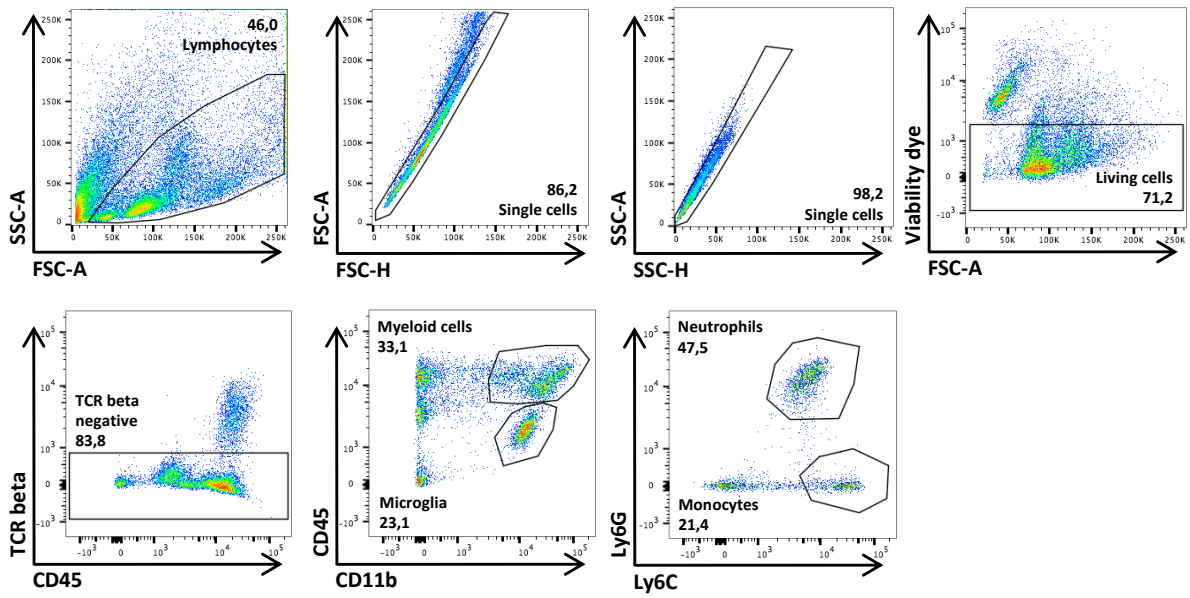

Figure 19: Gating strategy for different granulocytes in the CNS (example control brain during recovery)

The staining for granulocytes includes a viability dye, TCR beta, CD45, CD11b, Ly6G and Ly6C. After gating for lymphocytes with SSC-A and FSC-A, twice for single cells (FSC-A and FSC-H, SSC-A and SSC-H), only living viability negative cells were analysed. Only TCR beta negative cells are used for gating on myeloid od microglia cells by CD45 and CD11b. Myeloid cells can be further analysed and separated in neutrophils or monocytes with the markers Ly6G and Ly6C.

3.12.2. HMGCR$^{fl/wt}$/NFH-Cre Mice have More Microglia and Neutrophils in the CNS at the Peak of EAE

To analyse the severe EAE phenotype of the heterozygous knockout of HMGCR in neurons, granulocytes derived from brain and spinal cord were examined during peak and recovery phase of EAE according to the curse of the disease (Figure 17A). Staining for myeloid cells and microglia revealed that, even if in percentage there was no detectable difference between the genotypes of the examined mice, the experimental mice show significantly more microglia in the brain by cell count (p=0,0243) compared to their control littermates (Figure 19A+C). The myeloid cells were studied in detail and distinguished into neutrophils and monocytes by a staining of Ly6G and Ly6C. The analysis showed no difference in percentage between the groups, but in terms of cell count the knockout mice have indeed significant higher numbers of neutrophils (p=0,0367), whereas the monocytes seems to be higher as well but have no significance in statistics (Figure 20B+D).

The same analysis was performed for the spinal cord of the same mice but the results are slightly different. Myeloid cells, microglia and monocytes appear to be equal in percentage and cell count in both groups of mice at the peak of disease even though experimental mice show significant higher scores and a difference was observable in the brain (Figure 21A-C).

Regarding the neutrophils, there is a significant difference in the percentage, which is 10% higher in the experimental mice (p=0,0395) but cannot be seen in cell count (Figure 21B+D). Taken together the higher numbers of microglia and neutrophils in the brain and higher percentage of neutrophils in the spinal cord indicate more infiltration of granulocytes to the CNS matching the higher scores of disease and the higher observed neuronal damage, as described before (Rumble et al. 2015).

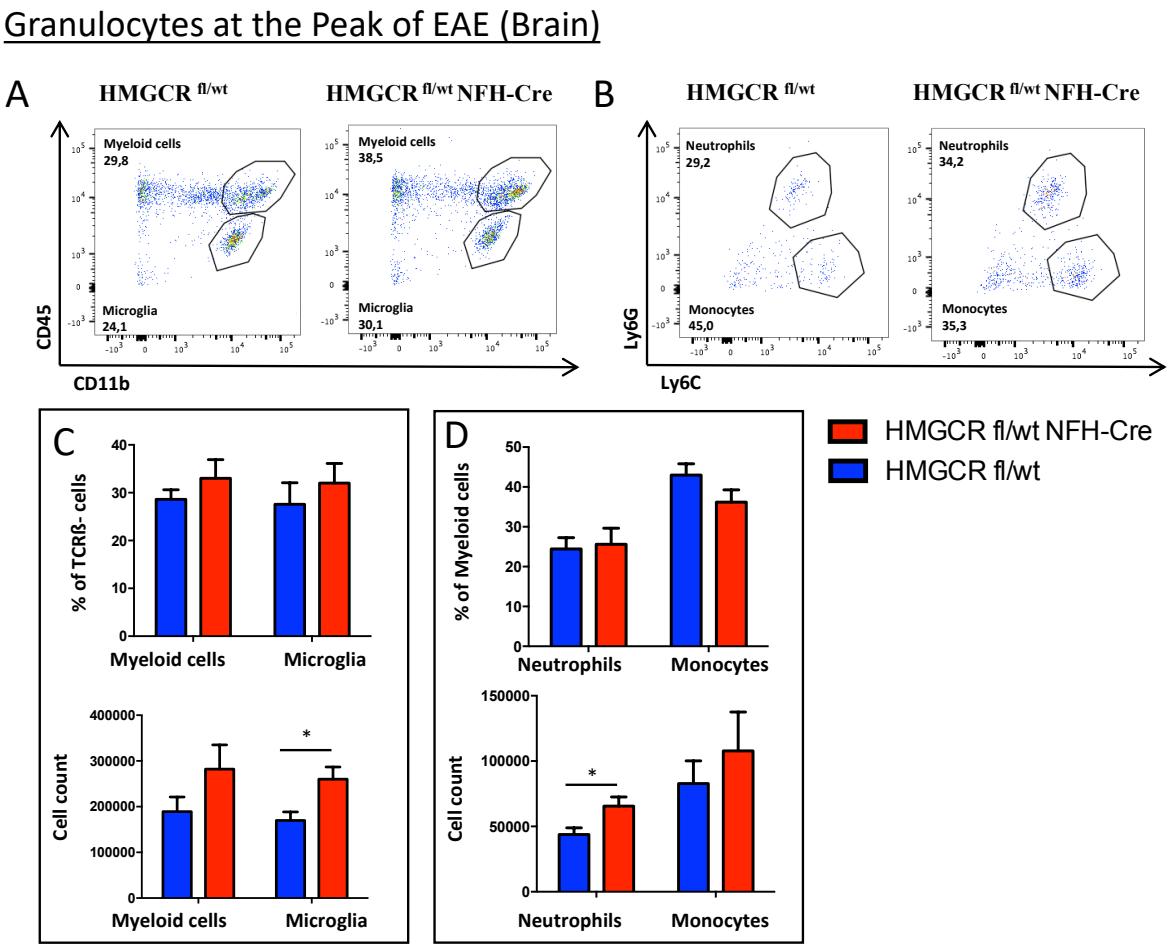

Figure 20: HMGCR$^{fl/wt}$/NFH-Cre mice have more microglia and neutrophils in the brain at the peak of EAE based on cell count

A: FACS plots with staining of CD45 versus CD11b to gate on myeloid cells and microglia in HMGCR$^{fl/wt}$/NFH-Cre mice and HMGCR$^{fl/wt}$ mice. Pregated on single living TCR beta negative lymphocytes.
B: FACS plots with gating for neutrophils and monocytes based on the staining for Ly6G and Ly6C in both experimental groups.
C: Statistics for myeloid cells and microglia, which do not show a difference in HMGCR$^{fl/wt}$/NFH-Cre mice and HMGCR$^{fl/wt}$ mice, neither in percentage nor in cell count.
D: Analysis of statistics for neutrophils and monocytes of the two different genotype of mice in percentage and cell count reveals a significant higher percentage of neutrophils in HMGCR$^{fl/wt}$/NFH-Cre mice (p=0,0395).
The experiments was repeated three times (N=9).

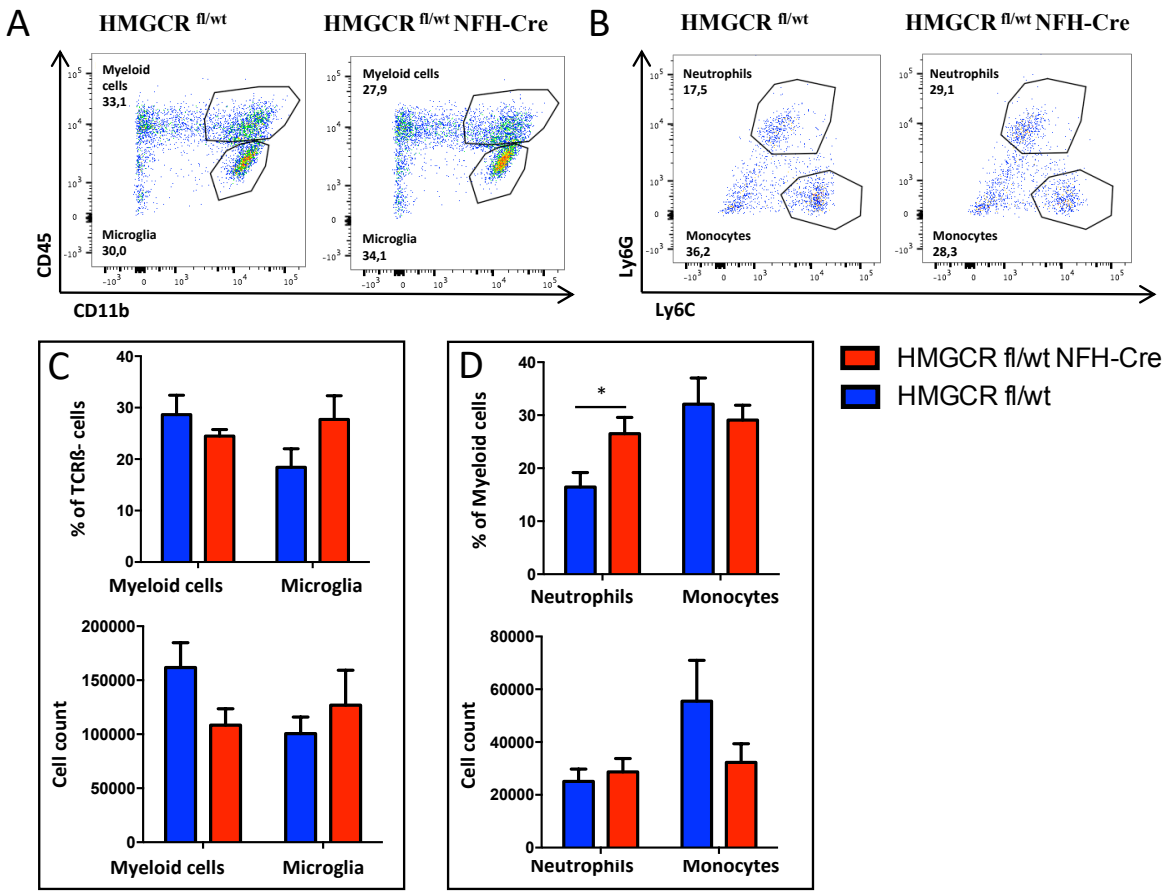

Figure 21: The spinal cord of HMGCR$^{fl/wt}$/NFH-Cre mice shows a higher percentage in neutrophils at the peak of disease

A: FACS plots with staining of CD45 versus CD11b to gate on myeloid cells and microglia in HMGCR$^{fl/wt}$/NFH-Cre mice and HMGCR$^{fl/wt}$ mice. Pregated on single living TCR beta negative lymphocytes.
B: FACS plots with gating for neutrophils and monocytes based on the staining for Ly6G and Ly6C in both experimental groups.
C: Statistics for myeloid cells and microglia, which do not show a difference in HMGCR$^{fl/wt}$/NFH-Cre mice and HMGCR$^{fl/wt}$ mice, neither in percentage nor in cell count.
D: Analysis of statistics for neutrophils and monocytes of the two different genotype of mice in percentage and cell count reveals a significant higher percentage of neutrophils in HMGCR$^{fl/wt}$/NFH-Cre mice (p=0,0395).
The FACS experiment was repeated three times (N=9).

3.12.3. Granulocytes of HMGCR$^{fl/wt}$/NFH-Cre Mice during Recovery Phase of EAE Match the Controls

The FACS analysis of microglia, neutrophils and monocytes was performed as described above during the recovery phase of EAE as well, to study the inability of a sufficient recovery in the HMGCR$^{fl/wt}$/NFH-Cre mice compared to their Cre-negative littermates. Even if the scores of disease are highly significant in this phase of EAE, staining for myeloid cells and microglia could not reveal a significant difference between both groups, this holds true for cell percentage

as well as cell count (Figure 22A+C and 23A+C). Also, the same percentage of neutrophils and monocytes could be detected in brain and spinal cord. Even though the number of neutrophils were slightly higher in spinal cord of the experimental mice, the difference did not reach statistical significance (Figure 23B+D). Cell counts of neutrophils and monocytes is remarkable lower in the recovery phase compared to the peak of EAE (Figure 20-23). But due to the characteristics of this disease with less infiltrates and healing during recovery this is nothing surprising and only shows the dynamics of the disease. It was shown before that a reduced number of myeloid cells indicate a declining inflammation which is typical for recovery phase (Rumble et al. 2015).

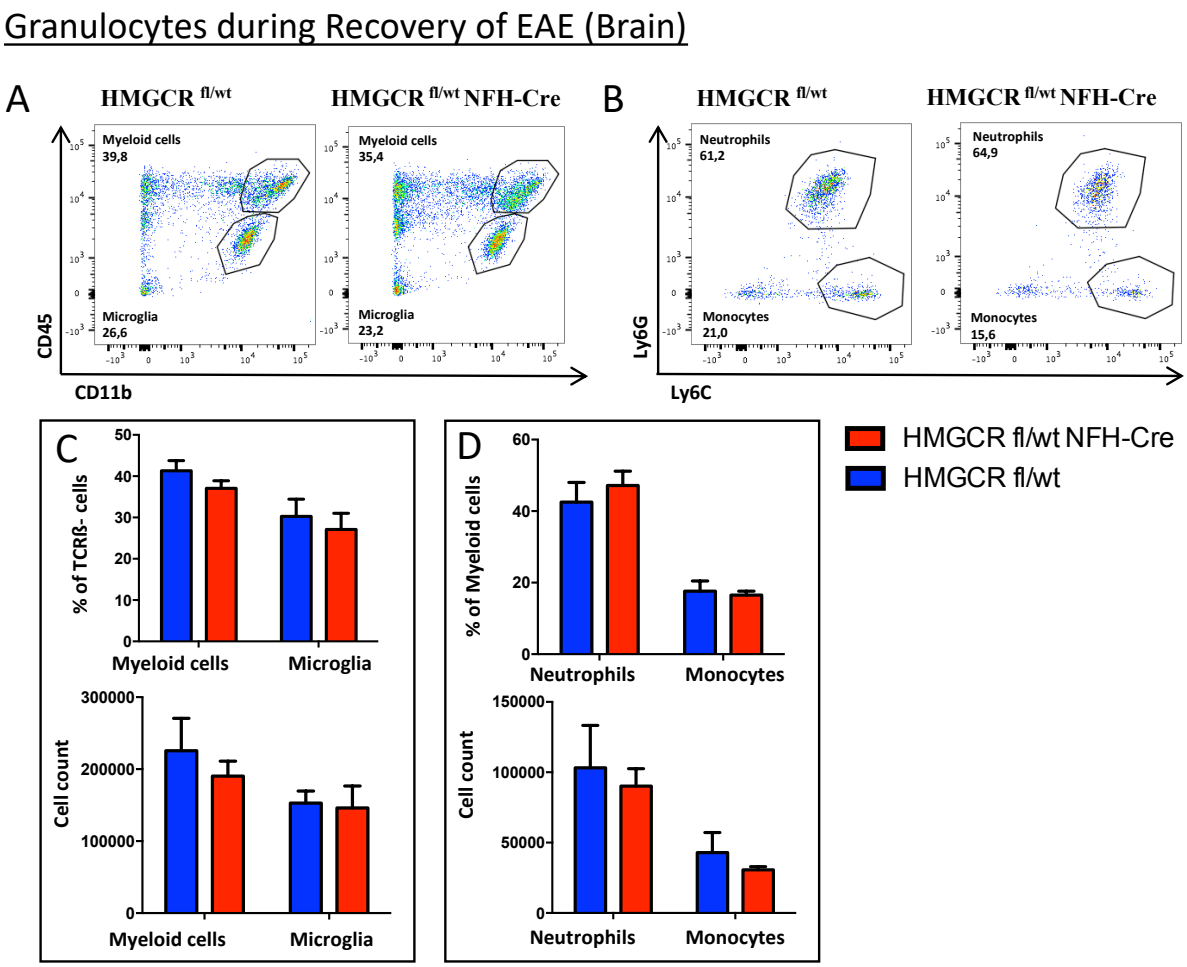

Figure 22: Granulocytes during recovery of the disease in the brain do not differ between the genotypes

A: FACS plots of HMGCR$^{fl/wt}$/NFH-Cre and HMGCR$^{fl/wt}$ mice with myeloid cells and microglia by staining of CD45 and CD11b. Pregated on single living TCR beta negative lymphocytes.
B: FACS plots of neutrophils and monocytes with Ly6G and Ly6C staining for both groups of mice.
C: Statistic analysis of myeloid cells and microglia in percentage and cell count are equal for HMGCR$^{fl/wt}$/NFH-Cre and HMGCR$^{fl/wt}$ mice.
D: Analysis of the statistic of neutrophils and monocytes could not reveal any significant difference in the experimental mouse groups.
The experiment was repeated three times (N=9).

Granulocytes during Recovery of EAE (Spinal cord)

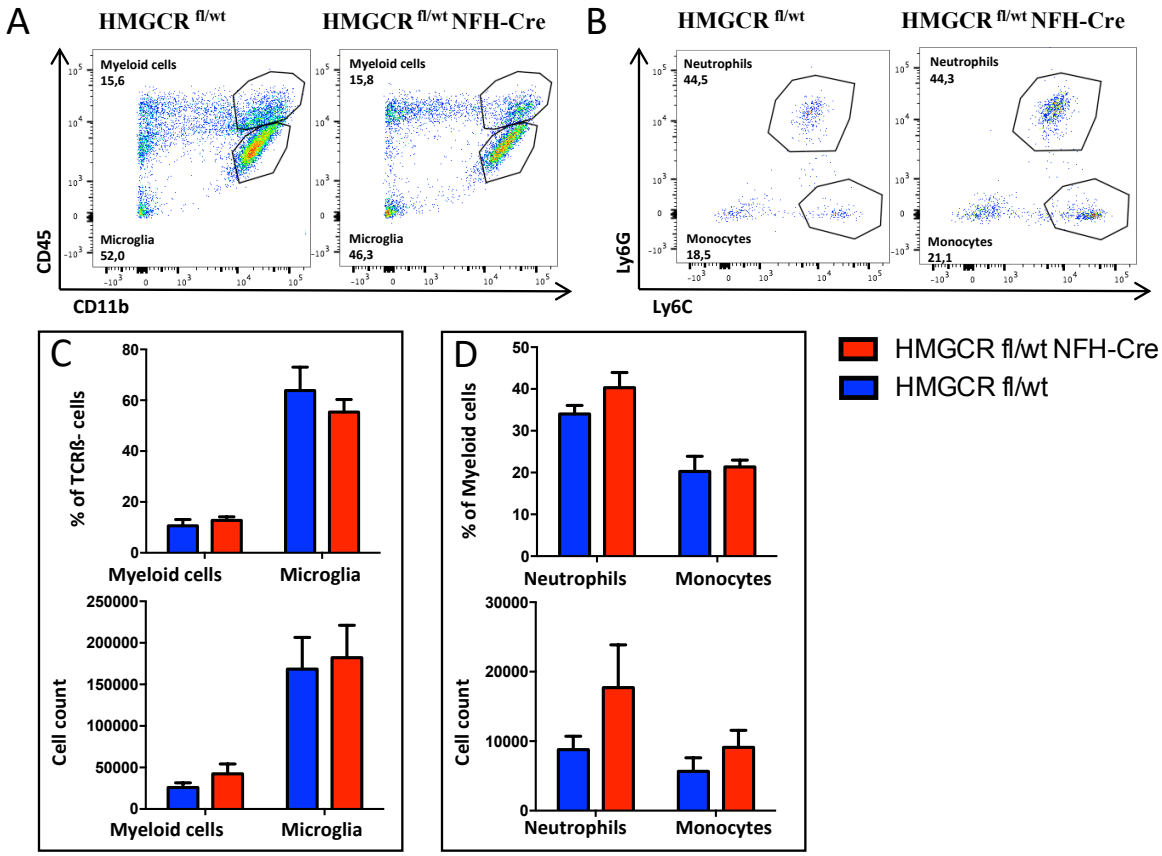

Figure 23: Granulocytes during recovery of EAE in the spinal cord do not show any significant differences between the experimental groups

A: FACS plots for staining of CD45 versus CD11b with myeloid cells and microglia in HMGCR$^{fl/wt}$/NFH-Cre and HMGCR$^{fl/wt}$ mice as controls. Pregated on single living TCR beta negative lymphocytes.
B: FACS plots showing neutrophils and monocytes of experimental mice after gating based on Ly6G and Ly6C staining.
C: Statistical analysis of myeloid cells as well as microglia for both groups of experimental groups show equal amount in percentage and cell count with no detectable difference.
D: For neutrophils and monocytes the analysis reveals slightly more cells in cell count in HMGCR$^{fl/wt}$/NFH-Cre, but it did not reach significant levels. There was no change in percentage neither in neutrophils nor for monocytes in comparison to HMGCR$^{fl/wt}$ control mice.
FACS experiments were repeated three times (N=9).

3.12.4. HMGCR^{fl7wt}/NFH-Cre Mice, have More Infiltrating T Cells in the Brain at the Peak of EAE

After analysing granulocytes in the CNS of HMGCR$^{fl/wt}$/NFH-Cre mice, also the infiltrating T cells were examined in brain, spinal cord, spleen and lymph nodes. Staining and gating strategy were performed as described above. CD4$^+$ T cells were studied in general and divided into activated T cells and MOG reactive T cells, with further analysis of IFNγ, IL17A and GM-CSF. In spleen, paraaortic and inguinal lymph nodes the CD4$^+$ cells were relatively low in both groups and no difference could be detected. In line, the MOG reactive cells were hardly detectable with less than 1% of the CD4$^+$ T cells (Figure 24B+E and Figure 25 B+E). This explains the low amount of cytokine producing cells. From those which could be analysed, no significant difference between experimental and control animals can be seen (Figure 24C+E and Figure 25C+E). The low number of MOG reactive T cells is a result of their migration into the CNS.

In the brain of the experimental mice a clear and significant phenotype can be observed. In line experimental mice have a significant higher number of CD4$^+$ T cells in cell count (p=0,0343) which can also be seen in percentage (Figure 26A+D). Furthermore, MOG reactive T cells are almost significantly higher (p=0,052) and results actually reach significance for the cytokine production (Figure 26 B+E). Explaining the higher scores of the knockout animals at the peak of disease, IFNγ (p=0,0188), IL17A (p=0,0365) and GM-CSF (p=0,0057) producing CD4$^+$ T cells are significantly higher in cell count in experimental mice, most likely causing the more severe EAE, even if there was not such a clear difference in percentage (Figure 26C+F).

Analysing the spinal cord, the difference as it was seen in the brain cannot be detected. CD4$^+$ T cells are equally high according percentage and cell count (Figure 27A+D). Also, MOG reactive T cells, with the cytokines IFNγ, IL17A and GM-CSF do not show any significant difference (Figure 27B+C+E+F). The phenotype of higher cell infiltration in HMGCR$^{fl/wt}$/NFH-Cre mice can only be seen in the brain but is still highly significant and explains the more severe disease in these mice compared to their littermate controls.

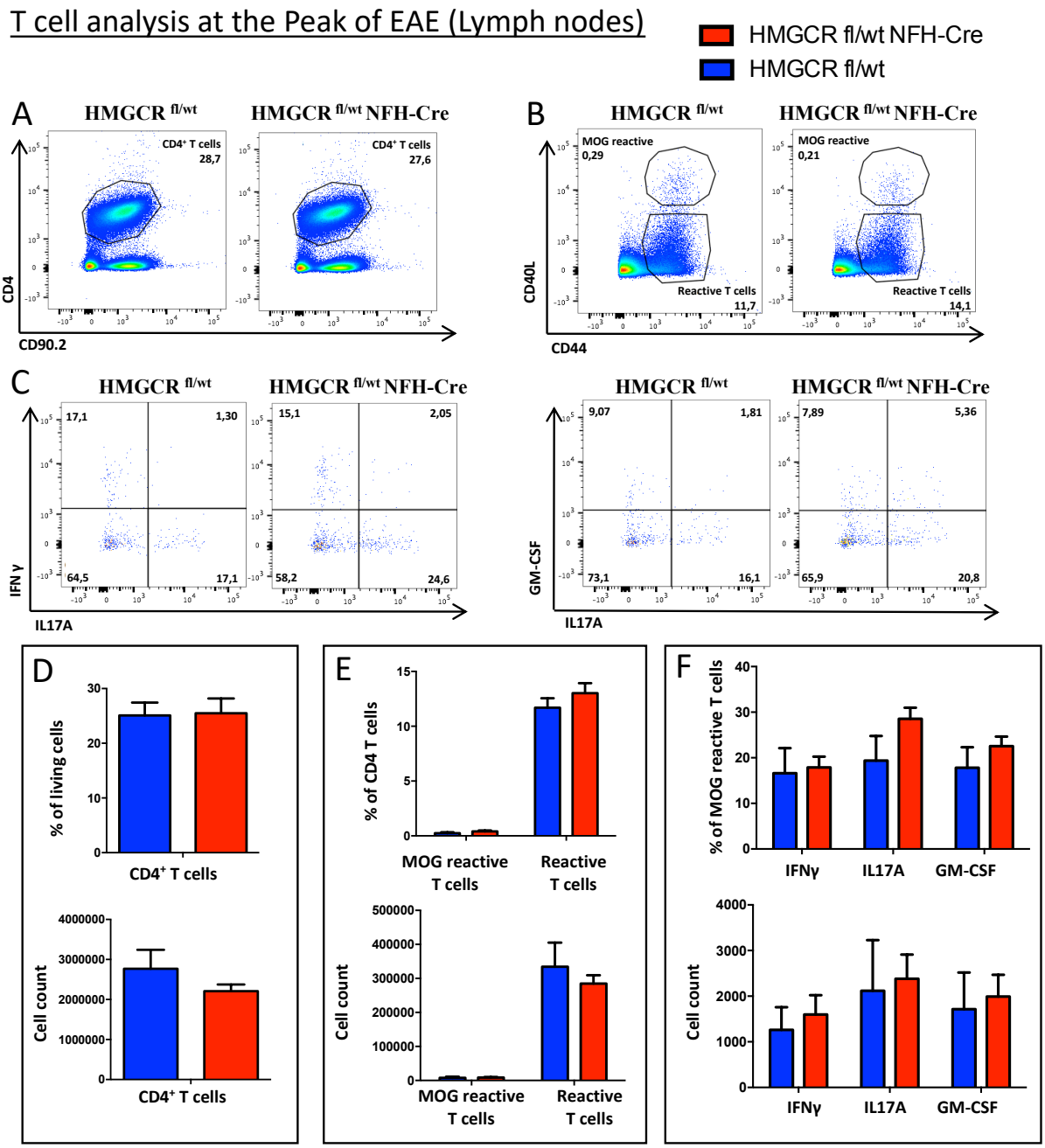

Figure 24: T cell analysis at the peak of EAE in paraaortic and inguinal lymph nodes shows equal results

A: FACs plots of CD4$^+$ T cell gating in lymph nodes based on CD4 and CD90.2 staining in HMGCR$^{fl/wt}$/NFH-Cre mice and HMGCR$^{fl/wt}$ control mice. Pregated on single living lymphocytes.
B: Gating of MOG reactive and activated CD4$^+$ T cells in the FACS plots by staining for CD40L and CD44 for both experimental groups shows equal percentage.
C: FACS plots of cytokine production in MOG reactive CD4$^+$ T cells, gating by IFNγ versus IL17A and GM-CSF versus IL17A for HMGCR$^{fl/wt}$/NFH-Cre and HMGCR$^{fl/wt}$ mice do not differ in percentage.
D: Statistics of CD4$^+$ T cells in comparison of the mouse groups shows equal amount of cells ins percentage as well as in cell count without significant difference.
E: Analysis of MOG reactive and activated T cells points out that MOG reactive T cells are equally low in both groups with less than 1%, there is no detectable difference in statistics.
F: Cytokine production in the few detectable MOG reactive T cells do not expose any difference comparing the experimental mouse groups.
Experiments were repeated three times (N=9).

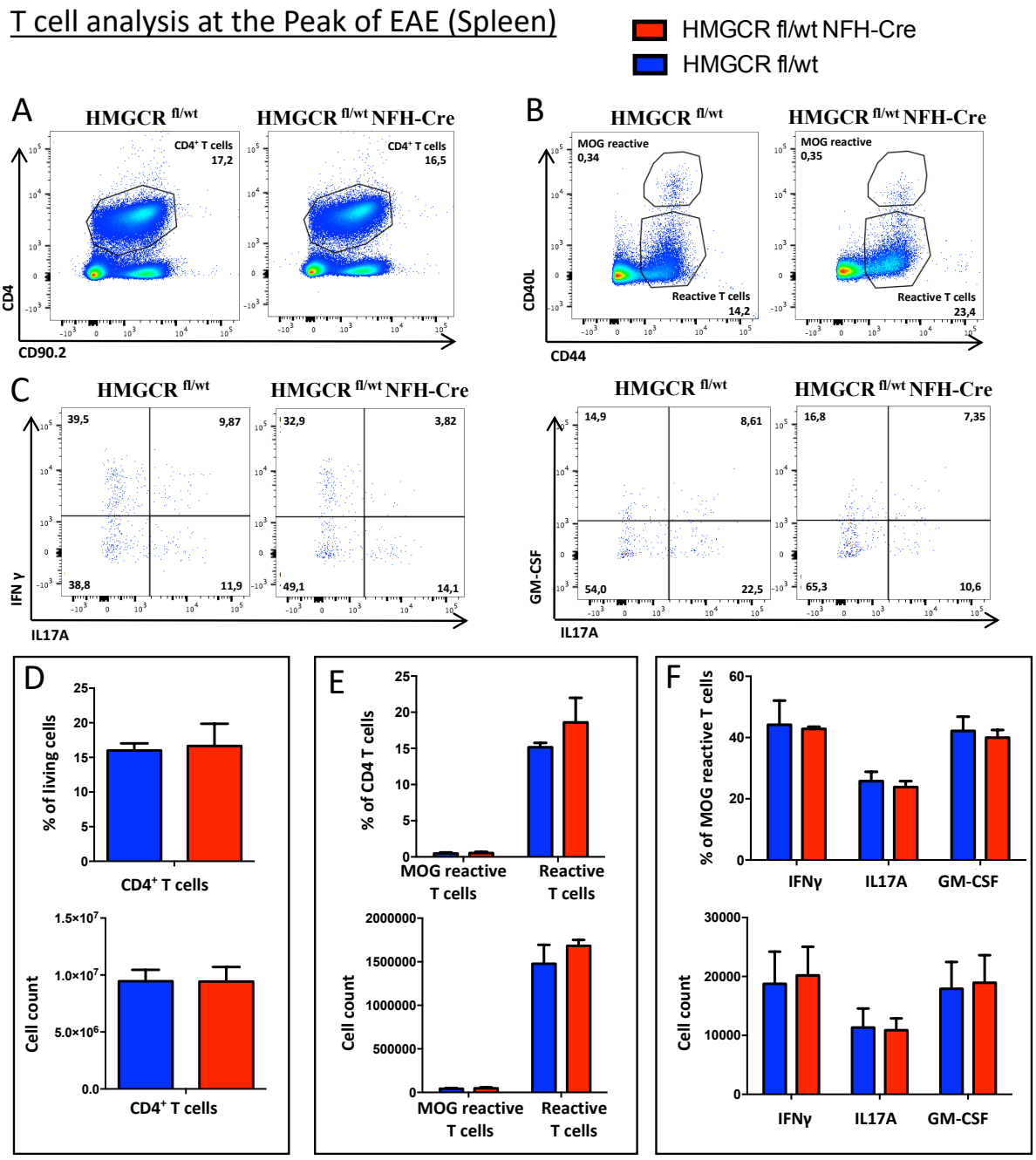

Figure 25: T cell analysis in the spleen of mice at the peak of EAE reveals no difference between the two groups of mice

A: FACS plots of $CD4^+$ T cells by gating based on CD4 and CD90.2 in $HMGCR^{fl/wt}$/NFH-Cre and $HMGCR^{fl/wt}$ mice. Pregated on single living lymphocytes.
B: MOG reactive $CD4^+$ T cells and activated $CD4^+$ T cells in the FACS plots of $HMGCR^{fl/wt}$/NFH-Cre mice and $HMGCR^{fl/wt}$ control mice after staining for CD40L and CD44.
C: FACS plots with focus on cytokine production in the few MOG reactive $CD4^+$ T cells by gating based on IFNγ, IL17A and GM-CSF intra cellular staining.
D: No significant difference can be seen by comparing $CD4^+$ T cells in the spleen of experimental mouse groups in percentage or cell count.
E: The reactive T cells as well as the sparsely MOG reactive $CD4^+$ T cells, do not show any disparity in percentage or cell count.
F: Statistical analysis of the cytokine production in the few MOG reactive cells which could be found in the spleen reveal equal amounts of IFNγ, IL17A and GM-CSF in $HMGCR^{fl/wt}$/NFH-Cre mice and $HMGCR^{fl/wt}$ mice.
FACS experiments were repeated three times (N=9).

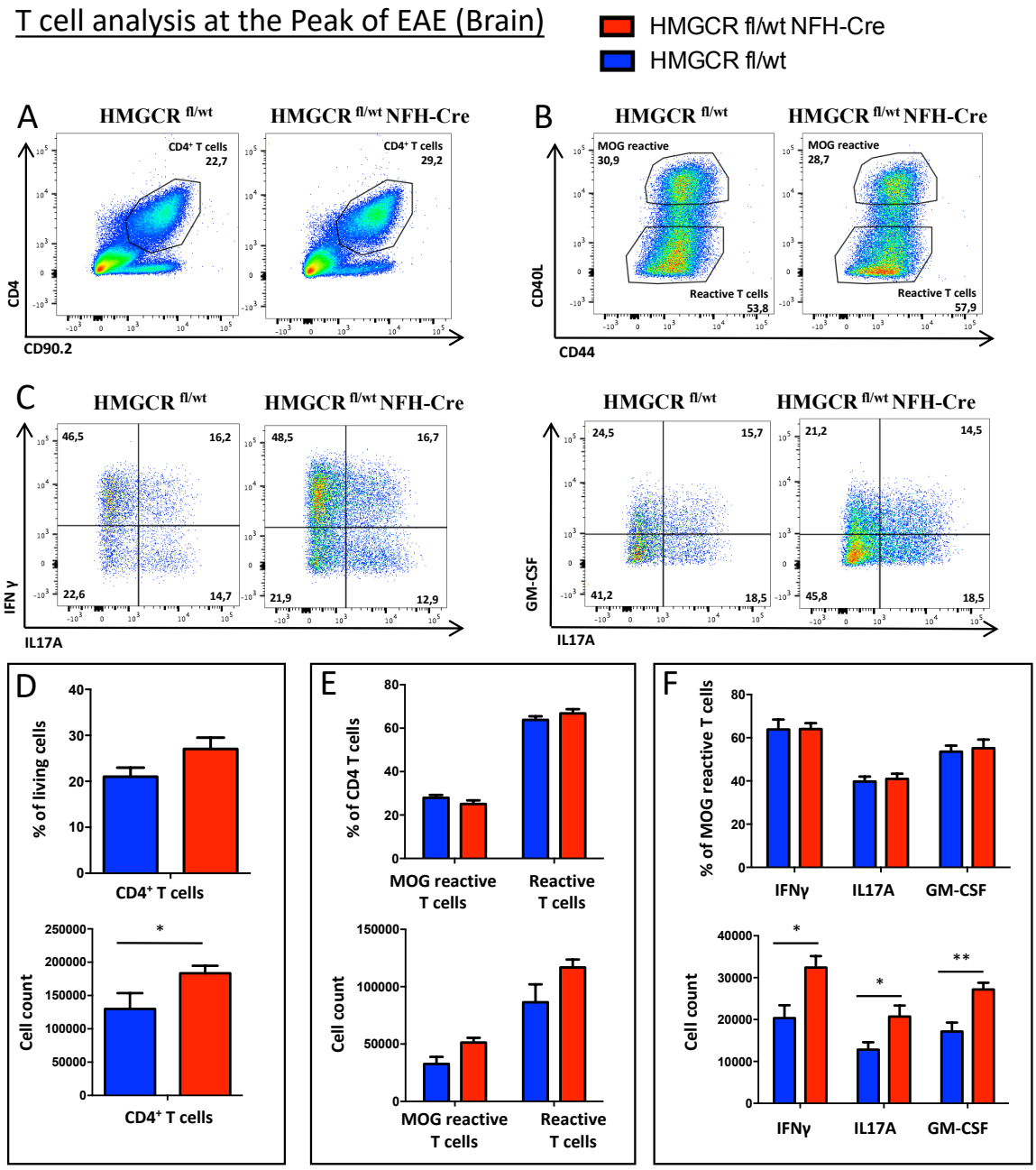

Figure 26: Significant higher numbers of CD4⁺ T cells and more IFNy, IL17A and GM-CSF can be found in HMGCR$^{fl/wt}$/NFH-Cre mice at the peak of disease

A: FACS plots of CD4 versus CD90.2 staining shows CD4⁺ T cell gating for HMGCR$^{fl/wt}$/NFH-Cre mice compared to HMGCR$^{fl/wt}$ control mice. Pregated on single living lymphocytes.
B: Gating of MOG reactive CD4⁺ T cells and activated CD4⁺ T cells in the FACS plots of CD40L and CD44 staining for both mouse groups in comparison.
C: FACS plots of IFNγ and IL17A staining in HMGCR$^{fl/wt}$/NFH-Cre and HMGCR$^{fl/w}$ mice and FACS plots of GM-CSF and IL17A gating to compare cytokine producing CD4 MOG reactive T cells in HMGCR$^{fl/wt}$/NFH-Cre and HMGCR$^{fl/w}$ mice.
D: Statistic analysis of CD4⁺ T cells in both mouse groups in percentage and cell count reveals significant higher numbers of infiltrating CD4⁺ T cells in the heterozygous knockout mice (p=0,0343).
E: MOG reactive and activated T cells in comparison between the two experimental mouse groups show no difference in percentage but a higher number of both cell types in HMGCR$^{fl/wt}$/NFH-Cre mice even this is not significant.
F: The analysis of the statistics of the cytokine producing MOG reactive CD4⁺ T cells shows again no difference regarding the percentage but a significant enrichment for IFNy (p=0,0188) and IL17A (p=0,0365) and a very significant enrichment for GM-CSF (p=0,0057) in cell count. Experiments were repeated three times (N=9).

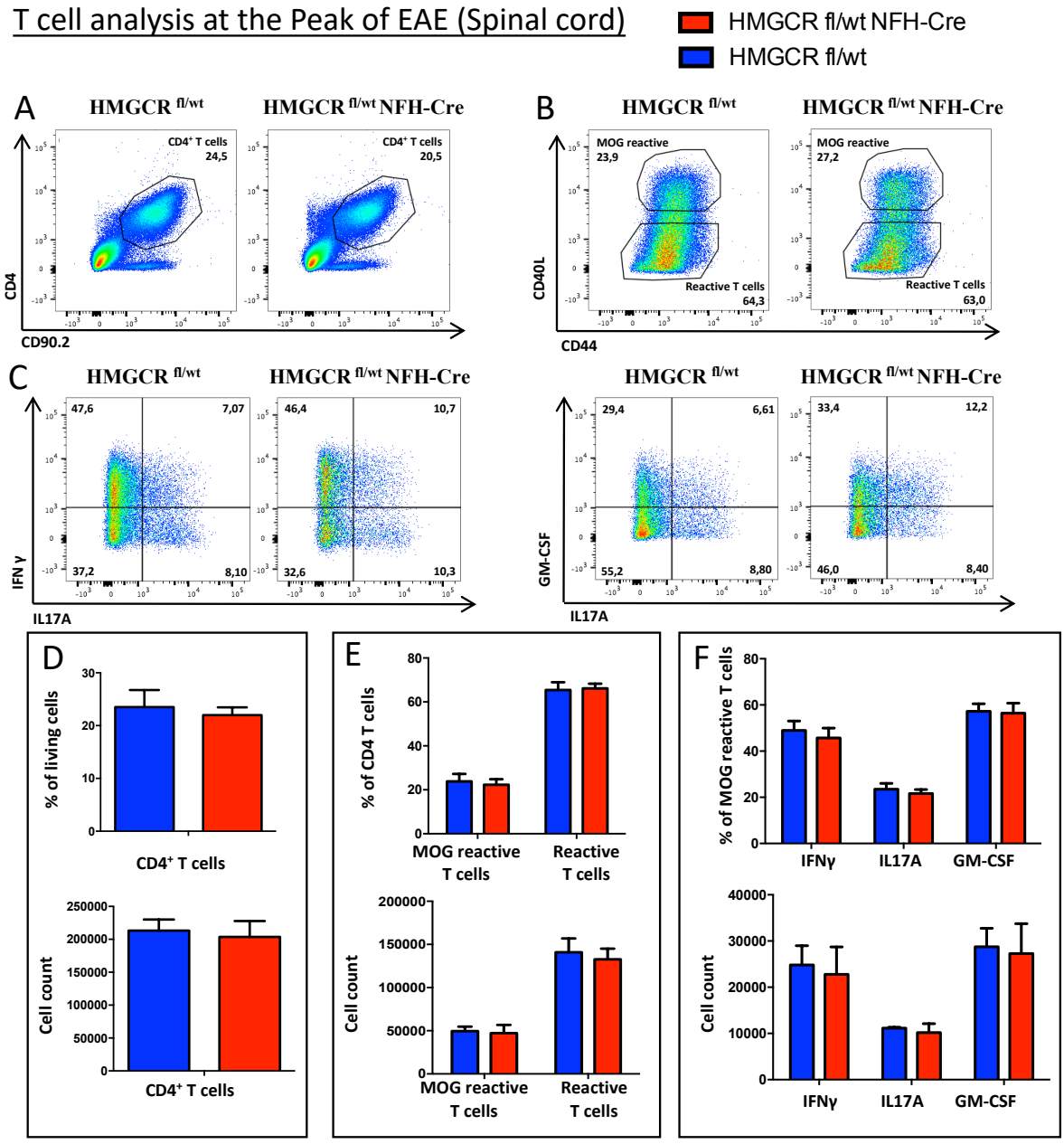

Figure 27: T cell analysis of the spinal cord for the peak of EAE does not differ between the genotypes

A: The FACS plots of CD4 versus CD90.2 staining compare HMGCR$^{fl/wt}$/NFH-Cre mice to HMGCR$^{fl/wt}$ control mice for their infiltrating CD4^{+} T cells to the spinal cord. Pregated on single living lymphocytes.
B: FACS plots including the gating of MOG reactive CD4^{+} T cells and activated CD4^{+} T cells stained for CD40L and CD44 in both mouse groups.
C: FACS plots of IFNγ and IL17A as well as GM-CSF and IL17A gating in HMGCR$^{fl/wt}$/NFH-Cre and HMGCR$^{fl/w}$ mice to compare cytokine producing CD4^{+} MOG reactive T cells.
D: Statistic analysis of CD4^{+} T cells in percentage and cell count reveals equal amount in both mouse groups.
E: MOG reactive and activated T cells in comparison between the two experimental mouse groups show no difference in percentage or cell count.
F: The statistical analysis of the cytokine producing MOG reactive CD4 T cells shows as well the same amount of cytokine production (IFNγ, IL17A and GM-CSF) in HMGCR$^{fl/wt}$/NFH-Cre and HMGCR$^{fl/w}$ mice.
FACS experiments were repeated three times (N=9).

3.12.5. More Infiltrating T Cells in the Spinal Cord of HMGCR$^{fl/wt}$/NFH-Cre Mice during Recovery Phase of EAE

For a complete analysis of the time course of EAE, also the recovery phase was analysed for the infiltrating immune cells, especially as this phase showed the highest difference between the mouse groups based on clinical EAE score. The inability of a sufficient recovery of the HMGCR$^{fl/wt}$/NFH-Cre mice has to be studied in detail.

CD4$^+$ T cells in spleen and lymph nodes were observable low compared to the peak of disease due to the fact that they migrate to the CNS. There was no significant difference between experimental mice and controls, as is was already seen at the peak of EAE (Figure 28+29).

The higher infiltration in the brain of the experimental mice is no longer existent during the recovery phase. Both mouse groups have an equal amount of CD4$^+$ T cells. Only a slightly higher percentage can be seen in the experimental animals but does not reach significance (Figure 30A+D). The MOG reactive cells are also similar regarding percentage and cell count, and reduced in amount due to the lower severity of EAE at this time point (Figure 30B+E). Even though, it does not reach significant levels, the difference in IL17A and GM-CSF which was detected in the brain at the peak of EAE can also be seen during recovery phase, but with an inferior difference (Figure 30C+F).

Spinal cord from control and experimental mice showed a lot of remarkable differences. HMGCR$^{fl/wt}$/NFH-Cre mice have a significantly increased number of CD4$^+$ T cells in spinal cord tissue in percentage ($p=0.0352$) and cell count ($p=0.0072$) (Figure 31A+D). Equally the activated T cells in the experimental mice are significantly higher in cell count than the control mice ($p=0.0039$). MOG reactive cells showed a significance in the cell count ($p = 0.0166$) as well as in percentage of CD4$^+$ T cells ($p = 0.0446$). In both cases the experimental mice revealed higher values (Figure 31B+E). The cytokine production emerged statistically significant, too. The IFNγ expression of HMGCR$^{fl/wt}$/NFH-Cre mice was significantly increased in cell count ($p=0.0168$) as well as for the percentage ($p=0.0063$). More MOG reactive cells of experimental mice produced IL17A with statistically significant results for the cell count ($p=0.0497$). For both, percentage ($p=0.0152$) and cell count ($p=0.0103$), GM-CSF showed a significantly higher number of cells in the experimental mice (Figure 31C+F). As the data revealed there is clearly an increased infiltration of T cells in the spinal cord of HMGCR$^{fl/wt}$/NFH-Cre mice. They show significantly more activated and MOG reactive T cells indicating the severity of EAE in these mice. This is also supported by the high amount of cytokine producing cells. Less cells produce IL17A than GM-CSF and IFNγ which indicates a slight recovery, as the inflammation is not further promoted. Nevertheless, the experimental animals show clearly an insufficient recovery

and exhibit more infiltration in the spinal cord, which can explain the higher damage and lower myelination of neurons.

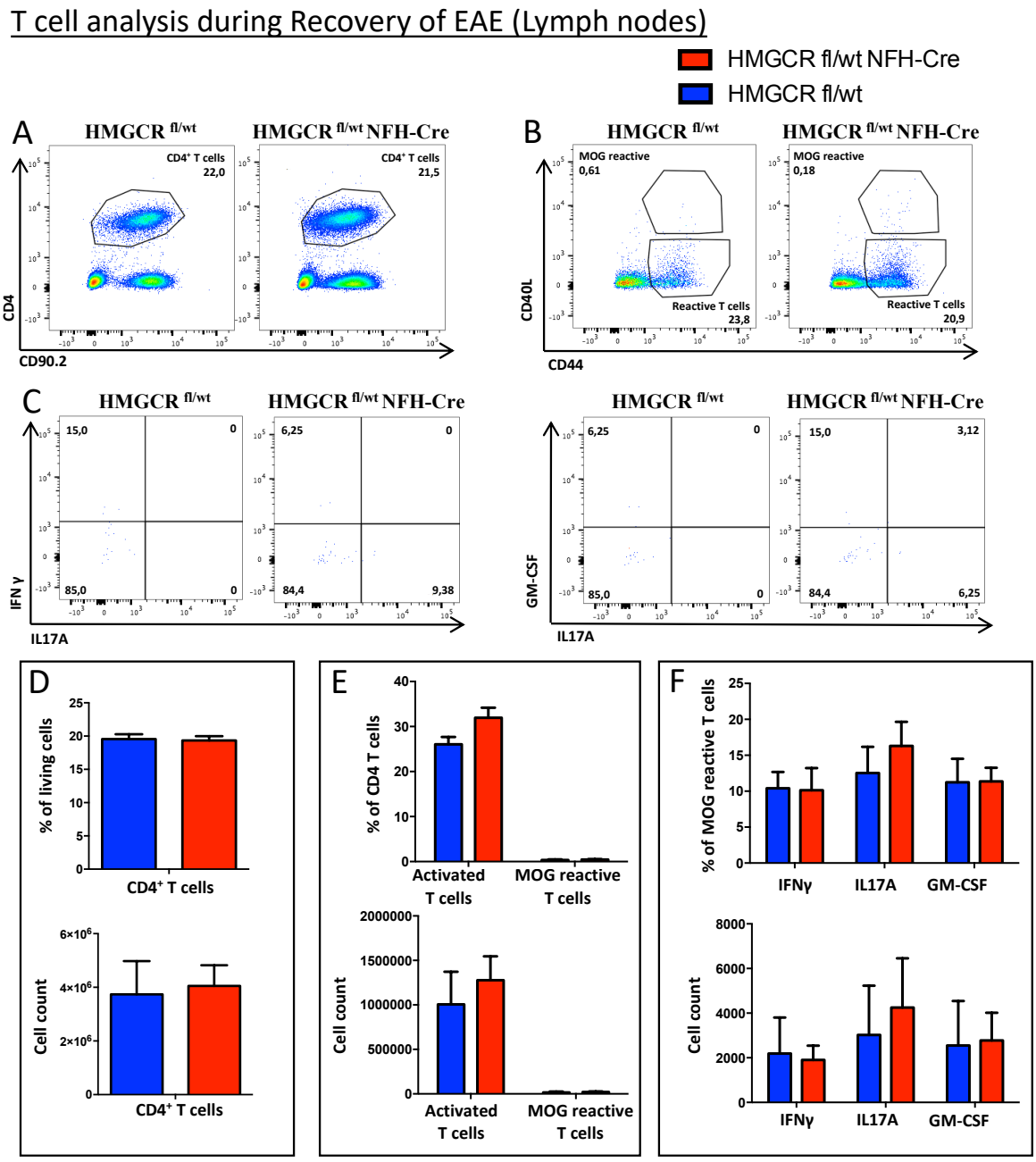

Figure 28: Paraaortic and inguinal lymph nodes show no difference in the groups of mice during recovery of EAE

A: FACs plots of $CD4^+$ T cell gating in lymph nodes based on CD4 and CD90.2 staining in $HMGCR^{fl/wt}$/NFH-Cre mice and $HMGCR^{fl/wt}$ control mice. Pregated on single living lymphocytes.
B: Gating of MOG reactive and activated $CD4^+$ T cells in the FACS plots by staining for CD40L and CD44 for both experimental groups.
C: FACS plots of cytokine production in MOG reactive $CD4^+$ T cells, gating by IFNγ versus IL17A and GM-CSF versus IL17A for $HMGCR^{fl/wt}$/NFH-Cre and $HMGCR^{fl/wt}$ mice.
D: Statistics of $CD4^+$ T cells in comparison of the mouse groups shows equal amount of cells ins percentage as well as in cell count.
E: Analysis of MOG reactive and activated T cells points out that MOG reactive T cells are equally low in both groups with less than 1%, there is no detectable difference in statistics.
F: Cytokine production in the few detectable MOG reactive T cells do not expose any difference comparing the experimental mouse groups. Experiments were performed three times (N=9).

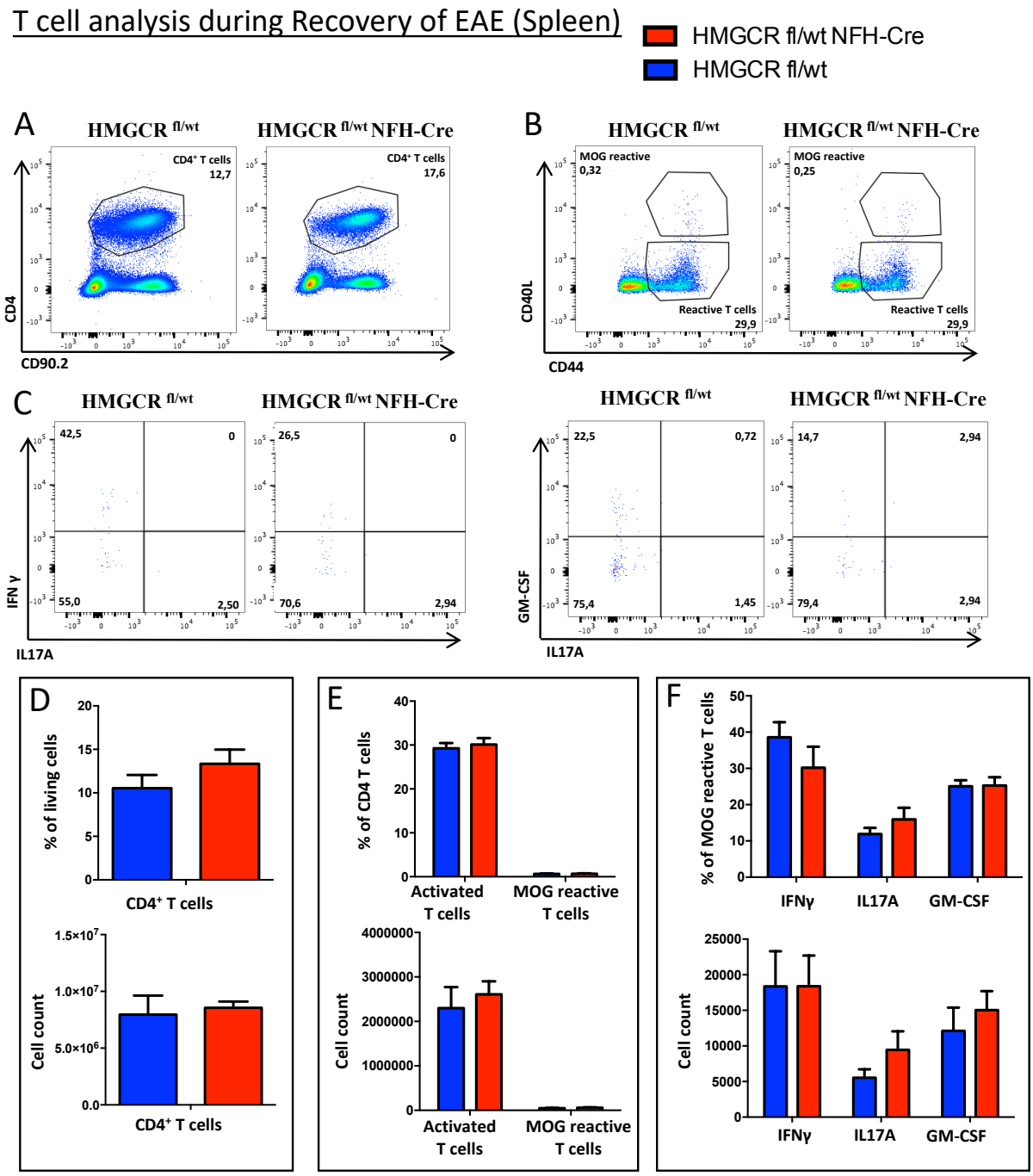

Figure 29: T cell analysis in the spleen of mice in the recovery phase of EAE is similar in both genotypes

A: FACs plots of $CD4^+$ T cell gating in lymph nodes based on CD4 and CD90.2 staining in $HMGCR^{fl/wt}$/NFH-Cre mice and $HMGCR^{fl/wt}$ control mice. Pregated on single living lymphocytes.
B: Gating of MOG reactive and activated $CD4^+$ T cells in the FACS plots by staining for CD40L and CD44 for both experimental groups.
C: FACS plots of cytokine production in MOG reactive $CD4^+$ T cells, gating by IFNγ versus IL17A and GM-CSF versus IL17A for $HMGCR^{fl/wt}$/NFH-Cre and $HMGCR^{fl/wt}$ mice.
D: Statistics of $CD4^+$ T cells in comparison of the mouse groups shows equal amount of cells ins percentage as well as in cell count.
E: Analysis of MOG reactive and activated T cells points out that MOG reactive T cells are equally low in both groups with less than 1%, there is no detectable difference in statistics.
F: Cytokine production in the few detectable MOG reactive T cells do not expose any difference comparing the experimental mouse groups.
Experiments were repeated three times (N=9).

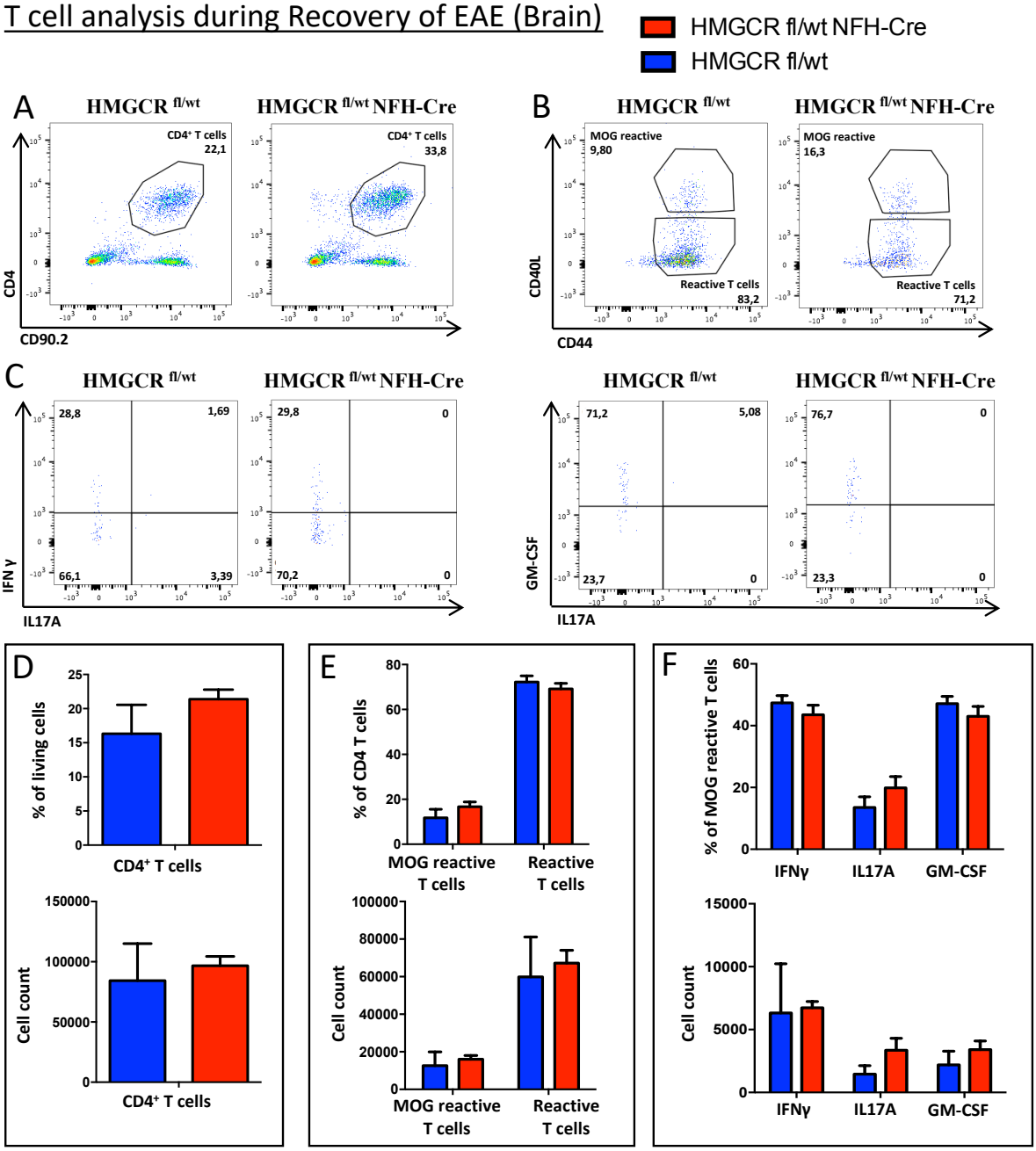

Figure 30: There is no significant difference between experimental mice and controls in the brain during recovery of EAE

A: FACS plots of HMGCR$^{fl/wt}$/NFH-Cre and HMGCR$^{fl/wt}$ mice with gating of CD4^{+} T cells based on CD4 and CD9.2 staining. Pregated on single living lymphocytes.
B: Gating on MOG reactive and activated T cells in FACS plots of both mouse groups with the help of CD40L and CD44.
C: FACS plots for cytokine production of IFNγ, IL17A and GM-CSF in HMGCR$^{fl/wt}$/NFH-Cre and HMGCR$^{fl/wt}$ mice.
D: Statistics in comparison between the two groups show no difference in percentage or cell count of the invading CD4^{+} T cells.
E: Analysis of MOG reactive and activated T cells also do not have a significant difference between HMGCR$^{fl/wt}$/NFH-Cre and HMGCR$^{fl/wt}$ mice
F: The diagram of IFNγ, IL17A and GM-CSF shows higher numbers of IL17A and GM-CSF without reaching significance as well as the percentages for the cytokine producing T cells.
FACS experiments were performed three times (N=9).

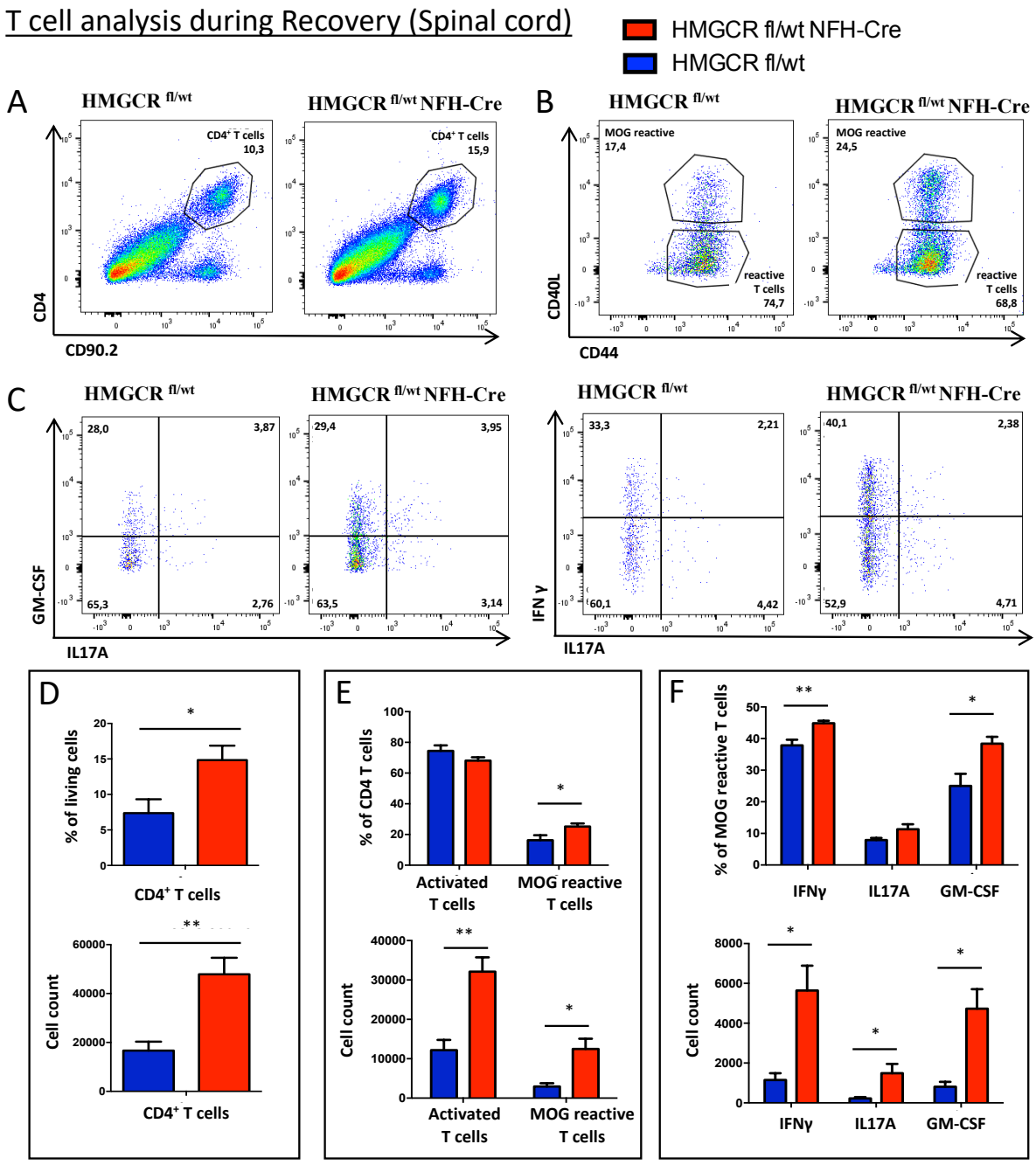

Figure 31: Spinal cord of HMGCR$^{fl/wt}$/NFH-Cre mice during recovery phase of EAE reveals a significant higher number of CD4$^+$ T cells, with more IFNγ, GM-CSF and IL17A

A+D: FACS analysis of invading immune cells in the spinal cord of HMGCR$^{fl/wt}$/NFH-Cre mice show a significant higher amount of CD4$^+$ T cells by percentage and number compared to HMGCR$^{fl/wt}$ littermate controls, pregated on living, single lymphocytes. Pregated on single living lymphocytes.
B+E: These CD4$^+$ T cells in HMGCR$^{fl/wt}$/NFH-Cre mice have significant more MOG reactive T cells compared to those in HMGCR$^{fl/wt}$ littermate controls by percentage as well as by cell count.
C+F: Cytokine staining of MOG reactive cells show significant higher IFNγ and GM-CSF in percentage and IFNγ, GM-CSF as well as IL17A in cell count in HMGCR$^{fl/wt}$/NFH-Cre mice compared to HMGCR$^{fl/wt}$ littermate controls.

3.13. Comparison of NGS Data with MS Patient Samples

Analysing the NGS data of neuronal response during EAE in mice focusing on genes related to certain disease we found a lot of coincidence to various different diseases (Analysis performed with iPathwayGuide). The inner ring of the circle plot highlights the different subtypes of disease groups in different colours. One can find for example Endocrine, nutritional and metabolic disease, Congenital malformations deformations and chromosomal abnormalities, Disease of the musculoskeletal system and connective tissue, Disease of the blood and blood-forming organs, Disease of the nervous system, which is from highest interest for this study, Disease of the eye and adnexa, neoplasms, Certain infectious and parasitic diseases, Disease of the circulatory system and many more (Figure 32A). Following the different layers of the circle plot towards the outside one reach single diseases out of the various subgroups and classifications. As the top 10 relevant disease for this study, the following were defined: Complement pathway defects and HMG-CoA synthase deficiency out of the group Endocrine, nutritional and metabolic diseases (dark blue). Behcet disease, Systemic sclerosis, Systemic lupus erythematosus and Seronegative Arthritis, which belong to the group of Disease of the musculoskeletal system and connective tissue (orange). Corresponding to the group Disease of the nervous tissue (green) there are Multiple Sclerosis and Amyotrophic lateral sclerosis, which reinforced strongly our experimental setup and the ability of translation of the EAE model to MS patients. The last two of the top 10 diseases are Leprosy/Hansen disease and Asthma (Figure 32B). The genes which are categorized to each of the disease can be found accordingly in the table (Figure 32C).

A

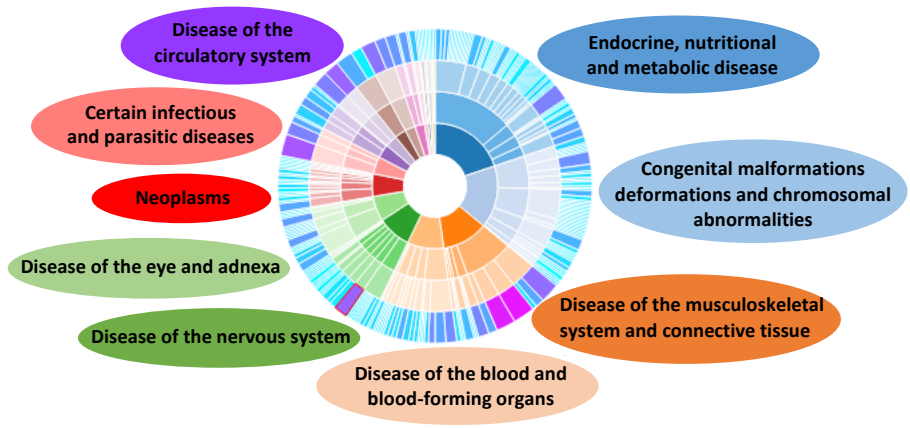

B

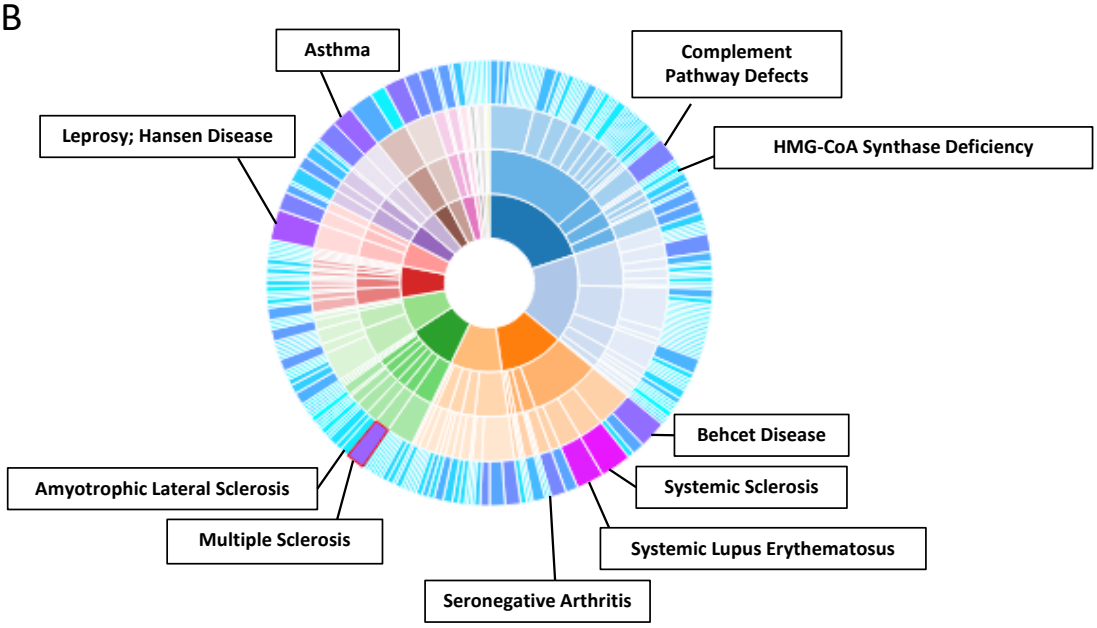

C

Disease	Genes
Systemic Sclerosis	H2-DMb1, H2-DMa, IL1b, IL1a, H2-Oa, H2-DMb2, Ptpn18, CD247, Ptpn22, Tnfaip3
Systhemic Lupus Erythematosus	Fcgr2b, H2-DMb1, H2-DMa, Fcgr4, H2-Oa, C4b, Tnf, H2-DMb2, Pdcd1
Complement Pathway Defects	C1s1, C1ra, C3, C4b, C1qa, C1qb
Leprosy; Hansen Disease	H2-T23, H2-T22, H2-Q7, H2-Q4. H2-K1, Tlr2, H2-Q6, H2-M3, H2-M2
Multiple Sclerosis	H2-DMb1, H2-DMa, H2-Oa, Tnfrsf1a, H2-DMb2, Pdcd1
Seronegative Arthritis	H2-T23, H2-T22, H2-Q7, H2-4, H2-D1, H2-K1, H2-Q6, H2-M3, H2-M2
Astma	H2-DMb1, H2-DMA, IL4ra, Cd14, H2-Oa, Tnf, H2-DMb2
Behcet Disease	H2-T23, H2-T22, H2-Q7, H2-D1, H2-K1, H2-Q6, H2-M3, H2-M2
Amyotrophic Lateral Sclerosis	Sod1
HMG-CoA Synthase Deficiency	Hmgcs1

Figure 32: Differentially expressed genes in neurons during EAE are crucial for various different diseases

A: Various diseases from diverse categories are impacted by the genes which were detected to be differentially expressed in neurons during the time course of EAE. In the inner ring of the circle one can find the categories, which are sorted clock-wise by the amount of involved diseases and affected genes (iPathwayGuide).
B: The top 10 disease which have the highest accordance with differentially expressed genes are assigned to their disease classification at the outer layer of the circle (iPathwayGuide).
C: The top 10 disease with associated differential expressed genes are listed in the table (iPathwayGuide).

After analysing the NGS data from mice in detail we wanted to verify if it can be compared to human MS patient samples. We used the data in collaboration with Prof. Dr. Hans Lassmann and colleagues, who have access to a huge collection of autopsy samples from MS patients. They isolated different kinds of regions from MS lesions by micro-dissection in different stages of the disease and performed whole genome arrays. The genome arrays have been made on archival, formaldehyde fixed and paraffin embedded material (Fischer et al., 2013, 2012). The micro-dissected regions include RNA of all kind of cell types in the CNS, including neurons, glial cells and invading immune cells, whereas our murine data is based on pure neuronal RNA. Also, the data is classified in different kind of MS stages, which are MS Cortical Lesions, MS White Matter Initial Lesions and MS White Matter Active Lesions, which makes it even harder to compare and make conclusions. We decided to put these three kinds of MS lesions side by side to our results of the peak of EAE and during recovery phase to point out similarities and contrasts. We show candidate genes and pathways which were discussed above and are most relevant for this study.

In our data *pirb* is highly upregulated, over 30-fold change, at the peak of disease (red) and is almost down to control level during recovery (blue). In accordance we see such an upregulation also in all three kinds of MS lesions, but it is most prominent in the MS White Matter Initial Lesions (dark green, Figure 33A). In the case of *b2m* which shows an upregulation by 15-fold change at the peak, we can see a clear but lower upregulation in initial and active white matter lesions, but a divergent result in the MS Cortical Lesions (bright green) were the gene is notably downregulated to -25-fold change (Figure 33B). The classical MHCI genes are different in mice and human. We compared the classical H2-K1, H2-D1 and H2-Q6 genes in mice to the human counterpart genes for HLA-A, HLA-B and HLA-C. In general, one can find a really clear coincidence between mice and human, we see an upregulation of the genes in mice at the peak of disease (red) and still slightly during recovery (blue) as well as for HLA-A and HLA-C genes in all three forms of MS lesions. The HLA-B gene shows an enrichment only in the initial and active white matter lesions (dark and light green), whereas the cortical lesions (bright green) show an opposing downregulation (Figure 33C+D). All in all, this mirrors the neuronal results in EAE mice for classical MHCI genes and pathway related genes.

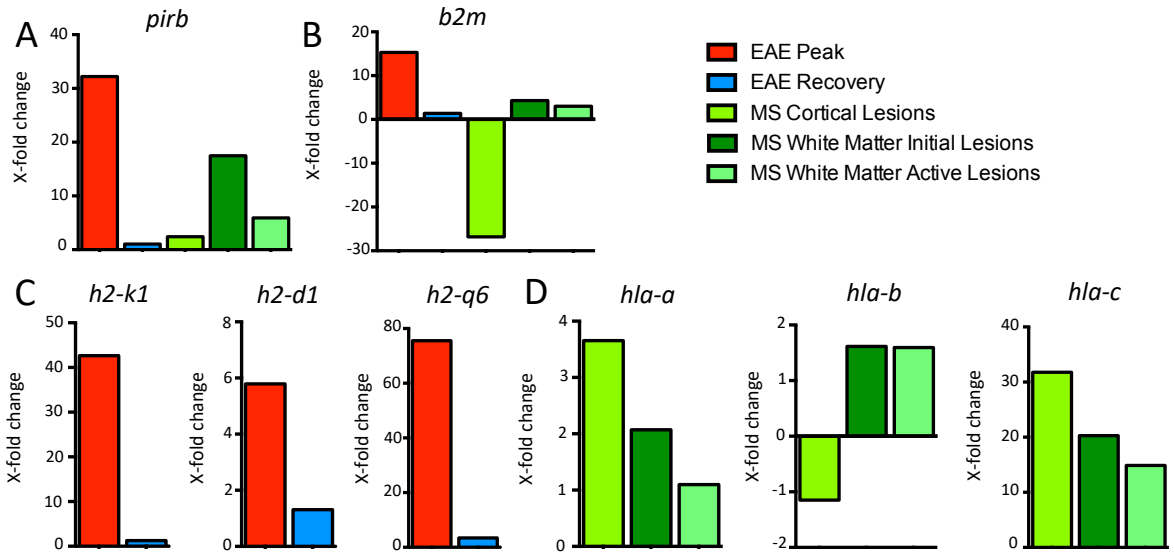

Figure 33: Comparison of the MHCI genes during EAE and MS shows obvious coincidence

A: Expression of *pirb* in the time course of EAE and its change in expression in MS lesions
B: Differential expression of *b2m* in peak and recovery of EAE and the expression seen in different MS lesions
C: Expression of the major MHCI genes *h2-k1, h2-d1* and *h2-q6* in mice, which show highly upregulation at the peak of disease and still during recovery phase.
D: Major MHCI genes in humans, *hla-a, hla-b* and *hla-c* mainly show an upregulation in gene expression as well, with MS cortical lesions as an exception.
Control, Peak and Recovery (N=3), Cortical lesions (N=1), White matter initial and active lesions (N=3).

Comparing genes from the mevalonate pathway (Figure 34A) and the cholesterol biosynthesis pathway (Figure 34B) which were prominently downregulated during recovery phase of EAE, we found varying results in humans. For *hmgcr* only the white matter lesions are in line with our results, whereas for *hmgcs1* only the cortical lesion shows the same downregulation. The gene *mvk* replicates the murine data, but *mvd* and *fdft1* in contrast show the opposite. For *sqle* and *lss* only the cortical lesions and the initial white matter lesions are comparable to our results, whereas for *cyp51*, both white matter lesions match. Another total overlap can be found for *tm7sf2*, were indeed all three human MS lesions show the same downregulation as we can see in the recovery phase of mice. In contrast, the next two genes downstream of *tm7sf2*, *nsdhl* and *dhcr24* are contrary to our data. The last gene *dhcr7*, we compared in this set of genes shows the same downregulation only in active white matter lesions. The pathway of cholesterol biosynthesis is hardly comparable between human and mice, as the data gives very contradictive results of differential gene expression (Figure 34A+B).

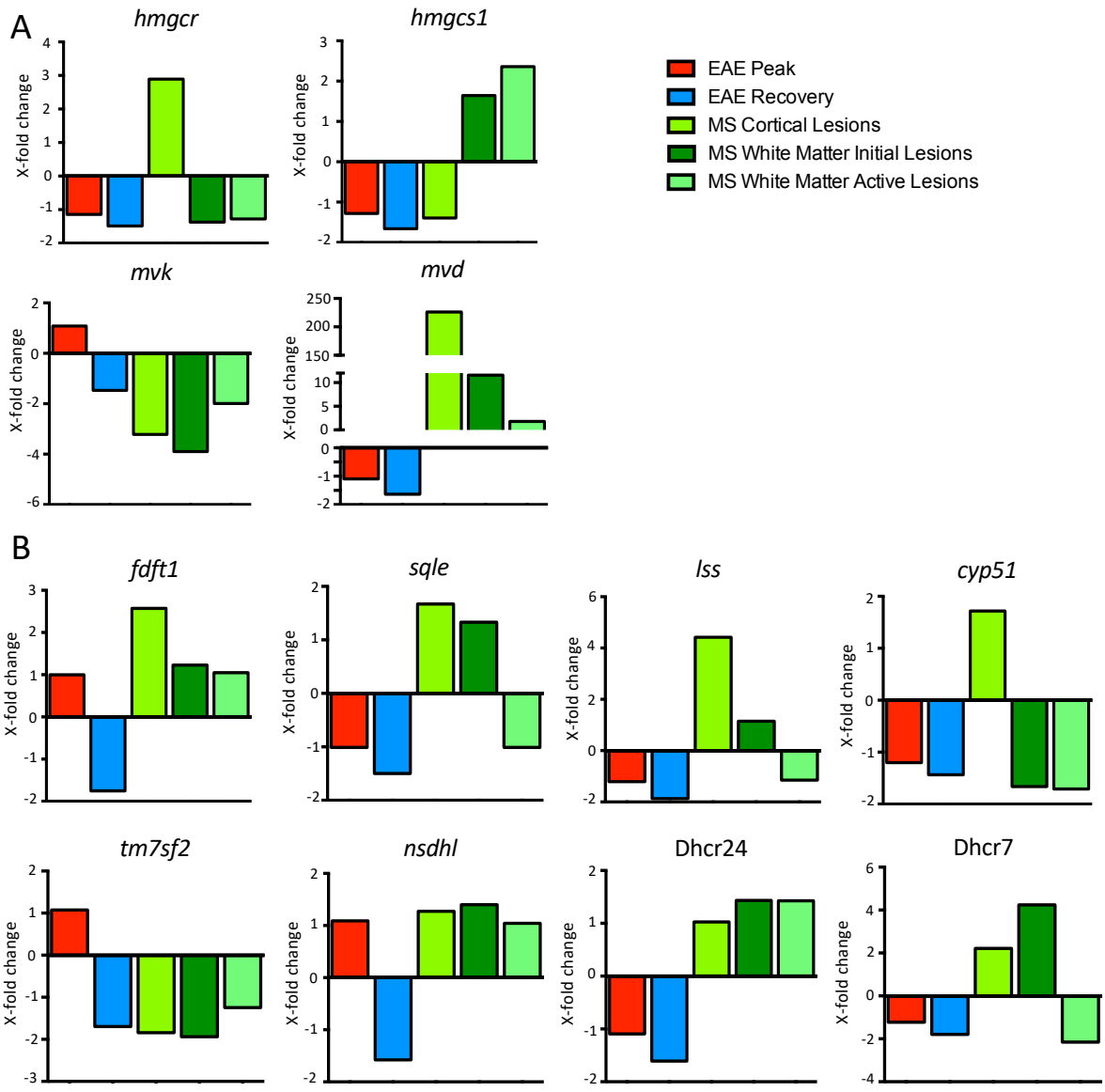

Figure 34: Differential expression of the Cholesterol biosynthesis shows barely correlation in EAE and MS

A: Expression of the mevalonate pathway genes *hmgcr*, *hmgcs1*, *mvk* and *mvd* compared in EAE mice and human MS patients.
B: Comparisson of the genes *fdft1, sqle, lss, cyp51, tm7sf2, msdhl, dhcr24* and *dhcr7*, of the cholesterol biosynthesis, which are highly downregulated during recovery phase of EAE in comparison to MS lesions from different regions.
The expression in humans do not follow the same consistent direction as is it seen in neurons during EAE. The expression profile of cortical lesions, white matter initial and white matter active lesions in general very uncommon. Only *mvk* and *tm7sf2* coincide in the downregulation of the genes for all kinds of lesions. Control, Peak and Recovery (N=3), Cortical lesions (N=1), White matter initial and active lesions (N=3).

For the IL17 receptor genes we could find correlations of the human and murine data sets for *il17ra* at peak of EAE and MS initial white matter lesions. Also for recovery phase of EAE and cortical as well as active white matter lesions correlations are detectable. For *il17rc* the murine data for peak and recovery only matches with the white matter lesions but not with the cortical lesions (Figure 35A). *Ifnγr1* corresponds in recovery phase data and all human MS lesions. The

neuronal AMPA receptor subunit gene *glur1* shows a slight downregulation in general, only in cortical lesions it seems to be up in expression level (Figure 35B+C).

Regarding the JAK/STAT pathway the results differ a lot. Already the different human datasets of MS lesions are so various that a comparison to the murine NGS data appears not to be possible (Figure 35D+E).

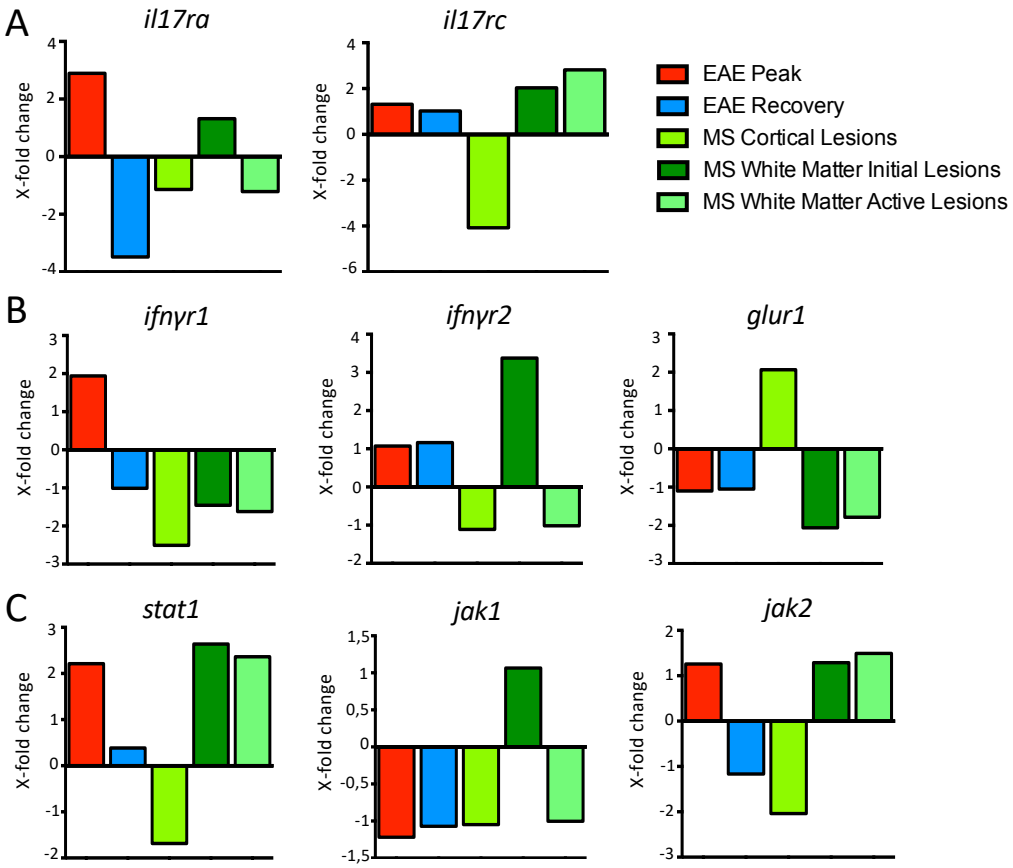

Figure 35: Expression profile of the IL17 and IFNγ receptor with downstream cascade has almost no correlation between EAE and MS

A: *il17ra* and *il17rc* expression profile in comparison between neurons of EAE mice and human MS patient lesions
B: Expression profile of *ifnγr1/2* with the interaction partner *glur1* at peak and recovery and lesions of MS patients.
C: The genes *stat1, jak1 and jak2* of the *JAK*/STAT pathway compared in human and mice in MS and EAE.
The data of human and mice shows hardly any correlation for the illustrated genes.
Control, Peak and Recovery (N=3), Cortical lesions (N=1), White matter initial and active lesions (N=3).

4. Discussion

4.1. Isolation of Neuronal RNA

Using papain for CNS tissue digestion results in relatively low cell death compared to the usage of collagenase, trypsin and other digestion enzymes (Kaiser et al., 2013). This is the major reason we used the kit from *Miltenyi Biotec* which is based on papain to break cell-cell interaction and separate CNS cells in adult mice to isolate neurons by FACS as well as for the depletion of non-neuronal cells. Still neuronal axons and dendrites will most likely be destroyed with this method and the mRNA being transported from the nucleus to the periphery of the cell will be lost (Aigner and Caroni, 1993; Cajigas et al., 2012; Müller et al., 2013). Not only mRNA, but also ribosomes, as an essential part of the translation machinery, were shown to be present in axons (Bunge, 1973; Tennyson and Brzin, 1970; Zelená, 1970). Focussing on mRNA derived from dendrites and axons, the digestion methods including mechanical force to split up the tissue are not optimal. Our focus was not only directed on axonal and dendritic mRNA, but rather to gather pure neuronal RNA with the best possible quantity and quality. The RiboTag technique prevents the loss of the mRNA information derived from axons and dendrites.

Removal of cell debris and myelin from a CNS cell suspension is usually performed by density gradients with percol or sucrose. Isolation of microglia and oligodendrocytes from the CNS could also be demonstrated using those methods (Berti Mattera et al., 1984; Bruttger et al., 2015; Wang et al., 2013). But for the isolation of neurons percol and sucrose gradients are not the best choice. The majority of neurons will settle in a layer together with myelin after centrifugation and will be lost after removing this part, which logically reduces the quantity of neuronal RNA. Motor neurons of foetal mice and hippocampal neurons of adult rats could be isolated using an Optiprep density gradient (Majd et al., 2008; Wang et al., 2017). We also used different kinds of Optiprep density gradients, but in our hands the protocols turned out to be not as efficient as the RiboTag method which we choose for our study. The resulting RNA of the isolated neurons using the Optiprep density gradient was not as pure as it was for the isolation by FACS, depletion of all non-neuronal cells or using RiboTag mice (data not shown). Therefor myelin was removed further on by Myelin Removal Beads from *Miltenyi Biotec* to achieve a separation of neurons and other glial cells from the myelin without stress induced by the gradient media itself or centrifugation which is part of the gradient protocol.

FACS sorting of neurons from adult rat brains based on an intracellular staining of NeuN, a commonly used neuronal marker, was done before (Guez-Barber et al., 2012), but the RNA

quality is decreased by the fixation which is necessary for the intracellular staining. The protocol for sorting eYFP$^-$ neurons by FACS was established before by panning purification of oligodendrocytes and FACS sorting of eYFP$^+$ astrocytes (Cahoy et al., 2008). But this was impossible for adult mice thus it only works for embryonic and young mice until an age of 8 days. The purification of juvenile and adult neurons from mouse brains by FACS was performed in a study from striatonigral and stratopallial neurons in the basal ganglia, located beneath the cerebral cortex, from GENSAT BAC transgenic mice and used for microarray analysis (Lobo et al., 2006). This study only focusses on specific subtypes of neurons whereas we want to purify all neurons from the brain to examine overall neuronal gene expression. Purifying neuron subtypes would not result in a representative neuronal RNA profile of the CNS. We used the expression of cytoplasmatic eYFP by the murine Thy1.2 minigene to FACS sort the neurons (Hirrlinger et al., 2005). The high output of 75.8% of eYFP positive viable cells might be due to fluorescence debris and fluorescence cell fragments as only 45.8% were NeuN positive viable neurons before FACS sorting. This is a consequence of the cytoplasmatic eYFP expression resulting in eYFP positive cell debris containing axon fragments and cannot be excluded. Some of these positive fragments also stick to glial cells, which explains the fact that we could only enrich neurons up to only 62% viable cells based on NeuN staining. The neuronal purity could not be increased by a more stringent gating of eYFP positive neurons during sort to exclude possible autofluorescence (data not shown). A further enrichment of neurons could be achieved by culturing sorted neurons under appropriate conditions. But this could lead to a complete change of neuronal RNA profile and would not allow for an *ex vivo* analysis, which was the aim of this study.

We see Dcx, a marker for neuronal precursor cells, higher enriched then Tubb3, which is a marker for mature neurons. It can be concluded that neuronal precursor cells, which are likely easier to separate from other CNS cells as they have fewer axonal branches, are preferentially isolated with this method. We do not observe a reduction of glial markers, even if an enrichment of neuronal markers could implicate even that. This might be because the neuronal enrichment is not high enough to see a reduction of RNA level by qPCR analysis. Also it is known that early neuronal precursors, which are already eYFP positive, still express Gfap, which explains the enrichment of Gfap after FACS sorting (Ming and Song, 2011).

A more efficient enrichment of neurons by FACS sorting could be obtained by using a mouse strain expressing eYFP or any other fluorescence protein in the nucleus instead of the cytoplasm, which could lower the amount of fluorescence debris and eYFP positive axonal fragments.

Isolating neurons by depleting all other non-neuronal cells of the CNS by specific antibodies leads to a high amount of cell debris together with the neurons in the flow through, if the kit is used as recommended in the user manual. Adult CNS contains much more myelin compared to embryonic tissue, for which the kit normally is used for. This leads to a high loss of neurons during the procedure as mature neurons are sticking to surrounding glial cells by myelin and are kept in the column during depletion. Only with our modifications the yield of neurons could be increased up to 86,5% purity based on viable cells and NeuN staining. NeuN negative cells could be damaged neurons without detectable NeuN or cell debris which cannot be stained with the Fixable Viability Dye eFluor®780 due to a low amount of DNA.

The biggest advantage of depleting non-neuronal cells to isolate neurons compared to FACS sorting of eYFP expressing neurons is that transgenic mice are redundant. As the neuronal isolation is based on depletion of all non-neuronal cells this method cannot be used if other cell types then in the healthy CNS are present. In the case of EAE immune cells invade the brain and must be depleted as well to ensure a proper isolation of neurons.

The RiboTag method is best suitable for our study. Neuronal RNA can be harvested without isolating adult neurons before. Thus damage to neurons especially axons and dendrites and potential change in gene expression during the procedure can be avoided. Furthermore, RNA can be isolated in high quality and quantity which is essential for NGS and deep-sequencing analysis. To perform RiboTag experiments special RiboTag transgenic mice must be used. The purity of isolated RNA is also dependent on the specific Cre mouse line used for each experiment. With the use of the neuron specific NFH-Cre mouse line, it was possible to isolate pure neuronal RNA. To also analyse genes with a low gene expression, the Input sample, taken before immunoprecipitation of neuronal ribosomes, must be considered to exclude potential background from unspecific binding during the procedure. Still our convincing results show the utility of the method so chosen.

4.2. Sequencing and Analysis of Neuronal RNA

Sequencing neuronal RNA, which was isolated by the RiboTag method, is limited for genes which are at a very low level of expression, due to the background of unspecific RNA bound to the beads during the procedure of immunoprecipitation. The level of this background is relatively low and cannot be detected by analysis with qPCR, but NGS is much more sensitive and detects also minor quantities of RNA. This must be considered especially when comparing EAE samples to those from healthy controls. RNA of invading immune cells during EAE potentially can bind unspecific to the beads during the RiboTag method and sequenced as

background. This could be avoided by sequencing the input sample, taken before immunoprecipitation, of each sample as well. With this data a normalization of each sample to the input is possible before analysing and comparing the samples of the different groups but also doubles the cost of the sequencing experiments. Without sequencing the input for each sample, genes with low expression level must be handled carefully to avoid comparing unspecific background which will result in false differential gene expression. Even if the data was handled carefully and this fact was considered as much as possible one cannot exclude all background and it is still possible that some of the upregulated genes, which outnumber the downregulated genes, are false positive.

The analysis of the sequence data was done with iPathwayGuide, an online tool to perform pathway analysis. Significant differentially expressed genes at the peak of disease and during recovery phase compared to controls are used to perform a meta-analysis to find pathways which are effected in the time course of EAE. This tool is a novel online tool, used by several scientists already and was found to be as practical and comparable as other sequence analysis tools like Ingenuity (Ahsan and Drăghici, 2017; Bober et al., 2019; Jiang et al., 2018; Kaur et al., 2018). The big disadvantage of this tool and the pathway analysis is the exclusion of all genes without significance after the threshold for statistics is set. Genes which are differentially expressed but do not reach statistical significance are not considered in the total pathway analysis. But these genes could still be relevant especially when performing a meta-analysis and comparing genes between the peak of EAE and the recovery phase. We only found 6 pathways with 21 genes overlapping in both time points of EAE, but there might be much more which are only significant in one or the other time point but are excluded in the analysis due to previous settings. With this analysis every pathway of interest must be checked manually for genes which might still be of importance but do not show up due to statistical relevance. Overall, there is a big loss of information which cannot be avoided using iPathwayGuide and might be also true for other tools of transcriptome analysis.

So far, the transcriptome analysis of neurons during EAE is totally novel. There were studies of differential gene expression in the spinal cord of rats during EAE (Inglis et al., 2012). But these microarrays were not neuron specific and included all invading immune cells during EAE as well. All genes being expressed exclusively by these cells and not by CNS resident cells are upregulated in this study. But interestingly already in this study they could show that cholesterol pathway genes are mainly downregulated in EAE rats compared to healthy controls (Inglis et al., 2012) in consistency with our results in neurons. Another study focusing on molecules for cholesterol biosynthesis (HMGCR), recycling (ApoE) and degradation (Cyp46A1) show with

qPCR and western blots that cholesterol biosynthesis in spinal cord of rats is reduced during peak of disease, whereas in the end of disease HMGCR levels are back to control (Lavrnja et al., 2017). That is in contrast to our results where HMGCR is even more reduced during recovery phase. One can conclude that the further reduction of HMGCR during the recovery phase is neuron specific and does not occur in the average analysis of all CNS resident cells and invading immune cells.

4.3. EAE with Knockout of Different Candidate Genes

To test the influence of PirB in neurons on EAE, we used Camk2-Cre/PirB$^{fl/fl}$ mice for EAE experiments in comparison with WT controls. The EAE does show the tendency of a reduced severity of the disease as we would expect due to the role of PirB in development and other diseases, but the results do not reach significance. This could possibly be since the knockout is not neuron specific and lack PirB as well in different glia cells, like microglia and astrocytes. Another possibility is the number of mice used for EAE. Due to breeding problems and few numbers of pubs from the breeding which harbour the right genotype, the EAE was performed in 3 rounds with small groups (N=1-3) and summarised for analysis (total N=7). Using higher amounts of animals in a big group could make the result significant as we already saw the tendency. A neuron specific knockout could be tested in further studies but was not carried out for this project. The knockout of MHCI, which can interacts with PirB and was already shown to be neuroprotective in stroke, could give further valuable insight into the mechanisms of neuronal response to EAE (Adelson et al., 2012).

The fact that MHCI presentation is mainly a defence mechanism for intracellular infections like viruses, which is not the case in EAE, the upregulation of MHC class I and other molecules of the mechanism could also only be a self-defence mechanism against destruction of the increasing numbers of T cells being present during EAE.

The knockout of IL17RA was neuron specific by crossing IL17RA$^{fl/fl}$ mice to the NFH-Cre line. Although the EAE did not show a significant difference compared to control littermates without NFH-Cre we could see a delayed onset of EAE symptoms in some animals and some of the performed EAEs. Nevertheless, the phenotype was not consistent and in conclusion of all performed EAEs did not reach significance. Il17RA is expressed on the surface of neurons, which was already known before, but in a minor quantity, as seen in our data as well. This few changes could be the reason for the absent phenotype even if the differential expression is significant. The expression of IL17RA might be restricted in its role to other cell types during EAE and does only play an important role in neurons.

The neuron specific knockout of IFNγR1 did not show any significant phenotype during EAE as well, even if it has a tendency to be less severe. We hypothesised that the interaction of IFNγR1 with the AMPA receptor GluR1 would lead to reduced Ca^{2+} influx to the neurons if IFNγR1 is removed (Mizuno et al., 2008). One reason why this hypothesis failed is the consistent expression of GluR1, which is not altered in expression level during the time course of EAE. Reduction of IFNγR1 might not be relevant if GluR1 is still be expressed on the neuronal surface. The actual Ca^{2+} influx during EAE was not tested for this knockout animals but does not seem to be relevant in this case as they do not show any effect during EAE due to IFNγR1 deficiency in neurons.

Genes which are differentially expressed during recovery might be from special interest for MS patients as they already have the disease and hope for recovery, which is not possible with the current medication. Maybe the genes differentially expressed during recovery phase in EAE are important for resolving the disease of the mice and could be translated to humans. For this reason, we decided to focus on the recovery phase and pick HMGCR as a candidate gene to study its role during EAE.

$HMGCR^{fl/wt}$/NFH-Cre mice develop phenotypically normal and have no obvious signs of any neurological deficit. Still this has to be tested performing behavioural studies and neurological test to exclude any phenotypes already present during steady-state with naïve conditions. For example the Smith-Lemli-Opitz syndrome results from a mutation on the 7-dehydrocholesterolreductase (Dhcr7) and causes profound brain development abnormalities, intellectual disability, emotional and sleep disorders (Nowaczyk and Irons, 2012). As Dhcr7 is one of the downstream enzymes of HMCGR in the cholesterol pathway, the knockout of HMGCR could result in a similar phenotype and must be evaluated. These studies have to be the destination of further experiments and are not included in this work.

EAE performed with heterozygous knockout of HMGCR specifically in neurons show a significantly more severe EAE with higher scores at the peak of disease and reduced recovery until dpi 30. This EAE phenotype is the result of more invading immune cells being present in the CNS causing higher neuronal damage and less myelination during recovery phase. The pathway of cholesterol biosynthesis has several possibilities of feed-back mechanisms, where the cholesterol content regulates the cholesterol homeostasis via negative-feedback for example the SREBP-2/SCAP/INSIG-1 pathway (Peake and Vance, 2012). In the heterozygous knockout of HMGCR the protein level of HMGCR shows a reduction by fluorescence of the antibody staining. But if a heterozygous knockout causes a halving of the expression level was not checked yet, due to missing of the right genotype. To study the RNA level of HMGCR by qPCR

neuronal RNA must be isolated from the heterozygous knockout mice. This is only possible with HMGCR$^{fl/wt}$/RiboTag$^{fl/fl}$/NFH-Cre mice and not with the experimental HMGCR$^{fl/wt}$/NFH-Cre mice, as immunoprecipitation of neuronal ribosomes with incorporated mRNA essentially needs the RiboTag. This needs to be part of further analysis and future studies and is not included in this thesis. The reason why there are more invading immune cells and more neuronal damage together with less myelination in HMGCR$^{fl/wt}$/NFH-Cre mice during EAE is not clear yet and can only be hypothesized about with the knowledge of the role of cholesterol in neurons and in other neurological diseases.

4.4. Role of Cholesterol in Neurons

Cholesterol has a high impact on neuronal function. It increases the velocity of action potential movement by playing a role in isolating the axons with a myelin sheath. Further, it allows to form a very compact myelin coat. Last, the information conduction is dependent on the permeability of the plasma membrane of axons. Cholesterol in interaction with other lipids is determining the membrane permeability. Consequently, the support of cholesterol is highly important for neurons to facilitate their large membrane surface and to conduct incoming information rapidly (Dietschy and Turley, 2004; Zhang and Liu, 2015).

To elucidate the role of HMGCR regarding the myelination of neurons, its function during embryonic development must be considered as well. It is suggested that HMGCR is essential in the myelination process in early development (Ohashi et al., 2003b). The enzyme is a major element in the cholesterol synthesis, and as mentioned cholesterol is necessary for myelination. A disturbed cholesterol synthesis during early stages of development has crucial impacts. It can lead to inhibition of dendritic and synaptic maturation, reduction of dendritic outgrow and neuronal cell death (Fan et al., 2002; Mauch et al., 2001) with severe consequences like brain disorders, holoprosencephaly and embryonic lethality (Ohashi et al., 2003b; Tozawa et al., 1999). This is the reason why the phenotype of mice with a homozygous knock-out of HMGCR are embryonic lethal and cannot be used as experimental mice. It elucidates how important a constant cholesterol supply is during development and highlights the major role of HMGCR for the cholesterol biosynthesis. In general, once the development is completed, adult neurons are not dependent of an own cholesterol production. Fünfschilling and colleagues discovered that some adult neurons can survive with a lack of own cholesterol synthesis. The phenotype of mice with interrupted cholesterol synthesis is indistinguishable from wild type mice and no motor deficits are observed (Fünfschilling et al., 2007). This might be due to other supply mechanisms as horizontal cholesterol flux from the BBB by apolipoprotein E (ApoE) uptake

and the supply by glia cells (Fünfschilling et al., 2007; Pfrieger, 2003). It is suggested that adult neurons have a very low turnover of cholesterol and become dependent on astrocytes after their development is completed (Morell and Jurevics, 1996b; Pfrieger, 2003; Toews et al., 1996). This might be one reason why adult neurons are not visibly affected by a interrupted cholesterol synthesis in steady-state in the heterozygous knockout mice and the phenotype becomes only substantial during EAE.

4.5. HMGCR in Other Cell Types During EAE

As mentioned above, HMGCR is necessary for the myelination of neurons and seems to play a major role in their development. But the enzyme is not only essential in neurons. Lacher et al. found that HMGCR is also important for the survival of T and B cells. By tissue-specific deletion of HMGCR in T cells, they detected an increased rate of apoptosis in $CD4^+$ and $CD8^+$ T cells. The T cell specific knock-out of HMGCR caused the death of those cells. It is further assumed that a deletion of HMGCR in any other cell type will in the end cause the death of the cell. Regarding this, it gets clear that HMGCR must play a key role in the survival of cells which is not only due to its function in cholesterol synthesis. When Lacher et al. induced EAE in mice deficient for one allele of HMGCR they detected no difference as the mice showed similar T cell numbers compared to control mice. This suggests that the heterozygous deletion of HMGCR did not affect the development of T cells, as one allele obviously expressed sufficient amounts of HMGCR (Lacher et al., 2017). In neurons, however, the heterozygous knock-out was sufficient to change the phenotype of mice during EAE. It would be informative to examine a HMGCR deletion for example in oligodendrocytes which are highly important for remyelination during EAE (Miron et al., 2009a) or in astrocytes which are the main suppliers of cholesterol for adult neurons (Nieweg et al., 2009b). These experiments must be performed in future and are not included in this study.

4.6. Results in Context to MS Treatment

For the treatment of several neurological diseases like Alzheimer's Disease (AD), Parkinson Disease (PD), ischemic and haemorrhagic stroke as well as Multiple Sclerosis (MS) drugs, known as statins, are most commonly prescribed, as they have a pleiotropic effect on disease progression (Willey and Elkind, 2010b). Statins impair the conversion of HMG-CoA to mevalonate by competitively inhibiting HMGCR (Chakravarti et al., 2018). In consequence, the biosynthesis of cholesterol is impaired.

This stands in contrast to the results of this study, because neuron specific HMGCR deletion worsened the disease progression of EAE. One reason could be that the potential therapeutic benefit of statin treatment do not only depend on a decreased cholesterol level but is also thought to be due to their function as immune modulators with anti-inflammatory properties (Greenwood et al., 2006). A step for leukocytes to pass the BBB is the degradation of the plasma membrane. Therefore, leukocytes produce matrix metalloproteinase (MMP) which ease the passage through the membrane. Statins interrupt the expression of MMP in leukocytes and so prevent migration of blood cells to the CNS (Greenwood et al., 2006). Furthermore, statins inhibit proinflammatory cytokine release by microglia and astrocytes (Goldman and Cohen, 2008a). Some cytokines in the brain induce iNOS (inducible nitric oxide synthase) expression which results in toxic NO (nitric oxide) production. This harms the myelin sheath of neurons and it is thought to contribute to oligodendrocyte degeneration during MS. Nevertheless, lovastatin showed to inhibit this cytokine-mediated iNOS expression and so decreased inflammation in the CNS (Greenwood et al., 2006). As presented, statins seem to have pleiotropic properties which appear to be beneficial on disease progression. Nevertheless, until now there is no satisfying answer to the question about the role of HMGCR during MS. But indeed, not only positive effects of statin treatment were reported. *In vivo* and *in vitro* models showed that statins can impair the remyelination during recovery phase. Two essential processes for remyelination can be inhibited by the treatment of statins: the oligodendrocyte maturation from oligodendrocyte precursor cells (OPC) and the myelin formation in mature oligodendrocytes (OLG) (Klopfleisch et al., 2008; Miron et al., 2009b). This was observed by Miron et al. in a long-term treatment with simvastatin where they used a cuprizone model to investigate the consequences of statin treatment on demyelination and remyelination in the brain. By using this model, similar observation as in MS lesions could be made, except there were no immune system related factors involved. They showed *in vivo* that simvastatin affects the myelin repair and maintenance by impacting OPC and OLG function and maturation. As simvastatin blocks the isoprenylation, survival of oligodendroglial cells is impaired through influencing the cell signalling. What is very important in OPC differentiation is the acquisition of signalling molecules of lipid rafts. This recruitment of cytoskeleton-associated proteins to lipid rafts in OLGs is essential for the initiation of myelin production. By statin treatment membrane cholesterol is decreased and so OPCs are kept in an immature state and are hindered to produce new myelin (Miron et al., 2009b).

This impairment of myelination supports the observations described in this thesis. The suppression of HMGCR in neurons led to an insufficient recovery, which could be caused by a

decreased remyelination by OLGs or increased demyelination. Consequently, the inhibition of HMGCR by statins should have a negative effect on EAE progression. Another possible explanation could be that statin treatment influences the cholesterol level in every cell type of the organism. In contrast to this, the knock-out of HMGCR in the experimental mice of this thesis was neuron specific. Maybe there are some important interactions between different cell types contributing to recovery in statin treatment which must be regarded. Furthermore, it must be considered that MS and EAE are still two different diseases, whereby EAE is just a model for the disease. Interspecies differences remain and pathways that are yet poorly understood but which could be important to fully understand the disease have to be studied further (Goldman and Cohen, 2008b).

4.7. Comparison with MS Patients Data

If we compare our data of neuronal response to EAE with data of MS patients we can find as many similarities as distinctions (Fischer et al., 2013, 2012). The main reason might be that EAE and MS are not comparable in many points (Fletcher et al., 2010; Pierson et al., 2012; Steinman, 1999; Van Kaer et al., 2019) and also that our study is only focussing on neurons specifically. The gene arrays of MS patients have been made on archival, formaldehyde fixed and paraffin embedded material. The sequencing does not work for all genes, being included in the arrays. It only works for genes with array sequences relatively close to the polyA tail. Thus, one will find many genes with very low expression levels and without dynamics in the expression in relation to controls, MS or activity stage of the lesions. Such genes must be excluded from the analysis since it can't be ensured whether there is really such a low expression or whether they are false negative due to higher distance to the polyA tail. In any way, the arrays are very useful, when one does concentrate on those genes, where one can find a clear signal, which in addition is related to lesion type and stage. Comparing given genes from EAE studies to this MS patient data sets on the other hand is very complicated and must be done with caution and will not work for all genes. Even if the data of Hans Lassmann and colleagues did not correspond completely to ours in case of HMGCR and the cholesterol pathway, other studies support our findings by showing that HMGCR and other enzymes involved in the pathway of lipid metabolism like stearoyl CoA desaturase (SCD), acetoacetyl-CoA thiolase, propionyl-CoA carboxylase and enoyl-CoA hydratase are downregulated in brain tissue of MS patients (Inglis et al., 2012).

5. Summary

In this study we aim to unravel the neuronal response to invading immune cells during the time course of EAE. After testing different isolation methods like FACS and MACS, we describe the isolation of pure neuronal mRNA from adult mice by the RiboTag technique. Isolated mRNA from mice at the peak of EAE (dpi16) and during the recovery phase (dpi30) was sequenced and compared in a detailed pathway analysis with healthy naive control mice. Meta-analysis of the three experimental groups revealed 1108 genes being differentially expressed at the peak of disease and 113 changed in expression level during recovery phase compared to control animals. These genes can be sorted in 108 and 24 different pathways respectively. Only 21 genes belonging to 6 pathways show overlapping between peak and recovery. After validation of the sequencing data by qPCR different candidate genes from the top 10 pathways of peak and recovery were picked to study their role in neurons during the time course of EAE. The candidate genes PirB, IL17RA and IFNγR1 were chosen due to their upregulation at the peak of disease and their known relevance during EAE itself or other neurological disorders. The knockout animals used for EAE studies were either used in collaboration (PirB) or were directly generated in our lab (IL17RA and IFNγR1). The EAE experiments performed with a neuronal specific knockout of either IL17RA or IFNγR1 as well as with a CNS resident cell specific knockout of PirB, showed a normal EAE phenotype. Thus leading to the clear conclusion that they do not play a major role in neuronal response to EAE. The forth candidate gene we picked due to its main appearance during recovery phase of EAE. The complete cholesterol biosynthesis with the key enzyme HMGCR was significantly downregulated already at the peak and even more prominently during recovery phase of EAE. The heterozygous neuron specific knockout of HMGCR ($HMGCR^{fl/wt}$/NFH-Cre) showed a more severe EAE with higher scores at the peak of disease and a reduced ability to recovery from the disease. FACS analysis revealed significant more microglia and neutrophils at the peak of disease as well as more invading $CD4^+$ T cells at the peak and during recovery phase. On top of that histology displays less myelination with higher neuronal damage in the spinal cord of the knockout mice explaining the higher clinical scores and the reduced recovery rate. Comparing the NGS data of EAE animals with data of MS patients we could identify several correlations. Especially comparing MHCI genes in mice and humans the agreement was blatantly obvious.

6. Zusammenfassung

Das Ziel dieser Studie ist es die neuronale Antwort auf einwandernde Immunzellen während dem Verlauf der EAE zu untersuchen. Nachdem unterschiedliche Methoden wie FACS und MACS getestet wurden, beschreiben wir die Isolation von neuronaler mRNA aus adulten Mäusen durch die RiboTag Methode. Isolierte mRNA von dem Höhepunkt der Krankheit (Tag 16) und während der Besserungsphase (Tag 30) wurde sequenziert und mit gesunden Kontrolltieren durch eine detaillierte Signalweganalyse verglichen. Eine Meta-Analyse der drei Experimentalgruppen zeigt eine differentielle Genexpression von 1108 Genen während dem Höhepunkt der Krankheit und 113 während der Besserungsphase. Diese Gene können 108 beziehungsweise 24 unterschiedlichen Signalwegen zugeordnet werden. 21 Gene aus 6 Signalwegen zeigen eine differentielle Genexpression zu beiden Zeitpunkten. Nach Validierung der Sequenzierung durch qPCR wurden verschiedene Kandidatengene aus den Top 10 der differentiell exprimierten Signalwege ausgewählt um ihre Rolle in der neuronalen Antwort während dem Verlauf der EAE genauer zu untersuchen. Die Kandidatengene PirB, IL17RA und IFNγR1 wurden aufgrund ihrer Hochregulierung auf dem Höhepunkt der Krankheit gewählt und wegen ihrer bekannten Relevanz während der EAE und anderen neurologischen Erkrankungen. Knockout Mäuse dieser Gene wurden entweder in Zusammenarbeit mit anderen Gruppen (PirB) untersucht oder durch Kreuzung in unserem Labor gezüchtet (IL17RA und IFNγR1) um EAE Experimente durchzuführen. Der Krankheitsverlauf keiner dieser drei knockout Tiere zeigte einen Phänotyp im Vergleich zu den Kontrolltieren woraus sich schließen lässt, dass alle drei Kandidatengene keine tragende Rolle bei der neuronalen Antwort während der EAE spielen. Das vierte Kandidatengen Hmgcr wurde Aufgrund der deutlichen Herrunterregelung von sich und seines gesamten Signalweges der Cholesterol Biosynthese, während dem Höhepunkt der Krankheit und noch signifikanter in der Besserungsphase, gewählt. Der heterozygote neuronale Knockout von Hmgcr ($HMGCR^{fl/wt}$/NFH-Cre) zeigt einen heftigeren Krankheitsverlauf mit höhere EAE Werte während dem Höhepunkt der Krankheit und signifikant reduzierter Verbesserung dieser Werte in der Besserungsphase. FACS Analyse zeigt erhöhte Anzahl von Mikroglia und neutrophilen Zellen zum Gipfel der Krankheit und zusätzlich mehr einwandernde $CD4^+$ T Zellen am Höhepunkt der EAE und in der Phase der Besserung. Darüber hinaus verdeutlicht Histologie eine reduzierte Myelinisierung und stärkeren neuronalen Schaden in der Lumbalregion des Rückenmarks was die höheren Krankheitswerte und das reduzierte Vermögen zur Besserung erklärt. Vergleicht man die Daten der Sequenzierung von EAE Mäusen mit MS Patientendaten kann man verschiedene Übereinstimmungen finden, besonders bei der differentiellen Expression der MHCI Gene in Mensch und Maus zeigen sich offensichtliche Korrelationen.

7. References

Abdarasulova, I.N., Serdiuk, S.E., Gmiro, V.E., n.d. [Combined blockade of GluR1 AMPA and NMDA receptors effectively eliminates neurological disorders in rats with experimental allergic encephalomyelitis]. Eksp. Klin. Farmakol. 70, 15–9.

Adelson, J.D., Barreto, G.E., Xu, L., Kim, T., Brott, B.K., Ouyang, Y.-B., Naserke, T., Djurisic, M., Xiong, X., Shatz, C.J., Giffard, R.G., 2012. Neuroprotection from Stroke in the Absence of MHCI or PirB. Neuron 73, 1100–1107. doi:10.1016/j.neuron.2012.01.020

Ahsan, S., Drăghici, S., 2017. Identifying Significantly Impacted Pathways and Putative Mechanisms with iPathwayGuide. Curr. Protoc. Bioinforma. 57, 7.15.1-7.15.30. doi:10.1002/cpbi.24

Aigner, L., Caroni, P., 1993. Depletion of 43-kD growth-associated protein in primary sensory neurons leads to diminished formation and spreading of growth cones. J. Cell Biol. 123, 417–429. doi:10.1083/jcb.123.2.417

Aktas, O., Smorodchenko, A., Brocke, S., Infante-Duarte, C., Topphoff, U.S., Vogt, J., Prozorovski, T., Meier, S., Osmanova, V., Pohl, E., Bechmann, I., Nitsch, R., Zipp, F., 2005. Neuronal Damage in Autoimmune Neuroinflammation Mediated by the Death Ligand TRAIL. Neuron 46, 421–432. doi:10.1016/j.neuron.2005.03.018

Alsterberg, G., 1956. [The physical and chemical structure of nerve fibers in the spinal cord]. Mikroskopie 10, 293–322.

Amatya, N., Garg, A. V, Gaffen, S.L., 2017. IL-17 Signaling: The Yin and the Yang. Trends Immunol. 38, 310–322. doi:10.1016/j.it.2017.01.006

Ballabh, P., Braun, A., Nedergaard, M., 2004. The blood–brain barrier: an overview. Neurobiol. Dis. 16, 1–13. doi:10.1016/j.nbd.2003.12.016

Berl, S., Karram, K., Scheller, A., Jungblut, M., Kirchhoff, F., Waisman, A., 2017. Enrichment and isolation of neurons from adult mouse brain for ex vivo analysis. J. Neurosci. Methods 283, 15–22. doi:10.1016/j.jneumeth.2017.03.015

Berti Mattera, L.N., Larocca, J.N., de Iraldi, A.P., Pasquini, J.M., Soto, E.F., 1984. Isolation of oligodendroglial cells from young and adult whole rat brains using an in situ generated percoll density gradient. Neurochem. Int. 6, 41–50.

Billiau, A., Matthys, P., 2001. Modes of action of Freund's adjuvants in experimental models of autoimmune diseases. J. Leukoc. Biol. 70, 849–60.

Bittner, S., Afzali, A.M., Wiendl, H., Meuth, S.G., 2014. Myelin Oligodendrocyte Glycoprotein (MOG₃₅₋₅₅) Induced Experimental Autoimmune Encephalomyelitis (EAE) in C57BL/6 Mice. J. Vis. Exp. doi:10.3791/51275

Bober, P., Tomková, Z., Alexovič, M., Ropovik, I., Sabo, J., 2019. The unfolded protein response controls endoplasmic reticulum stress-induced apoptosis of MCF-7 cells via a high dose of vitamin C treatment. Mol. Biol. Rep. 46, 1275–1284. doi:10.1007/s11033-019-04598-w

Bochner, D.N., Sapp, R.W., Adelson, J.D., Zhang, S., Lee, H., Djurisic, M., Syken, J., Dan, Y., Shatz, C.J., 2014. Blocking PirB up-regulates spines and functional synapses to unlock visual cortical plasticity and facilitate recovery from amblyopia. Sci. Transl. Med. 6, 258ra140. doi:10.1126/scitranslmed.3010157

Brownlee, W.J., Miller, D.H., 2014. Clinically isolated syndromes and the relationship to multiple sclerosis. J. Clin. Neurosci. 21, 2065–2071. doi:10.1016/j.jocn.2014.02.026

Bruttger, J., Karram, K., Wörtge, S., Regen, T., Marini, F., Hoppmann, N., Klein, M., Blank, T., Yona, S., Wolf, Y., Mack, M., Pinteaux, E., Müller, W., Zipp, F., Binder, H., Bopp, T., Prinz, M., Jung, S., Waisman, A., 2015. Genetic Cell Ablation Reveals Clusters of Local Self-Renewing Microglia in the Mammalian Central Nervous System. Immunity 43, 92–106. doi:10.1016/j.immuni.2015.06.012

Bunge, M.B., 1973. Fine structure of nerve fibers and growth cones of isolated sympathetic neurons in culture. J. Cell Biol. 56, 713–35. doi:10.1083/jcb.56.3.713

Cahoy, J.D., Emery, B., Kaushal, A., Foo, L.C., Zamanian, J.L., Christopherson, K.S., Xing, Y., Lubischer, J.L., Krieg, P.A., Krupenko, S.A., Thompson, W.J., Barres, B.A., 2008. A Transcriptome Database for Astrocytes, Neurons, and Oligodendrocytes: A New Resource for Understanding Brain Development and Function. J. Neurosci. 28, 264–278. doi:10.1523/JNEUROSCI.4178-07.2008

Cajigas, I.J., Tushev, G., Will, T.J., tom Dieck, S., Fuerst, N., Schuman, E.M., 2012. The Local Transcriptome in the Synaptic Neuropil Revealed by Deep Sequencing and High-Resolution Imaging. Neuron 74, 453–466. doi:10.1016/j.neuron.2012.02.036

Chakravarti, A., Selvadurai, K., Shahoei, R., Lee, H., Fatma, S., Tajkhorshid, E., Huang, R.H., 2018. Reconstitution and substrate specificity for isopentenyl pyrophosphate of the antiviral radical SAM enzyme viperin. J. Biol. Chem. 293, 14122–14133. doi:10.1074/jbc.RA118.003998

Chang, A., Staugaitis, S.M., Dutta, R., Batt, C.E., Easley, K.E., Chomyk, A.M., Yong, V.W., Fox, R.J., Kidd, G.J., Trapp, B.D., 2012. Cortical remyelination: A new target for repair therapies in multiple sclerosis. Ann. Neurol. 72, 918–926. doi:10.1002/ana.23693

Chang, A., Tourtellotte, W.W., Rudick, R., Trapp, B.D., 2002. Premyelinating Oligodendrocytes in Chronic Lesions of Multiple Sclerosis. N. Engl. J. Med. 346, 165–173. doi:10.1056/NEJMoa010994

Chen, Y., Zhao, L., Li, Q., Wheeler, D.C., Varghese, Z., Moorhead, J.F., Powis, S.H., Ruan, X.Z., 2014. Inflammatory stress reduces the effectiveness of statins in the kidney by disrupting HMGCoA reductase feedback regulation. Nephrol. Dial. Transplant 29, 1864–78. doi:10.1093/ndt/gfu203

Chevalier, G., Suberbielle, E., Monnet, C., Duplan, V., Martin-Blondel, G., Farrugia, F., Le Masson, G., Liblau, R., Gonzalez-Dunia, D., 2011. Neurons are MHC class I-dependent targets for CD8 T cells upon neurotropic viral infection. PLoS Pathog. 7, e1002393. doi:10.1371/journal.ppat.1002393

Chisholm, S.P., Cervi, A.L., Nagpal, S., Lomax, A.E., 2012. Interleukin-17A Increases Neurite Outgrowth from Adult Postganglionic Sympathetic Neurons. J. Neurosci. 32, 1146–1155. doi:10.1523/JNEUROSCI.5343-11.2012

Czuba, E., Steliga, A., Lietzau, G., Kowiański, P., 2017. Cholesterol as a modifying agent of the neurovascular unit structure and function under physiological and pathological conditions. Metab. Brain Dis. 32, 935–948. doi:10.1007/s11011-017-0015-3

Daneman, R., Prat, A., 2015. The blood-brain barrier. Cold Spring Harb. Perspect. Biol. 7, a020412. doi:10.1101/cshperspect.a020412

DeGrella, R.F., Simoni, R.D., 1982. Intracellular transport of cholesterol to the plasma membrane. J. Biol. Chem. 257, 14256–62.

Díaz-Hernández, M., Hernández, F., Martín-Aparicio, E., Gómez-Ramos, P., Morán, M.A., Castaño, J.G., Ferrer, I., Avila, J., Lucas, J.J., 2003. Neuronal induction of the immunoproteasome in Huntington's disease. J. Neurosci. 23, 11653–61.

Dietschy, J.M., Turley, S.D., 2004. Thematic review series: brain Lipids. Cholesterol metabolism in the central nervous system during early development and in the mature animal. J. Lipid Res. 45, 1375–97. doi:10.1194/jlr.R400004-JLR200

Ding, X., Yan, Y., Li, X., Li, K., Ciric, B., Yang, J., Zhang, Y., Wu, S., Xu, H., Chen, W., Lovett-Racke, A.E., Zhang, G.-X., Rostami, A., 2015. Silencing IFN-γ binding/signaling in astrocytes versus microglia leads to opposite effects on central nervous system autoimmunity. J. Immunol. 194, 4251–64.

doi:10.4049/jimmunol.1303321

Fan, Q.-W., Yu, W., Gong, J.-S., Zou, K., Sawamura, N., Senda, T., Yanagisawa, K., Michikawa, M., 2002. Cholesterol-dependent modulation of dendrite outgrowth and microtubule stability in cultured neurons. J. Neurochem. 80, 178–90.

Farrokhi, M., Saadatpour, Z., Fadaee, E., Saadatpour, L., Rezaei, A., Moeini, P., Amani Beni, A., 2016. A Novel Approach to Discriminate Subgroups in Multiple Sclerosis. Iran. J. Allergy. Asthma. Immunol. 15, 536–546.

Fellows, K., Uher, T., Browne, R.W., Weinstock-Guttman, B., Horakova, D., Posova, H., Vaneckova, M., Seidl, Z., Krasensky, J., Tyblova, M., Havrdova, E., Zivadinov, R., Ramanathan, M., 2015. Protective associations of HDL with blood-brain barrier injury in multiple sclerosis patients. J. Lipid Res. 56, 2010–2018. doi:10.1194/jlr.M060970

Fischer, M.T., Sharma, R., Lim, J.L., Haider, L., Frischer, J.M., Drexhage, J., Mahad, D., Bradl, M., van Horssen, J., Lassmann, H., 2012. NADPH oxidase expression in active multiple sclerosis lesions in relation to oxidative tissue damage and mitochondrial injury. Brain 135, 886–899. doi:10.1093/brain/aws012

Fischer, M.T., Wimmer, I., Höftberger, R., Gerlach, S., Haider, L., Zrzavy, T., Hametner, S., Mahad, D., Binder, C.J., Krumbholz, M., Bauer, J., Bradl, M., Lassmann, H., 2013. Disease-specific molecular events in cortical multiple sclerosis lesions. Brain 136, 1799–1815. doi:10.1093/brain/awt110

Fletcher, J.M., Lalor, S.J., Sweeney, C.M., Tubridy, N., Mills, K.H.G., 2010. T cells in multiple sclerosis and experimental autoimmune encephalomyelitis. Clin. Exp. Immunol. 162, 1–11. doi:10.1111/j.1365-2249.2010.04143.x

Foster, M.; Sherrington, C.S., 1897. Textbook of Physiology, 7th ed. London.

Foster, J.A., Quan, N., Stern, E.L., Kristensson, K., Herkenham, M., 2002. Induced neuronal expression of class I major histocompatibility complex mRNA in acute and chronic inflammation models. J. Neuroimmunol. 131, 83–91.

Franklin, R.J.M., ffrench-Constant, C., Edgar, J.M., Smith, K.J., 2012. Neuroprotection and repair in multiple sclerosis. Nat. Rev. Neurol. 8, 624–634. doi:10.1038/nrneurol.2012.200

Fünfschilling, U., Saher, G., Xiao, L., Möbius, W., Nave, K.-A., 2007. Survival of adult neurons lacking cholesterol synthesis in vivo. BMC Neurosci. 8, 1. doi:10.1186/1471-2202-8-1

Furtado, G.C., Marcondes, M.C.G., Latkowski, J.-A., Tsai, J., Wensky, A., Lafaille, J.J., 2008. Swift entry of myelin-specific T lymphocytes into the central nervous system in spontaneous autoimmune encephalomyelitis. J. Immunol. 181, 4648–55. doi:10.4049/jimmunol.181.7.4648

Galea, I., Bechmann, I., Perry, V.H., 2007. What is immune privilege (not)? Trends Immunol. 28, 12–18. doi:10.1016/j.it.2006.11.004

Gilbert, S.F., 2000. Tissue Architecture of the Central Nervous System.

Goldman, M.D., Cohen, J.A., 2008. Statins to treat multiple sclerosis: Friend or foe? Neurology 71, 1386–1387. doi:10.1212/01.wnl.0000327876.72639.e7

Greenwood, J., Steinman, L., Zamvil, S.S., 2006. Statin therapy and autoimmune disease: from protein prenylation to immunomodulation. Nat. Rev. Immunol. 6, 358–70. doi:10.1038/nri1839

Guez-Barber, D., Fanous, S., Harvey, B.K., Zhang, Y., Lehrmann, E., Becker, K.G., Picciotto, M.R., Hope, B.T., 2012. FACS purification of immunolabeled cell types from adult rat brain. J. Neurosci. Methods 203, 10–18. doi:10.1016/j.jneumeth.2011.08.045

Handel, A.E., Lincoln, M.R., Ramagopalan, S. V., 2011. Of mice and men: experimental autoimmune encephalitis and multiple sclerosis. Eur. J. Clin. Invest. 41, 1254–1258. doi:10.1111/j.1365-

2362.2011.02519.x

Harrington, S.M., Strauman, M.C., Abe, C.M., Nataro, J.P., 2005. Aggregative adherence fimbriae contribute to the inflammatory response of epithelial cells infected with enteroaggregative Escherichia coli. Cell. Microbiol. 7, 1565–1578. doi:10.1111/j.1462-5822.2005.00588.x

Harrison, D.A., 2012. The JAK/STAT Pathway. Cold Spring Harb. Perspect. Biol. 4, a011205–a011205. doi:10.1101/cshperspect.a011205

Hawkins, B.T., 2005. The Blood-Brain Barrier/Neurovascular Unit in Health and Disease. Pharmacol. Rev. 57, 173–185. doi:10.1124/pr.57.2.4

Hirrlinger, P.G., Scheller, A., Braun, C., Quintela-Schneider, M., Fuss, B., Hirrlinger, J., Kirchhoff, F., 2005. Expression of reef coral fluorescent proteins in the central nervous system of transgenic mice. Mol. Cell. Neurosci. 30, 291–303. doi:10.1016/j.mcn.2005.08.011

Ikonen, E., 2008. Cellular cholesterol trafficking and compartmentalization. Nat. Rev. Mol. Cell Biol. 9, 125–138. doi:10.1038/nrm2336

Inglis, H.R., Greer, J.M., McCombe, P.A., 2012. Gene Expression in the Spinal Cord in Female Lewis Rats with Experimental Autoimmune Encephalomyelitis Induced with Myelin Basic Protein. PLoS One 7, e48555. doi:10.1371/journal.pone.0048555

Iwanowski, P., Losy, J., 2015. Immunological differences between classical phenothypes of multiple sclerosis. J. Neurol. Sci. 349, 10–14. doi:10.1016/j.jns.2014.12.035

Jaiswal, M., Zech, W.-D., Goos, M., Leutbecher, C., Ferri, A., Zippelius, A., Carrì, M., Nau, R., Keller, B.U., 2009. Impairment of mitochondrial calcium handling in a mtSOD1 cell culture model of motoneuron disease. BMC Neurosci. 10, 64. doi:10.1186/1471-2202-10-64

Jawabri, K.H., Sharma, S., 2019. Physiology, Cerebral Cortex Functions, StatPearls.

Jeske, D.J., Dietschy, J.M., 1980. Regulation of rates of cholesterol synthesis in vivo in the liver and carcass of the rat measured using [3H]water. J. Lipid Res. 21, 364–76.

Jiang, J., Shihan, M.H., Wang, Y., Duncan, M.K., 2018. Lens Epithelial Cells Initiate an Inflammatory Response Following Cataract Surgery. Investig. Opthalmology Vis. Sci. 59, 4986. doi:10.1167/iovs.18-25067

Kaiser, O., Aliuos, P., Wissel, K., Lenarz, T., Werner, D., Reuter, G., Kral, A., Warnecke, A., 2013. Dissociated Neurons and Glial Cells Derived from Rat Inferior Colliculi after Digestion with Papain. PLoS One 8, e80490. doi:10.1371/journal.pone.0080490

Kaur, G., Helmer, R.A., Smith, L.A., Martinez-Zaguilan, R., Dufour, J.M., Chilton, B.S., 2018. Alternative splicing of helicase-like transcription factor (Hltf): Intron retention-dependent activation of immune tolerance at the feto-maternal interface. PLoS One 13, e0200211. doi:10.1371/journal.pone.0200211

Kerlero de Rosbo, N., Milo, R., Lees, M.B., Burger, D., Bernard, C.C., Ben-Nun, A., 1993. Reactivity to myelin antigens in multiple sclerosis. Peripheral blood lymphocytes respond predominantly to myelin oligodendrocyte glycoprotein. J. Clin. Invest. 92, 2602–2608. doi:10.1172/JCI116875

Kiu, H., Nicholson, S.E., 2012. Biology and significance of the JAK/STAT signalling pathways. Growth Factors 30, 88–106. doi:10.3109/08977194.2012.660936

Klopfleisch, S., Merkler, D., Schmitz, M., Kloppner, S., Schedensack, M., Jeserich, G., Althaus, H.H., Bruck, W., 2008. Negative Impact of Statins on Oligodendrocytes and Myelin Formation In Vitro and In Vivo. J. Neurosci. 28, 13609–13614. doi:10.1523/JNEUROSCI.2765-08.2008

Kostic, M., Dzopalic, T., Zivanovic, S., Zivkovic, N., Cvetanovic, A., Stojanovic, I., Vojinovic, S., Marjanovic, G., Savic, V., Colic, M., 2014. IL-17 and Glutamate Excitotoxicity in the Pathogenesis of Multiple Sclerosis. Scand. J. Immunol. 79, 181–186. doi:10.1111/sji.12147

Kremer, D., Küry, P., Dutta, R., 2015. Promoting remyelination in multiple sclerosis: Current drugs and future prospects. Mult. Scler. J. 21, 541–549. doi:10.1177/1352458514566419

Kubagawa, H., Burrows, P.D., Cooper, M.D., 1997. A novel pair of immunoglobulin-like receptors expressed by B cells and myeloid cells. Proc. Natl. Acad. Sci. U. S. A. 94, 5261–6.

Lacher, S.M., Bruttger, J., Kalt, B., Berthelet, J., Rajalingam, K., Wörtge, S., Waisman, A., 2017a. HMG-CoA reductase promotes protein prenylation and therefore is indispensible for T-cell survival. Cell Death Dis. 8, e2824. doi:10.1038/cddis.2017.221

Lavrnja, I., Smiljanic, K., Savic, D., Mladenovic-Djordjevic, A., Tesovic, K., Kanazir, S., Pekovic, S., 2017. Expression profiles of cholesterol metabolism-related genes are altered during development of experimental autoimmune encephalomyelitis in the rat spinal cord. Sci. Rep. 7, 2702. doi:10.1038/s41598-017-02638-8

Li, Z., Li, K., Zhu, L., Kan, Q., Yan, Y., Kumar, P., Xu, H., Rostami, A., Zhang, G.-X., 2013. Inhibitory effect of IL-17 on neural stem cell proliferation and neural cell differentiation. BMC Immunol. 14, 20. doi:10.1186/1471-2172-14-20

Lobo, M.K., Karsten, S.L., Gray, M., Geschwind, D.H., Yang, X.W., 2006. FACS-array profiling of striatal projection neuron subtypes in juvenile and adult mouse brains. Nat. Neurosci. 9, 443–52. doi:10.1038/nn1654

Lodish, H., Berk, A., Zipursky, S.L., Matsudaira, P., Baltimore, D., Darnell, J., 2000. Neurotransmitters, Synapses, and Impulse Transmission.

Lucchinetti, C.F., Popescu, B.F.G., Bunyan, R.F., Moll, N.M., Roemer, S.F., Lassmann, H., Brück, W., Parisi, J.E., Scheithauer, B.W., Giannini, C., Weigand, S.D., Mandrekar, J., Ransohoff, R.M., 2011. Inflammatory Cortical Demyelination in Early Multiple Sclerosis. N. Engl. J. Med. 365, 2188–2197. doi:10.1056/NEJMoa1100648

Ludowyk, P.A., Willenborg, D.O., Parish, C.R., 1992. Selective localisation of neuro-specific T lymphocytes in the central nervous system. J. Neuroimmunol. 37, 237–50.

Maehlen, J., Schröder, H.D., Klareskog, L., Olsson, T., Kristensson, K., 1988. Axotomy induces MHC class I antigen expression on rat nerve cells. Neurosci. Lett. 92, 8–13.

Mailman, T., Hariharan, M., Karten, B., 2011. Inhibition of neuronal cholesterol biosynthesis with lovastatin leads to impaired synaptic vesicle release even in the presence of lipoproteins or geranylgeraniol. J. Neurochem. 119, 1002–1015. doi:10.1111/j.1471-4159.2011.07474.x

Majd, S., Zarifkar, A., Rastegar, K., Takhshid, M.A., 2008. Culturing adult rat hippocampal neurons with long-interval changing media. Iran. Biomed. J. 12, 101–7.

Manev, H., Favaron, M., Guidotti, A., Costa, E., 1989. Delayed increase of Ca2+ influx elicited by glutamate: role in neuronal death. Mol. Pharmacol. 36, 106–12.

Maton, A., 1993. Human biology and health. Prentice Hall.

Mauch, D.H., Nägler, K., Schumacher, S., Göritz, C., Müller, E.C., Otto, A., Pfrieger, F.W., 2001. CNS Synaptogenesis Promoted by Glia-Derived Cholesterol. Science (80-.). 294, 1354–1357. doi:10.1126/science.294.5545.1354

McConnell, M.J., Huang, Y.H., Datwani, A., Shatz, C.J., 2009. H2-Kb and H2-Db regulate cerebellar long-term depression and limit motor learning. Proc. Natl. Acad. Sci. 106, 6784–6789. doi:10.1073/pnas.0902018106

McIntosh, T.J., Simon, S.A., 2006. ROLES OF BILAYER MATERIAL PROPERTIES IN FUNCTION AND DISTRIBUTION OF MEMBRANE PROTEINS. Annu. Rev. Biophys. Biomol. Struct. 35, 177–198. doi:10.1146/annurev.biophys.35.040405.102022

Medana, I., Martinic, M.A., Wekerle, H., Neumann, H., 2001. Transection of Major Histocompatibility Complex

Class I-Induced Neurites by Cytotoxic T Lymphocytes. Am. J. Pathol. 159, 809–815. doi:10.1016/S0002-9440(10)61755-5

Medana, I.M., Gallimore, A., Oxenius, A., Martinic, M.M.A., Wekerle, H., Neumann, H., 2000. MHC class I-restricted killing of neurons by virus-specific CD8+ T lymphocytes is effected through the Fas/FasL, but not the perforin pathway. Eur. J. Immunol. 30, 3623–3633. doi:10.1002/1521-4141(200012)30:12<3623::AID-IMMU3623>3.0.CO;2-F

Mendel, I., de Rosbo, N.K., Ben-Nun, A., 1995. A myelin oligodendrocyte glycoprotein peptide induces typical chronic experimental autoimmune encephalomyelitis in H-2b mice: Fine specificity and T cell receptor Vβ expression of encephalitogenic T cells. Eur. J. Immunol. 25, 1951–1959. doi:10.1002/eji.1830250723

Ming, G., Song, H., 2011. Adult Neurogenesis in the Mammalian Brain: Significant Answers and Significant Questions. Neuron 70, 687–702. doi:10.1016/j.neuron.2011.05.001

Miron, V.E., Zehntner, S.P., Kuhlmann, T., Ludwin, S.K., Owens, T., Kennedy, T.E., Bedell, B.J., Antel, J.P., 2009. Statin Therapy Inhibits Remyelination in the Central Nervous System. Am. J. Pathol. 174, 1880–1890. doi:10.2353/ajpath.2009.080947

Miziorko, H.M., 2011. Enzymes of the mevalonate pathway of isoprenoid biosynthesis. Arch. Biochem. Biophys. 505, 131–143. doi:10.1016/j.abb.2010.09.028

Mizuno, T., Zhang, G., Takeuchi, H., Kawanokuchi, J., Wang, J., Sonobe, Y., Jin, S., Takada, N., Komatsu, Y., Suzumura, A., 2008. Interferon-γ directly induces neurotoxicity through a neuron specific, calcium-permeable complex of IFN-γ receptor and AMPA GluR1 receptor. FASEB J. 22, 1797–1806. doi:10.1096/fj.07-099499

Morell, P., Jurevics, H., 1996a. Origin of cholesterol in myelin. Neurochem. Res. 21, 463–70.

Müller, C., Bauer, N.M., Schäfer, I., White, R., Stangel, M., Klugmann, M., 2013. Making myelin basic protein – from mRNA transport to localized translation 25, 19–1. doi:10.3389/fncel.2013.00169

Neumann, H., Schmidt, H., Cavalié, A., Jenne, D., Wekerle, H., 1997. Major Histocompatibility Complex (MHC) Class I Gene Expression in Single Neurons of the Central Nervous System: Differential Regulation by Interferon (IFN)-γ and Tumor Necrosis Factor (TNF)-α. J. Exp. Med. 185, 305–316. doi:10.1084/jem.185.2.305

Nieweg, K., Schaller, H., Pfrieger, F.W., 2009a. Marked differences in cholesterol synthesis between neurons and glial cells from postnatal rats. J. Neurochem. 109, 125–134. doi:10.1111/j.1471-4159.2009.05917.x

Nowaczyk, M.J.M., Irons, M.B., 2012. Smith-Lemli-Opitz syndrome: Phenotype, natural history, and epidemiology. Am. J. Med. Genet. Part C Semin. Med. Genet. 160C, 250–262. doi:10.1002/ajmg.c.31343

Ohashi, K., Osuga, J., Tozawa, R., Kitamine, T., Yagyu, H., Sekiya, M., Tomita, S., Okazaki, H., Tamura, Y., Yahagi, N., Iizuka, Y., Harada, K., Gotoda, T., Shimano, H., Yamada, N., Ishibashi, S., 2003. Early embryonic lethality caused by targeted disruption of the 3-hydroxy-3-methylglutaryl-CoA reductase gene. J. Biol. Chem. 278, 42936–41. doi:10.1074/jbc.M307228200

Ottum, P.A., Arellano, G., Reyes, L.I., Iruretagoyena, M., Naves, R., 2015. Opposing Roles of Interferon-Gamma on Cells of the Central Nervous System in Autoimmune Neuroinflammation. Front. Immunol. 6, 539. doi:10.3389/fimmu.2015.00539

Peake, K.B., Vance, J.E., 2012. Normalization of Cholesterol Homeostasis by 2-Hydroxypropyl-β-cyclodextrin in Neurons and Glia from Niemann-Pick C1 (NPC1)-deficient Mice. J. Biol. Chem. 287, 9290–9298. doi:10.1074/jbc.M111.326405

Pender, M.P., Sears, T.A., 1986. Involvement of the dorsal root ganglion in acute experimental allergic encephalomyelitis in the Lewis rat. A histological and electrophysiological study. J. Neurol. Sci. 72, 231–42.

Pfrieger, F.W., 2003. Cholesterol homeostasis and function in neurons of the central nervous system. Cell. Mol.

Life Sci. 60, 1158–1171. doi:10.1007/s00018-003-3018-7

Pickering, A.M., Davies, K.J.A., 2012. Differential roles of proteasome and immunoproteasome regulators Pa28αβ, Pa28γ and Pa200 in the degradation of oxidized proteins. Arch. Biochem. Biophys. 523, 181–90. doi:10.1016/j.abb.2012.04.018

Pierson, E., Simmons, S.B., Castelli, L., Goverman, J.M., 2012. Mechanisms regulating regional localization of inflammation during CNS autoimmunity. Immunol. Rev. 248, 205–15. doi:10.1111/j.1600-065X.2012.01126.x

Plantone, D., De Angelis, F., Doshi, A., Chataway, J., 2016. Secondary Progressive Multiple Sclerosis: Definition and Measurement. CNS Drugs 30, 517–526. doi:10.1007/s40263-016-0340-9

Prineas, J.W., Connell, F., 1979. Remyelination in multiple sclerosis. Ann. Neurol. 5, 22–31. doi:10.1002/ana.410050105

Purves, D., Augustine, G.J., Fitzpatrick, D., Katz, L.C., LaMantia, A.-S., McNamara, J.O., Williams, S.M., 2001. Cerebellar Circuitry and the Coordination of Ongoing Movement.

Ransohoff, R.M., Engelhardt, B., 2012. The anatomical and cellular basis of immune surveillance in the central nervous system. Nat. Rev. Immunol. 12, 623–635. doi:10.1038/nri3265

Rawson, R.B., 2003. The SREBP pathway — insights from insigs and insects. Nat. Rev. Mol. Cell Biol. 4, 631–640. doi:10.1038/nrm1174

Robinson, A.P., Harp, C.T., Noronha, A., Miller, S.D., 2014. The experimental autoimmune encephalomyelitis (EAE) model of MS, in: Handbook of Clinical Neurology. pp. 173–189. doi:10.1016/B978-0-444-52001-2.00008-X

Rostami, A., Ciric, B., 2013. Role of Th17 cells in the pathogenesis of CNS inflammatory demyelination. J. Neurol. Sci. 333, 76–87. doi:10.1016/j.jns.2013.03.002

Saher, G., Brügger, B., Lappe-Siefke, C., Möbius, W., Tozawa, R., Wehr, M.C., Wieland, F., Ishibashi, S., Nave, K.-A., 2005. High cholesterol level is essential for myelin membrane growth. Nat. Neurosci. 8, 468–475. doi:10.1038/nn1426

Sanz, E., Yang, L., Su, T., Morris, D.R., McKnight, G.S., Amieux, P.S., 2009. Cell-type-specific isolation of ribosome-associated mRNA from complex tissues. Proc. Natl. Acad. Sci. 106, 13939–13944. doi:10.1073/pnas.0907143106

Sarma, J., Ciric, B., Marek, R., Sadhukhan, S., Caruso, M.L., Shafagh, J., Fitzgerald, D.C., Shindler, K.S., Rostami, A., 2009. Functional interleukin-17 receptor A is expressed in central nervous system glia and upregulated in experimental autoimmune encephalomyelitis. J. Neuroinflammation 6, 14. doi:10.1186/1742-2094-6-14

Sever, N., Yang, T., Brown, M.S., Goldstein, J.L., DeBose-Boyd, R.A., 2003. Accelerated degradation of HMG CoA reductase mediated by binding of insig-1 to its sterol-sensing domain. Mol. Cell 11, 25–33.

Shatz, C.J., 2009. MHC Class I: An Unexpected Role in Neuronal Plasticity. Neuron 64, 40–45. doi:10.1016/j.neuron.2009.09.044

Siffrin, V., Radbruch, H., Glumm, R., Niesner, R., Paterka, M., Herz, J., Leuenberger, T., Lehmann, S.M., Luenstedt, S., Rinnenthal, J.L., Laube, G., Luche, H., Lehnardt, S., Fehling, H.-J., Griesbeck, O., Zipp, F., 2010. In Vivo Imaging of Partially Reversible Th17 Cell-Induced Neuronal Dysfunction in the Course of Encephalomyelitis. Immunity 33, 424–436. doi:10.1016/j.immuni.2010.08.018

Simons, K., Vaz, W.L.C., 2004. Model systems, lipid rafts, and cell membranes. Annu. Rev. Biophys. Biomol. Struct. 33, 269–95. doi:10.1146/annurev.biophys.32.110601.141803

Stampachiacchiere, B., Aloe, L., 2005. Differential modulatory effect of NGF on MHC class I and class II expression in spinal cord cells of EAE rats. J. Neuroimmunol. 169, 20–30.

doi:10.1016/j.jneuroim.2005.07.022

Steinman, L., 1999. Assessment of animal models for MS and demyelinating disease in the design of rational therapy. Neuron 24, 511–4.

Steinman, L., Zamvil, S., 2003. Transcriptional analysis of targets in multiple sclerosis. Nat. Rev. Immunol. 3, 483–492. doi:10.1038/nri1108

Stromnes, I.M., Goverman, J.M., 2006. Active induction of experimental allergic encephalomyelitis. Nat. Protoc. 1, 1810–1819. doi:10.1038/nprot.2006.285

Suidan, H.S., Bouvier, J., Schaerer, E., Stone, S.R., Monard, D., Tschopp, J., 1994. Granzyme A released upon stimulation of cytotoxic T lymphocytes activates the thrombin receptor on neuronal cells and astrocytes. Proc. Natl. Acad. Sci. 91, 8112–8116. doi:10.1073/pnas.91.17.8112

Syken, J., Grandpre, T., Kanold, P.O., Shatz, C.J., 2006. PirB restricts ocular-dominance plasticity in visual cortex. Science 313, 1795–800. doi:10.1126/science.1128232

Tennyson, V.M., Brzin, M., 1970. THE APPEARANCE OF ACETYLCHOLINESTERASE IN THE DORSAL ROOT NEUROBLAST OF THE RABBIT EMBRYO: A Study by Electron Microscope Cytochemistry and Microgasometric Analysis with the Magnetic Diver. J. Cell Biol. 46, 64–80. doi:10.1083/jcb.46.1.64

Tettey, P., Simpson, S., Taylor, B., Blizzard, L., Ponsonby, A.-L., Dwyer, T., Kostner, K., van der Mei, I., 2014. An adverse lipid profile is associated with disability and progression in disability, in people with MS. Mult. Scler. J. 20, 1737–1744. doi:10.1177/1352458514533162

Toews, A.D., Jurevics, H., Hostettler, J., Roe, E.B., Morell, P., 1996. Tissue-specific coordinate regulation of enzymes of cholesterol biosynthesis: sciatic nerve versus liver. J. Lipid Res. 37, 2502–9.

Tozawa, R., Ishibashi, S., Osuga, J., Yagyu, H., Oka, T., Chen, Z., Ohashi, K., Perrey, S., Shionoiri, F., Yahagi, N., Harada, K., Gotoda, T., Yazaki, Y., Yamada, N., 1999. Embryonic lethality and defective neural tube closure in mice lacking squalene synthase. J. Biol. Chem. 274, 30843–8. doi:10.1074/jbc.274.43.30843

Trapp, B.D., Stys, P.K., 2009. Virtual hypoxia and chronic necrosis of demyelinated axons in multiple sclerosis. Lancet Neurol. 8, 280–291. doi:10.1016/S1474-4422(09)70043-2

Trinchieri, G., 1997. Cytokines acting on or secreted by macrophages during intracellular infection (IL-10, IL-12, IFN-gamma). Curr. Opin. Immunol. 9, 17–23.

Van Kaer, L., Postoak, J.L., Wang, C., Yang, G., Wu, L., 2019. Innate, innate-like and adaptive lymphocytes in the pathogenesis of MS and EAE. Cell. Mol. Immunol. 16, 531–539. doi:10.1038/s41423-019-0221-5

Vance, J.E., 2006. Lipid imbalance in the neurological disorder, Niemann-Pick C disease. FEBS Lett. 580, 5518–5524. doi:10.1016/j.febslet.2006.06.008

Waisman, A., Hauptmann, J., Regen, T., 2015. The role of IL-17 in CNS diseases. Acta Neuropathol. 129, 625–637. doi:10.1007/s00401-015-1402-7

Wang, Weifang, Qi, B., Lv, H., Wu, F., Liu, L., Wang, Wei, Wang, Q., Hu, L., Hao, Y., Wang, Y., 2017. A new method of isolating spinal motor neurons from fetal mouse. J. Neurosci. Methods 288, 57–61. doi:10.1016/j.jneumeth.2017.06.014

Wang, Y., Tan, Z., Qin, L., Yu, Y., 2013. Simplified protocol for isolation of multipotential NG2 cells from postnatal mouse. J. Neurosci. Methods 219, 252–261. doi:10.1016/j.jneumeth.2013.08.001

Waterham, H.R., 2006. Defects of cholesterol biosynthesis. FEBS Lett. 580, 5442–5449. doi:10.1016/j.febslet.2006.07.027

Weinstock-Guttman, B., Zivadinov, R., Mahfooz, N., Carl, E., Drake, A., Schneider, J., Teter, B., Hussein, S., Mehta, B., Weiskopf, M., Durfee, J., Bergsland, N., Ramanathan, M., 2011. Serum lipid profiles are associated with disability and MRI outcomes in multiple sclerosis. J. Neuroinflammation 8, 127.

doi:10.1186/1742-2094-8-127

Willey, J.Z., Elkind, M.S. V., 2010. 3-Hydroxy-3-methylglutaryl–Coenzyme A Reductase Inhibitors in the Treatment of Central Nervous System Diseases. Arch. Neurol. 67, 1062–7. doi:10.1001/archneurol.2010.199

Yokoyama, C., Wang, X., Briggs, M.R., Admon, A., Wu, J., Hua, X., Goldstein, J.L., Brown, M.S., 1993. SREBP-1, a basic-helix-loop-helix-leucine zipper protein that controls transcription of the low density lipoprotein receptor gene. Cell 75, 187–97.

Zelená, J., 1970. Ribosome-like particles in myelinated axons of the rat. Brain Res. 24, 359–63.

Zhang, J., Liu, Q., 2015. Cholesterol metabolism and homeostasis in the brain. Protein Cell 6, 254–64. doi:10.1007/s13238-014-0131-3

8. Acknowledgements

First of all, I have to thank [redacted] who gave me the opportunity to perform my PhD thesis in this outstanding research group with an interesting and challenging project.

Also thanks to my thesis committee [redacted] and [redacted] for reading and evaluating my PhD thesis.

I would like to thank all members of the Waisman group for the nice atmosphere in the lab, especially to [redacted], [redacted], [redacted], [redacted] and [redacted] for the fun in the lab and afterwards!

Thanks to [redacted], [redacted], [redacted], [redacted] and [redacted] who always helped with experiments and experienced advice.

Also thanks to the collaboration partners [redacted], [redacted], [redacted], [redacted], [redacted], [redacted] and [redacted], for their help with the RiboTag method, sequencing and data analysis.

I also want to thank my students [redacted], [redacted] and [redacted] for their help in the lab.

Last but not least I have to thank my family from the bottom of my heart for their moral support and unconditionally love during these years!

9. Erklärung

Ich versichere, dass ich die von mir vorgelegte Dissertation selbständig angefertigt, die benutzten Quellen und Hilfsmittel vollständig angegeben und die Stellen der Arbeit – einschließlich Tabellen, Karten und Abbildungen -, die anderen Werken im Wortlaut oder dem Sinn nach entnommen sind, in jedem Einzelfall als Entlehnung kenntlich gemacht habe; dass diese Dissertation noch keiner anderen Fakultät oder Universität zur Prüfung vorgelegen hat; dass sie - abgesehen von unten angegebenen Teilpublikationen - noch nicht veröffentlicht worden ist sowie, dass ich eine solche Veröffentlichung vor Abschluss des Promotionsverfahrens nicht vornehmen werde. Die Bestimmungen dieser Promotionsordnung sind mir bekannt. Die von mir vorgelegte Dissertation ist von Herrn [redacted] betreut worden.

Mainz, im Juni 2019 Sabina Berl

10. Curriculum Vitae

Persönliche Daten

Name:	Sabina Melanie Berl
Geburtsdatum:	08.07.1985
Geburtsort:	Frankfurt am Main
Adresse:	Am Fort Elisabeth 5, 55131 Mainz
E-Mail:	berls@uni-mainz.de
Familienstand:	verheiratet
Nationalität:	deutsch

Schulische Ausbildung

1992-1996	Grundschule am Landgraben Frankfurt am Main
1996-2005	Integrierte Gesamtschule am Ried Frankfurt am Main

Studium

2005-2011	Studium der Biologie an der Johannes-Gutenberg Universität Mainz
2011	Diplomprüfung in den Hauptfächern Genetik, Immunologie und Zoologie Diplomprüfung im Nebenfach Anthropologie
2011	Diplomarbeit am Institut für Entwicklungsgenetik bei [redacted] mit dem Thema: "Identifizierung und Charakterisierung glialer Enhancersequencen in *Drosophila melanogaster*"

Promotion

Seit 2012	"Neuronal Response to Experimental Autoimmune Encephalomyelitis" am Institut für Molekulare Medizin Mainz bei [redacted]

11. Publication

Enrichment and isolation of neurons from adult mouse brain for ex vivo analysis

Berl S., Karram K., Scheller A., Jungblut M., Kirchhoff F. and Waisman A.

Journal of Neuroscience Methods 2017